UNIVERSIDADE FEDERAL DO RIO GRANDE DO SUL

INSTITUTO DE QUÍMICA

USO DE SILICATOS MODIFICADOS NA REMOÇÃO DE CORANTES DE EFLUENTES AQUOSOS

Doutoranda: ***Betina Royer***

Outubro de 2012

Porto Alegre, RS

UNIVERSIDADE FEDERAL DO RIO GRANDE DO SUL

INSTITUTO DE QUÍMICA

USO DE SILICATOS MODIFICADOS NA REMOÇÃO DE CORANTES DE EFLUENTES AQUOSOS

Doutoranda: ***Betina Royer***

Orientador: Prof. Dr. Éder Cláudio Lima

Tese de doutorado submetido ao Programa de Pós-Graduação em Química-UFRGS como parte dos requisitos para obtenção do título de Doutor em Química.

Outubro de 2012

Porto Alegre, RS

A presente tese foi realizada inteiramente pelo autor, exceto as colaborações as quais serão devidamente citadas nos agradecimentos, no período entre (abril/2008) e (setembro/2012), no Instituto de Química da Universidade Federal do Rio Grande do Sul sob Orientação do Professor Doutor Éder Cláudio Lima. A tese foi julgada adequada para a obtenção do título de Doutor em Química pela seguinte banca examinadora:

Comissão Examinadora:

Orientador Prof. Dr. Éder Cláudio Lima	Prof. Dr. Edilson V. Benvenutti
Prof. Dr. Flávio André Pavan	Prof. Dr. Sílvio Luis Pereira Dias
Prof. Dr. Fernando M. Machado	Prof. Dr. Caciano P. Z. Noreña

Dedico este trabalho aos meus pais Darcy José e Ivete Maria e aos meus irmãos André, Tiago e Sabrina, que, próximos ou distantes, estiveram sempre presentes durante mais esta etapa de minha vida acadêmica.

AGRADECIMENTOS

Agradeço de forma carinhosa a todas as pessoas que me incentivaram e me apoiaram durante esses quatro anos de trabalho, compartilhando comigo todos os momentos de dedicação e zelo.

Ao meu orientador Prof. Dr. Éder Cláudio Lima, pelos ensinamentos, amizade, apoio e principalmente paciência e desprendimento nos momentos em que precisei do seu auxílio.

Ao Prof. Dr. Cláudio Airoldi e a sua aluna de doutorado Thais Regi Macedo, do Instituto de Química da Unicamp, pelo fornecimento dos silicatos empregados nessa tese de doutorado.

Aos colegas de laboratório, Bruna Martins, Bruna Cunha, Bruna Dinarte, Camila, Felipe, Fernando, Elie, Marta Cunha, Natali, Nathália, Rodrigo, Tatiana, Thais, Suzimara pelo companheirismo e auxílio durante os trabalhos e pela descontração em muitos momentos.

A todos colegas do Programa de Pós Graduação em Química pelo coleguismo durante os estudos e aos inúmeros amigos que conquistei durante essa etapa.

Aos meus pais, Darcy José e Ivete Maria, que apesar da distância, jamais deixaram que eu desistisse do meu sonho. Pai, és meu porto seguro, meu exemplo de dedicação, organização e zelo. Mãe, és minha fortaleza, presente em todos horas, boas e difíceis, sempre com palavras de amor e carinho. Amo vocês mais que tudo na vida.

Aos meus irmãos, André, Tiago e Sabrina, aturando mau humor, participando das alegrias e apoiando sempre durante a busca do meu ideal profissional, também amo vocês.

E enfim, aos meus grandes e bons amigos, que de perto ou de longe, sempre compreenderam minha ausência em alguns momentos e demostraram muito apoio, compreensão e carinho até hoje.

Ao **CNPq** e a **CAPES** pela bolsa concedida.

LISTA DE TRABALHOS GERADOS A PARTIR DOS RESULTADOS DESCRITOS NA TESE

- Royer, B., Cardoso, N.F., Lima, E.C., Ruiz, V.S.O., Macedo, T.R., Airoldi, C. "*Organofunctionalized kenyaite for dye removal from aqueous solution*". **Journal of Colloid and Interface Science, 2009**, v.336, pp. 398-405. doi:10.1016/j.jcis.2009.04.025

- Royer, B., Cardoso, N.F., Lima, E.C., Macedo, T.R., Airoldi, C. "*Sodic and acidic crystalline lamellar magadiite adsorbents for removal of methylene blue from aqueous solutions. Kinetic and equilibrium studies."* **Separation Science and Technology, 2010**, v.45, pp.129-141. doi: 10.1080/01496390903256257.

- Royer, B.,Cardoso, N.F., Lima, E.C., Macedo, T.R., Airoldi, C. *"A useful organofunctionalized layered silicate for textile dye removal"* **Journal of Hazardous Materials, 2010,** v.181, pp. 366-374. doi:10.1016/j.jhazmat.2010.05.019

Publicações de B. Royer no Grupo de Pesquisa LATAMA

1. Lima, E.C., Royer, B., Vaghetti, J.C.P., Brasil, J.L., Simon, N.M., dos Santos Jr., A.A., Pavan, F.A., Dias, S.L.P., Benvenutti, E.V., da Silva, E.A. "*Adsorption of Cu(II) on Araucaria angustifolia wastes: Determination of the optimal conditions by statistic design of experiments*". **Journal of Hazardous Materials, 2007** v.140, pp. 211-220. Autor Correspondente: **Lima, E.C.** DOI:10.1016/j.jhazmat.2006.06.073
2. Brasil, J.L., Vaghetti, J.C.P., Royer, B., dos Santos Jr., A.A., Simon, N.M., Pavan, F.A., Dias, S.L.P., Lima E.C. "*Planejamento estatístico de experimentos como uma ferramenta para otimização das condições de biossorção de Cu(II) em batelada utilizando-se casca de nozes pecã como biossorvente"*. **Química Nova**, **2007**, v.30, pp 548-553. Autor Correspondente: **Lima, E.C.** doi.10.1590/S0100-40422007000300008.
3. Lima, E.C., Royer, B., Vaghetti, J.C.P, Simon, N.M., da Cunha, B.M., Pavan, F.A., Benvenutti, E.V., Veses, R.C., Airoldi,C. "*Application of Brazilian-pine fruit coat as a biosorbent to removal of reactive red 194 textile dye from aqueous solution. Kinetics and equilibrium stud*y". **Journal of Hazardous Materials**, **2008**, v.155, pp 536-550. Autor Correspondente: **Lima, E.C.** doi: 10.1016/j.jhazmat.2007.11.101
4. Vaghetti, J.C.P., Lima E.C., Royer B., Brasil, J.L., da Cunha, B.M., Simon, N.M., Cardoso, N.F., Noreña, C.P. Z., "*Application of Brazilian-pine fruit coat as a biosorbent to removal of Cr(VI) from aqueous solution. Kinetics and equilibrium study*". **Biochemical Engineering Journal, 2008**, v.42, pp 67-76. Autor Correspondente: **Lima, E.C.** doi: 10.1016/j.bej.2008.05.021
5. Vaghetti, J.C.P., Lima, E.C., Royer, B., da Cunha, B.M., Cardoso, N.F., Brasil, J. L., Dias, S.L.P. "*Pecan nutshell as biosorbent to remove Cu(II), Mn(II) and Pb(II) from aqueous solutions*". **Journal of Hazardous Materials**, **2009,** v.162, PP 270-280. Autor Correspondente: **Lima, E.C.** DOI: 10.1016/j.jhazmat.2008.05.039
6. Vaghetti, J.C.P., Lima, E.C., Royer, B., Cardoso, N.F., Martins, B., Calvete, T. "*Pecan nutshell as biosorbent to remove toxic metals from aqueous solution*", **Separation Science and Technology**, **2009**, v. 44, pp. 615-644. Autor Correspondente: **Lima, E.C.** DOI: 10.1080/01496390802634331
7. Royer, B., Cardoso, N.F., Lima, E.C., Vaghetti, J.C.P., Simon, N.M., Calvete, T., Veses, R.C., "*Applications of Brazilian-pine fruit shell in natural and carbonized forms as adsorbents to removal of methylene blue from aqueous solutions - Kinetic and equilibrium study*". **Journal of Hazardous Materials**, **2009**, v. 164, pp. 1213-1222. Autor Correspondente: **Lima, E.C.** DOI: 10.1016/j.jhazmat.2008.05.039

8. Royer, B., Cardoso, N.F., Lima, E.C., Ruiz, V.S.O., Macedo, T.R., Airoldi, C. "*Organofunctionalized kenyaite for dye removal from aqueous solution*". **Journal of Colloid and Interface Science, 2009**, v.336, pp. 398-405. Autor Correspondente: **Lima, E.C** doi:10.1016/j.jcis.2009.04.025
9. Royer, B., Lima, E.C., Cardoso, N.F., Calvete, T., Bruns, R.E., "*Statistical design of experiments for optimization of batch adsorption conditions for removal of reactive red 194 textile dye from aqueous effluents*". **Chemical Engineering Communications, 2010**, v.197, pp. 775-790**.** Autor Correspondente: **Lima, E.C** DOI: 10.1080/00986440903359004
10. Royer, B., Cardoso, N.F., Lima, E.C., Macedo, T.R., Airoldi, C. "*Sodic and acidic crystalline lamellar magadiite adsorbents for removal of methylene blue from aqueous solutions. Kinetic and equilibrium studies."* **Separation Science and Technology, 2010**, v.45, pp.129-141. Autor Correspondente: **Lima, E.C** doi: 10.1080/01496390903256257.
11. Royer, B., Cardoso, N.F., Lima, E.C., Macedo, T.R., Airoldi, C., "*A useful organofunctionalized layered silicate for textile dye removal*". **Journal of Hazardous Materials, 2010**, v.181, pp 366-374. Autor Correspondente: **Lima, E.C** doi:10.1016/j.jhazmat.2010.05.019
12. Cardoso, N.F., Lima, E.C., Pinto I.S., Amavisca C.V., Royer B., Pinto R.B., Alencar W.S., Pereira S.F.P., "*Application of cupuassu shell as biosorbent for the removal of textile dyes from aqueous solution"*. **Journal of Environmental Management**, **2011**, v.92, pp. 1237-1247. Autor Correspondente: **Lima, E.C** doi:10.1016/j.jenvman.2010.12.010
13. Cardoso, N.F., Pinto, R.B., Lima, E.C., Calvete, T., Amavisca, C.V., Royer, B., Cunha, M.L., Fernandes, T.H.M., Pinto, I.S., "*Removal of remazol black B textile dye from aqueous solution by adsorption*", **Desalination**, **2011**, v.269, pp. 92-103 Autor Correspondente: **Lima, E.C.** doi:10.1016/j.desal.2010.10.047
14. da Silva, L.G., Ruggiero, R., Gontijo, P.M., Pinto, R.B., Royer, B., Lima E.C., Fernandes,T.H.M., Calvete, T., "*Adsorption of Brilliant Red 2BE dye from water solutions by a chemically modified sugarcane bagasse lignin*". **Chemical Engineering Journal, 2011**, v.168, pp. 620-628**.** Autor Correspondente: **Lima, E.C.** doi:10.1016/j.cej.2011.01.040
15. Machado, F.M., Bergmann, C.P., Fernandes, T.H.M., Lima, E.C., Royer, B., Calvete, T., Fagan, S.B., "*Adsorption of Reactive Red M-2BE dye from water solutions by multi-walled carbon nanotubes and activated carbon"*. **Journal of Hazardous Materials**, **2011**, v.192, pp 1122-1131. Autor Correspondente: **Lima, E.C.** doi:10.1016/j.jhazmat.2011.06.020.

16. Alencar, W.S., Lima, E.C., Royer, B., dos Santos, B.D., Calvete, T., da Silva, E.A., Alves, C.N., "*Application of aqai stalks as biosorbents for the removal of the dye Procion Blue MX-R from aqueous solution".* **Separation Science and Technology**, **2012**, v.47, pp.513-526. Autor Correspondente: **Lima, E.C.** doi:10.1080/01496395.2011.616568

17. de Menezes, E.W., Lima, E.C., Royer, B., de Souza, F.E., dos Santos, B.D., Gregório, J.R., Costa, T.M.H., Gushikem, Y., Benvenutti, E.V. "*Ionic silica based hybrid material containing the pyridinium group used as adsorbent for textile dye*", **Journal of Colloid and Interface Science**, **2012**, v.378, pp.10-20. Autor Correspondente: **Lima, E.C.** Doi:10.1016/j.jcis.2012.04.021

18. Machado, F.M., Bergmann, C.P., Lima, E.C., Royer, B., de Souza, F.E., Jauris, I.M., Calvete, T., Fagan, S.B. "*Adsorption of Reactive Blue 4 dye from water solutions by carbon nanotubes: experiment and theory*", **Physical Chemistry Chemical Physics**, **2012**, v.14 pp.11139-11153. Autor Correspondente: **Fagan, S.B**. DOI:10.1039/C2CP41475A

19. Alencar, W.S., Acayanka, E., Lima, E.C., Royer, B., dos Santos, F.E., Lameira, J., Alves, C.N., "*Application of Mangifera indica (mango) seeds as a biosorbent for removal of Victazol Orange 3R dye from aqueous solution and study of the biosorption mechanism"*, **Chemical Engineering Journal**, aceito para publicação. Autor Correspondente: **Lima, E.C.** DOI: 10.1016/j.cej.2012.08.053

20. Cardoso, N.F., Lima, E.C., Royer, B., Bach, M.V., Dotto, G.L., Pinto, L.A.A., Calvete, T.," *Comparison of Spirulina platensis microalgae and commercial activated carbon as adsorbents for the removal of Reactive Red 120 dye from aqueous effluents*", Journal of Hazardous Materials, **2012**, **aceito para publicação**. Autor Correspondente: **Lima, E.C.** DOI: 10.1016/j.jhazmat.2012.09.026

LISTA DE FIGURAS

LISTA DE TABELAS

LISTA DE ABREVIATURAS

Na-mag: magadeíta básica

Na-ken: keniaíta básica

Na-RUB-18: octossilicato RUB-18 básica ou octossilicato lamelar hidratado

H-mag: magadeíta ácida

H-ken: keniaíta ácida

2N-ken: H-ken organofuncionalizada com N-3-trimetóxissililpropiletilenodiamina

CTA-RUB-18: RUB-18 intercalado com Brometo de cetiltrimetilamônio

C-RUB-U: CTA-RUB-18 organofuncionalizado com 3-trimetóxissililpropiluréia

AM: corante básico Azul de Metileno

LR16: corante Laranja Reativo 16

PR5: corante Preto Reativo 5

FTIR: Espectroscopia vibracional na região do infravermelho com transformada de Fourier

SEM: Microscopia Eletrônica de varredura

CHN: Análise Elementar de Carbono, Hidrogênio e Nitrogênio

BET: Método de Brunauer, Emmet e Teller para determinação de áreas supeficiais

BJH: Método de Barret, Joyner e Halenda para determinação de tamanho de poros

NMR de ^{29}Si e ^{13}C com CP-MAS: ressonância magnética nuclear no estado sólido com polarização cruzada e rotação do ângulo mágico

TGA: termogravimetria

ÍNDICE

RESUMO

Este trabalho descreve a preparação, caracterização e aplicação de novos materiais híbridos inorgânico/orgânicos, obtidos a partir de processos de organofuncionalização da superfície lamelar de derivados de keniaíta, magadeíta e RUB-18. Os produtos obtidos foram tratados com agentes sililantes por diferentes métodos. Os materiais foram caracterizados por Espectroscopia vibracional da região do infravermelho com transformada de Fourier (FTIR) quanto à presença de grupos funcionais característicos. Os difratogramas de raio-X mostraram a cristalinidade e a microscopia eletrônica de varredura (SEM) forneceu pelas micrografias, a morfologia estrutural dos silicatos. As áreas superficiais específicas e a porosidade dos adsorventes foram obtidas através de cálculos de área e de volume de poros utilizando os métodos de BET e BJH. Espectros de ressonância magnética nuclear (RMN) de ^{29}Si e ^{13}C no estado sólido mostraram o sucesso das sínteses. Os resultados de análise elementar determinaram as quantidades de grupos orgânicos imobilizados na superfície e por termogravimetria (TGA) os resultados das temperaturas em que os materiais apresentaram estabilidade térmica. Efeitos da dosagem de adsorvente e do efeito de acidez pela variação de pH das soluções foram estudados para os diferentes materiais para otimizar as melhores condições de trabalho nos estudos de adsorção.

As isotermas de adsorção foram obtidas por processos em batelada e os dados experimentais ajustados aos modelos de Langmuir, Freundlich, Sips e Redlich-Peterson, considerando superfícies heterogêneas. Pelo estudo cinético foi possível obter informações valiosas a respeito de um possível mecanismo de adsorção por interação eletrostática, no qual foram testados os modelos de ordem fracionária de Avrami, pseudo- primeira ordem, pseudo-segunda ordem e quimiossorção de Elovich. Os resultados obtidos mostraram a viabilidade da aplicação destes silicatos lamelares modificados como eficientes adsorventes para remoção de corantes têxteis de efluentes aquosos contaminados.

ABSTRACT

This thesis describes the preparation, characterization and application of new inorganic/organic hybrid materials, obtained from organo-functionalization of lamellar surface of derivatives of keniaíta, magadeíta and RUB-18 silicates. The products obtained were treated with silylating agents by different methods. The materials were characterized by FTIR for verifying the presence of characteristic functional groups. The X-ray diffraction showed the crystallinity and scanning electron microscopy micrographs provided by the structural morphology of silicates. The specific surface area and porosity of the adsorbent was obtained by calculation of area and pore volume using the BET and BJH methods. Nuclear magnetic resonance spectra ^{29}Si and ^{13}C solid state have shown the success of the synthesis. The results of elemental analysis determined the amounts of organic groups on the surface and immobilized by thermogravimetric analysis (TGA) results of the temperatures at which the materials exhibited thermal stability. Effects of adsorbent dosage and effect of acidity by varying pH of the solutions were studied for different materials to optimize the best working conditions for adsorption.

The adsorption isotherms were obtained by batch process and experimental data used to fit the Langmuir, the Freundlich, the Sips and the Redlich-Peterson isotherm models, considering heterogeneous surfaces. For kinetic models were utilized to obtain valuable information about a possible mechanism of adsorption in which the tested models were Avrami fractional order, pseudo-first order, pseudo-second order and chemisorption of Elovich. The results showed the feasibility of applying these lamellar silicates modified as efficient adsorbents for the removal of textile dyes from contaminated aqueous effluents.

1 INTRODUÇÃO

As atividades industriais são responsáveis por gerar grande volume de espécies nocivas em efluentes de águas residuais. Entre essas espécies, os corantes representam uma classe de compostos indesejáveis que inevitavelmente exigem um tratamento especial, pelo fato de que a simples presença desses compostos na água reduz a penetração de luz, impedindo fotossíntese da flora aquosa. Além disso, outras características associadas com muitos corantes são aquelas que afetam seres humanos por serem extremamente tóxicos, carcinogênicos e até mesmo mutagênicos.

Uma das formas de controlar contaminações de efluentes por corantes provenientes da indústria têxtil é utilizar processos que removam ao máximo essas espécies tóxicas do ambiente aquífero. Vários métodos têm sido desenvolvidos para remoção de corante sintético de águas e efluentes, a fim de diminuir seu impacto sobre o meio ambiente.

O procedimento mais barato e eficiente para tais processos está relacionada com a adsorção, onde as espécies de corante são transferidas do efluente para uma fase sólida. Posteriormente, o adsorvente pode ser regenerado ou ainda mantido em local seco sem contato direto com o meio ambiente.

De uma série de materiais naturais e sintéticos, silicatos lamelares, e sílicas organofuncionalizadas têm despertado enorme interesse, devido à sua boa capacidade de adsorção, e boa capacidade de troca iônica, intercalações e possibilidade de participar de reações de organofuncionalização. Todas estas propriedades inferem o uso destes valiosos materiais para aplicações como adsorventes, trocadores iônicos, catalisadores e peneiras moleculares.

Os silicatos lamelares hidratados, pertencentes ao grupo dos polissilicatos, são formados pelos materiais keniaíta, makatita, kanemita, octossilicatos e magadeíta e compreendem uma classe definida de compostos com diferentes arranjos cristalinos em lamelas. Toda a pureza destes materiais se dá pelo sucesso de sínteses em laboratórios, por tratamentos hidrotermais, através de condições controladas de tempo, temperatura, pressão, estequiometria e a razão de reagente, para a obtenção destes compostos, principalmente na forma sódica, que é o procedimento operacional preferido. Com exceção dos octossilicatos, todos

outros polissilicatos são encontrados naturalmente. Apesar da grande importância desta classe de compostos formados por lamelas, a estrutura correta de alguns deles ainda é desconhecida. Alguns estudos consideram que a estrutura desses compostos seja constituída por lamelas tetraédricas regulares de SiO_4, com átomos de oxigênio terminal os quais podem ser neutralizados por íons sódio.

Da mesma forma, para alterar a superfície das sílicas, um grande número de grupos silanol estarão disponíveis, com ligação de hidrogênio para um grande número de compostos orgânicos polares de bases para facilitar o processo de adsorção ou favorecer tanto interações como também, reações de intercalação.

A presente investigação trata da utilização de três diferentes silicatos lamelares sódicos cristalinos: magadeíta (Na-mag), keniaíta (Na-ken) e o octossilicato ou ilerita RUB-18 (Na-RUB-18), bem como as conversão na forma ácida (H-mag e H-ken), além de outros novos materiais organofuncionalizados 2N-ken, CTA-RUB-18 e C-RUB-U.

Estes materiais apresentam alta área superficial, alta estabilidade térmica e mecânica, resistência a solventes e ácidos e por apresentarem grande capacidade de interagir com os corantes. Por essa última habilidade, os silicatos lamelares e os novos materiais híbridos obtidos por reações de organofuncionalização foram testados como adsorventes alternativos para remoção dos corantes têxteis Azul de metileno (AM), Laranja Reativo 16 (LR16) e Preto Reativo 5 (PR5) de soluções aquosas, através do processo de adsorção em batelada.

2 REVISÃO BIBLIOGRÁFICA

2.1 Silicatos

Os silicatos são a principal classe de minerais em toda crosta terrestre, representando 25% dos minerais conhecidos. São compostos formados por unidades estruturais extremamente estáveis contendo tetraedros, representados por SiO_4, que, dependendo do tipo de polimerização envolvido, pode formar diferentes grupos de compostos [1].

A estrutura dos silicatos pode consistir em tetraedros independentes, cadeias simples, cadeias duplas, lamelas ou armações tridimensionais [2]. Assim conforme o

arranjo cristalino, os silicatos podem ser agrupados em classes, conforme mostra a Tabela 1 e Figura 1.

Tabela 1 - *Classificação dos silicatos conforme arranjo cristalino dos grupos tetraédricos* SiO_4 [1] .

Classe	**Arranjo cristalino dos tetraedros** sio_4
Nesossilicatos	Tetraedros isolados de $(SiO_4)^{4-}$
Sorossilicatos	Pares de tetraedros de $(SiO_4)^{4-}$
Ciclossilicatos	Anéis de tetraedros de $(SiO_4)^{4-}$
Inossilicatos	Cadeias simples ou duplas de tetraedros de $(SiO_4)^{4-}$
Tectossilicatos	Arranjos tridimensionais de tetraedros de $(SiO_4)^{4-}$ com os 4 O^{2-} ligados a outros tetraedros
Filossilicatos	Lamelas de tetraedros de $(SiO_4)^{4-}$

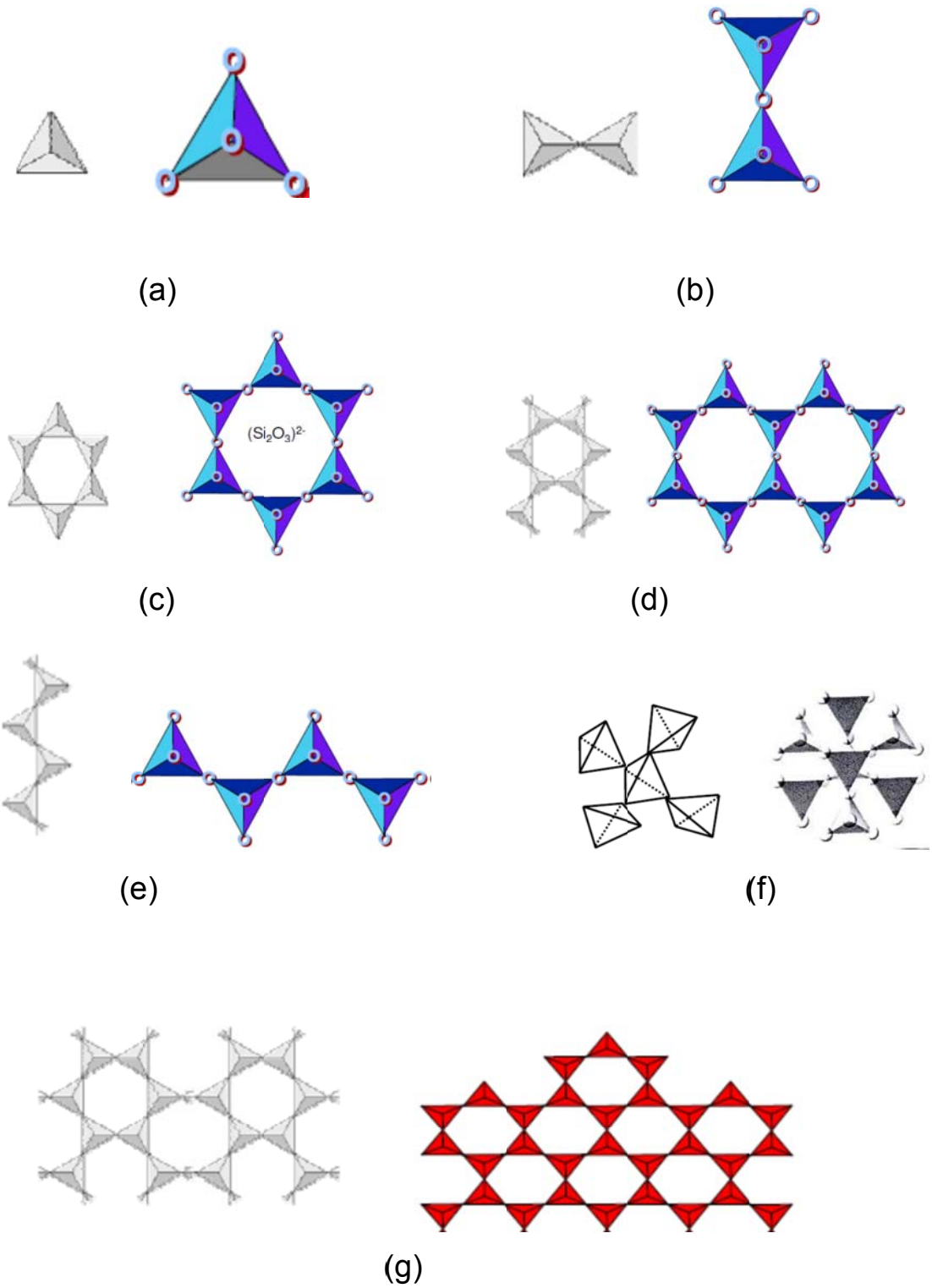

Figura 1 – Tipos de silicatos: (a) nesossilicato; (b) sorossilicato; (c) ciclossilicato; (d) inossilicato de cadeia dupla; (e) inossilicato de cadeia simples; (f) tectossilicato; (g) filossilicato.

Os nesossilicatos são formados por grupos independentes de tetraedros de SiO_4^{4-}. As cargas negativas dos tetraedros são neutralizadas por cátions. Exemplos dessa classe são as olivinas, $(Mg,Fe)_2SiO_4$, as granadas, $(Ca,Mg,Fe,Mn)_3(Al,Fe,Cr)_2(SiO_4)_3$ e as pedras preciosas topázio e zirconita [3-7].

Os sorossilicatos [3-7] são formados quando dois tetraedros SiO_4^{4-} estão interligados, compartilhando um átomo de oxigênio gerando o íon $(Si_2O_7)^{6-}$. Estes minerais aparecem como epídoto, $Ca_5(Al,Fe)Al_2O(SiO_4)(SiO_7)(OH)$, thortveítita, $Sc_2Si_2O_7$ e hemimorfita, $Zn_4(OH)_2Si_2O_7H_2O$.

Os ciclossilicatos são formados quando tetraedros de SiO_4^{4-} se polimerizam gerando uma estrutura com forma de anéis. Alguns exemplos são a turmalina, $Na(Mg,Fe)_3Al_6(BO_3)_3(Si_6O_{18})(OH)_4$ e o berilo[3-7].

Quando várias unidades de SiO_4^{4-} se unem em cadeia infinita, a unidade estrutural é o grupo piroxênio $(SiO_3)^{2-}$ que dá origem aos minerais piroxênios como a augita, $Ca(Mg,Fe,Al)(Al,Si)_2O_6$ e o hiperstênio, $(Mg,Fe)SiO_3$. A ligação de duas cadeias $(SiO_3)^{2-}$ produz uma cadeia dupla, com estrutura unitária $(Si_4O_{11})^{6-}$ gerando os minerais anfibólios como a tremolita $Ca_2Mg_5(Si_4O_{11})_2.(OH)_2$ e a hornblenda, $NaCa_2(Mg,Fe,Al)_5((Si,Al)_8)_{22}(OH)_2$. Esta classe é denominada de inossilicatos[3-7].

O compartilhamento de todos os átomos de oxigênio por silício significa a formação de uma estrutura tridimensional, os tectossilicatos [3-7]. Alguns exemplos são o quartzo e o feldspato como os mais comuns e mais abundantes dessa classe.

E por fim, o compartilhamento de três átomos de oxigênio dos vértices por átomos de silício, resulta em estruturas lamelares, os filossilicatos, cuja unidade é $(Si_2O_5)^{2-}$. As argilas (vermiculita, montmorilonita e caulinita) e as micas (biotita, $K(Al,Fe)_3(AlSi_3O_{10})(OH)_2$ e a muscovita, $KAl_3(AlSi_3O_{10})(OH)_2$) são exemplos dessa classe [3-7].

2.2 Filossilicatos

As espécies de filossilicatos (do grego *phyllos*) são, atualmente, uma das que mais despertam interesses de pesquisadores da área de materiais lamelares[1]. Os filossilicatos constituem um grupo de minerais, com grande importância para a geologia, pedologia e para a indústria.

A estrutura cristalina dos filossilicatos apresenta camadas constituídas por tetraedros de silício ou alumínio (minerais argilosos, que são os aluminossilicatos) e

oxigênio (SiO_4) ou $(AlO_4)^-$, e camadas formadas por octaedros de alumínio, magnésio ou ferro, oxigênio e hidroxilas[1,8].

Cada uma dessas camadas pode se unir à outra, formando uma estrutura do tipo 1:1 ou T-O (tetraédrica-octaédrica). Quando se tem uma segunda folha tetraédrica ligada ao octaedro forma-se uma estrutura 2:1 ou T-O-T (tetraédrica-octaédrica-tetraédrica). Cada uma destas folhas complexas T-O ou T-O-T podem se ligar a outra folha idêntica formando a estrutura lamelar, através de interações de van der Waals[1,8]. Na Figura 2, estão representadas as estruturas dos filossilicatos dos tipos 1:1 e 2:1, que ocorrem nas argilas caulinita e pirofilita[3,7,8], respectivamente.

(a) (b)

Figura 2 - Estruturas de filossilicatos do tipo 1:1 (a) e 2:1 (b). Os o representam grupos hidroxilas (OH) ou oxigênio, ● cátions octaédricos e • cátions tetraédricos.

Portanto os filossilicatos, também chamados de silicatos lamelares, serão um pouco mais explorados, uma vez que é o objeto de estudo deste trabalho.

2.3 Definições e características dos sólidos lamelares

Os materiais com estrutura lamelar são sólidos bidimensionais que possuem átomos firmemente ligados entre si em duas direções do espaço formando lamelas (planos) e fracamente ligados na direção perpendicular a estas lamelas. A região de interação fraca entre as lamelas é conhecida como região interlamelar. Quando as lamelas são eletricamente neutras, as camadas estão em contato através de interações de van der Waals [9-11].

Está associada a estas matrizes inorgânicas uma alta estabilidade térmica, bem como uma relativa resistência química à oxidação e alta seletividade a certos íons e moléculas[12].

Nos sólidos lamelares a região interlamelar (d_f) é definida como a distância entre duas camadas adjacentes de silicato enquanto o espaço basal ou a distância interplanar (d_b), é a distância compreendida entre a região interlamelar e a espessura da lamela[13], como pode ser observado na Figura 3.

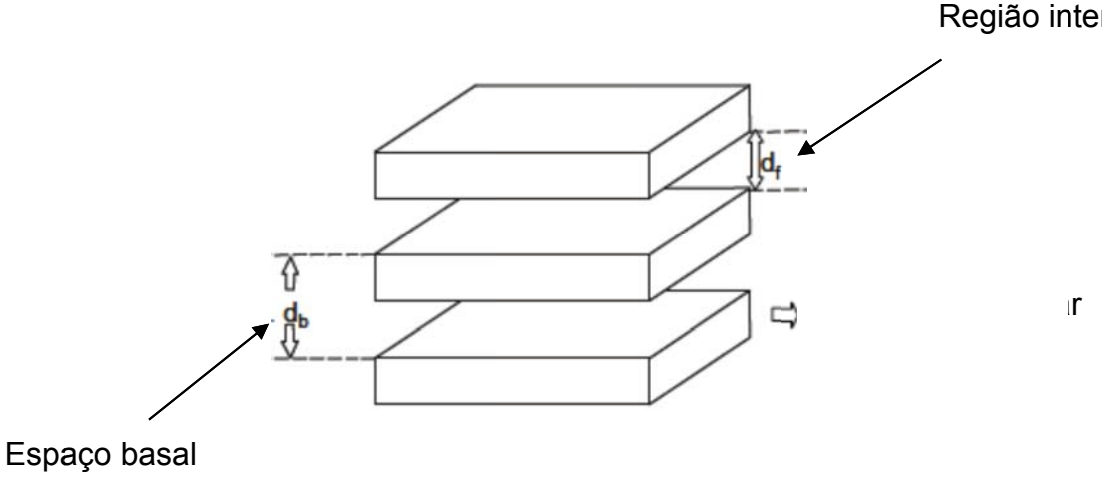

Figura 3 – Representação esquemática de um sólido lamelar.

A densidade superficial dos sítios ativos de uma lamela é geralmente expressa como um número de sítios por área superficial lamelar. Esse valor é uma característica importante do sólido, pois é a quantidade de sítios disponíveis para uma determinada reação[13].

Cada sítio ativo pode interagir com uma molécula, assim o recobrimento total dos sítios pode ser obtido somente se a área da molécula for menor que a área livre do sítio ativo da lamela. A disposição dos sítios ativos na superfície da lamela e sua área livre podem ser exatamente determinadas somente quando a estrutura cristalina do sólido lamelar é devidamente conhecida e caracterizada[13].

De acordo com a estrutura dos materiais lamelares são possíveis reações que ocorrem somente nas superfícies externas do material, como na lacuna interlamelar[1] e também no próprio esqueleto inorgânico que formam as camadas de silicato, caracterizando modificações isomórficas nas lamelas[14].

A estrutura cristalina dos sólidos lamelares é formada por efetiva ligação intralamelar, principalmente ligações covalentes (pela rigidez das camadas) e interações fracas do tipo van der Waals, que são as presentes nas regiões interlamelares e favorecem reações de intercalação e organofuncionalização, uma vez que existe grande possibilidade de flexibilidade e da expansão do espaço interlamelar [13].

A superfície das lamelas apresenta cargas que determinam a natureza dos sítios ativos disponíveis para determinadas reações. Por isso é considerada uma característica muito importante, determinando a presença de interações hidrofílicas e hidrofóbicas[15].

A acidez superficial e a porosidade de sólidos ácidos são as propriedades físicas que mais afetam e determinam o comportamento catalítico destes materiais, em função da natureza da lamela. A espessura da lamela também é um fator importante, pois tem relação direta com a rigidez dos constituintes lamelares. Existem algumas reações em que é preciso considerar essa propriedade para que não haja colapso do espaço interlamelar. Por exemplo, algumas reações de funcionalização podem modificar a estrutura lamelar organizada e esfoliar o material, o que pode promover uma desorganização da estrutura[15,16].

Muitos materiais estudados são naturais, porém busca-se sempre a melhoria das condições sintéticas, com objetivo de obter em laboratório materiais semelhantes aos encontrados na natureza, ou mesmo trabalhar com materiais sintéticos que podem trazer vantagens por apresentar baixa ou quase nenhuma contaminação com outros elementos.

2.4 Silicatos lamelares hidratados

Os silicatos lamelares hidratados, formado por um grupo de polissilicatos, cuja utilização vem despertando um grande interesse são uma das classes de materiais lamelares[13,17]. Eles apresentam fórmula geral $Na_2O{\cdot}(4\text{-}22)SiO_2{\cdot}(5\text{-}10)H_2O$ e são formados pelos materiais makatita, kanemita, magadeíta, keniaíta e octossilicato ou ilerita. Podem ser encontrados na natureza em lagos de alta estabilidade ou obtidos em laboratório através de sínteses hidrotérmicas, com exceção dos octossilicatos que são obtidos apenas por síntese[17].

Cada um dos materiais é caracterizado pela variação do espaço basal de 0,9 a 2,0 nm, como mostra a Tabela 2 e pela espessura da camada lamelar [13].

Tabela 2 - *Espaço Basal dos silicatos lamelares hidratados[18].*

Silicato	Espaço Basal (nm)
Makatita	0,90
Kanemita	1,00
Octossilicato ou Ilerita (RUB-18)	1,10
Magadeíta	1,56
Keniaíta	2,00

De todos os silicatos apresentados apenas a estrutura da makatita é conhecida com precisão. Pela composição de sua cela unitária permitiu-se a proposição de um modelo que apresenta uma fita unitária de tetraedros de silício interligados[19], o que permitiu então a suposição de modelos para os silicatos lamelares hidratados magadeíta e keniaíta, os quais apresentam a estrutura cristalina mais complexa e ainda não foram determinadas[18,19]. Essas estruturas propostas são apresentadas na Figura 4.

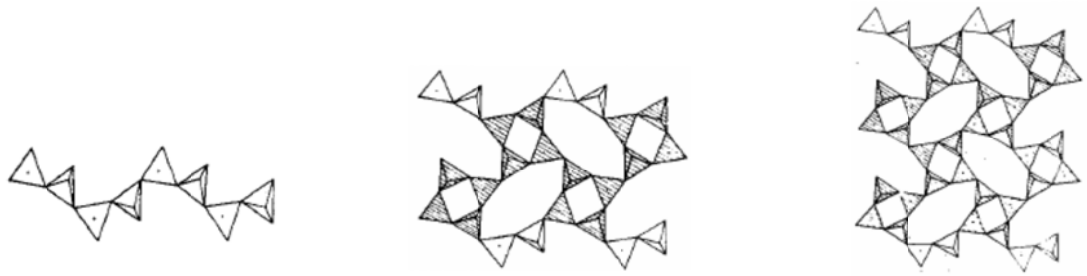

(a) (b) (c)

Figura 4 – Estrutura proposta dos silicatos lamelares makatita (a), magadeíta (b) e keniaíta (c).

Mesmo com inúmeros estudos para compreender a estrutura dos silicatos hidratados as estruturas cristalinas detalhadas dos compostos magadeíta e keniaíta ainda não foram elucidadas até o momento [18,19].

Porém o interesse nesses materiais se dá pela grande possibilidade utilizá-los como matrizes para reações de intercalação de várias espécies químicas na região interlamelar com inúmeras aplicações [20,21].

Essas estruturas possuem diferentes arranjos tetraédricos de silício formando grupos siloxanos e silanóis, carregados negativamente cujas lamelas são separadas por cátions hidratados, que podem se tornar ácidos após reação de troca iônica[17]. Em cada unidade o átomo de oxigênio forma ponte com átomos de silício, sendo que a parte superficial da lamela é coberta por grupos silanóis (SiOH), os quais apresentam acidez de Brönsted superficial[22].

Um maior destaque será dado aos materiais hidratados Na-magadeíta, Na-keniaíta e Na-RUB-18, produto sintético da família de silicatos lamelares, por serem os compostos utilizados neste trabalho. A magadeíta e a keniaíta natural foram descobertas em 1967 no lago Magadi no Kênia[23]. As formulações químicas propostas para esses materiais são $Na_2Si_{14}O_{29}\cdot 9H_2O$ (magadeíta) e $Na_2Si_{22}O_{45}\cdot 10H_2O$ (keniaíta).

O RUB-18, apresenta dados estruturais de alguns derivados que foram sintetizados, como sua forma ácida, H-RUB-18, e a forma intercalada com acetona [24]. A primeira síntese data de 1964, foi feita por Iler [25], e o material passou a ser chamado de octossilicato, de acordo com a sua composição química, que apresenta razão molar SiO_2/Na_2O igual a 8 [25,26]. Porém, esse nome não refletia nenhum aspecto estrutural do material, e então passou a ser conhecido também como ilerita, em homenagem ao autor que o sintetizou. Recentemente, com a determinação exata da estrutura cristalina e algumas mudanças na rota de síntese em 2008 [24], o material passou a ser conhecido como Na-RUB-18, pois foi sintetizado na Ruhr-Universität Bochum, e este nome se tornou a tendência da literatura atual.

Estes materiais apresentam muitas propriedades, tais como: adsorção de moléculas no espaço interlamelar, troca iônica, inchamento (*"swelling"*) e enxertia ("*grafting"*) [27]. Dessa forma um número grande de aplicações desses sólidos lamelares hidratados pode ser observado, por exemplo, como adsorvente de metais e corantes, catalisador, trocador iônico e peneira molecular [28-31].

Neste trabalho, destaca-se a aplicação destes materiais com alta capacidade de troca iônica e de alta habilidade de remoção de contaminantes inorgânicos e orgânicos de águas como adsorventes de baixo custo para remoção de corantes de efluentes contaminados.

2.5 Corantes

Nos últimos 100 anos, mais de 20.000 novos corantes foram sendo sintetizados e como a demanda por corantes é grande e variada [32,33], pesquisadores das grandes empresas fabricantes de corantes são desafiados a produzir compostos com propriedades particulares para os diferentes fins, como por exemplo, para indústrias de couro, papel, cosméticos, plásticos, alimentícia, automotiva, madeireira, vernizes, solventes e tintas, farmacêuticas, de saponáceos e detergentes e principalmente para a indústria têxtil [34].

Somente na indústria têxtil já estão catalogados mais de 8.000 corantes sintéticos [33], diversidade esta justificada pelos diferentes critérios que influenciam na escolha de determinado corante, como por exemplo, natureza da fibra têxtil, características estruturais do corante e da fibra, classificação e disponibilidade do corante para aplicação, propriedades de fixação, custo econômico, dentre outras propriedades [32].

Corantes têxteis são compostos orgânicos cuja finalidade é conferir coloração a um determinado substrato, ou seja, a uma determinada fibra, seja ela sintética ou natural. Os corantes apresentam dois componentes principais na sua estrutura: o grupo cromóforo, responsável pela cor e o grupo funcional que permite a fixação nas fibras dos tecidos [35,36]. A forma da fixação da molécula do corante as fibras geralmente é feita em solução aquosa e pode envolver basicamente quatro tipos de interações: ligações iônicas, ligações de hidrogênio, de van der Walls e ligações covalentes [32].

Os corantes utilizados neste trabalho foram o corante catiônico ou básico, Azul de Metileno (AM) obtido da Sigma (CI 52030, azul básico 9, $C_{16}H_{18}N_3SCl$) para os materiais magadeíta, o corante reativo Laranja Reativo 16 (LR16) obtido da Sigma (Reactive Orange 16, CI 17757, $C_{20}H_{17}N_3O_{10}S_3Na_2$) para materiais keniaíta e o corante Preto Reativo 5 obtido da Sigma (Reactive Black 5, CI 20505, $C_{26}H_{21}N_5O_{19}S_6Na_4$) para o RUB-18.

Os corantes reativos são os que contêm um grupo eletrofílico (reativo) capaz de formar ligação covalente com grupo hidroxila das fibras celulósicas, com grupos amino, hidroxila e tióis das fibras protéicas e também com grupos amino das poliamidas. Existem numerosos tipos de corantes reativos, porém os principais contêm a função azo e antraquinona como grupos cromóforos e os grupos

clorotriazinila e sulfatoetilsulfonila como grupos reativos. Neste tipo de corante, a reação química se processa diretamente através da substituição do grupo nucleofílico pelo grupo hidroxila da celulose [35,37].

Este grupo de corantes apresenta como característica uma alta solubilidade em água e o estabelecimento de uma ligação covalente entre o corante e a fibra, cuja ligação confere maior estabilidade na cor do tecido tingido quando comparado a outros tipos de corantes em que o processo de coloração se opera através de ligações de maior intensidade [36].

Os corantes catiônicos ou básicos são solúveis em água e ligações iônicas (atração eletrostática) são formadas entre o cátion da molécula do corante, e os sítios aniônicos na fibra. São fortemente ligados e não migram facilmente. Produzem cores brilhantes e boa resistência (exceto em fibras naturais), e apresentam uma variedade de cores ilimitada [32].

2.6 Consequências do uso de corantes

Com a extensiva utilização de corantes reativos pelas indústrias têxteis, ocorre a geração de um grande volume de efluentes contaminados durante os processos de tingimento têxtil. Os processos de tinturaria e lavagem são as principais fontes de poluição da água, sendo produzidos de 45 a 65 litros de água por quilograma de tecido processado [38]. Esta contaminação se dá, pelas perdas ocorridas durante os processos de fixação da tintura às fibras e pode ser facilmente detectada a olho nu, sendo visível mesmo em concentrações tão baixas quanto 1 $mg.L^{-1}$.

Por este motivo, uma pequena quantidade de corantes lançada em efluentes aquáticos promove uma alteração na coloração da água, gerando um possível comprometimento do sistema aquático [32]. Este fato tornou-se um dos aspectos mais importantes do ponto de vista ambiental, uma vez que alterações ecológicas e toxicológicas podem ser observadas após a contaminação de efluentes geradas pelo uso de corantes em indústrias têxteis [39-41].

2.7 Tratamentos para remoção da cor de efluentes

O maior problema observado quando se trata de efluentes contaminados por corantes têxteis é com relação à alta estabilidade desses compostos, que são extremamente resistentes à luz e a agentes oxidantes moderados, logo o desenvolvimento de tecnologia adequada para o tratamento de efluentes, tem sido objeto de grande interesse nós últimos anos pela comunidade científica.

Neste trabalho, será abordado o processo de adsorção como tratamento para remoção de corantes de efluentes contaminados.

2.7.1 Processo de Adsorção

De acordo com informações na literatura, adsorção em suspensões sólido-líquido (adsorvente sólido e adsorvato dissolvido em solução líquida) é um dos métodos mais utilizados e eficientes para remoção de poluentes de efluentes aquosos. O processo de adsorção sólido-líquido explora a habilidade que certos sólidos têm de concentrar na sua superfície substâncias específicas presentes em soluções aquosas. Dessa forma, os componentes das soluções aquosas podem ser separados. O material inicial a ser adsorvido é o adsorvato, e o material sólido onde ocorre a adsorção é chamado de adsorvente. Devido às diferentes forças de interações envolvidas no fenômeno de adsorção, este é comumente distinguido em adsorção física (fisiossorção) ou química (quimiossorção) [42]. Adsorção física, ou adsorção de van de Waals, é um fenômeno reversível. A fisiossorção é o resultado de forças intermoleculares de atração relativamente fracas entre as moléculas do sólido e a substância adsorvida. Esta substância adsorvida não penetra dentro da estrutura do cristal do sólido e não se dissolve nele, mas permanece inteiramente sobre a superfície [43, 44].

Adsorção química é o resultado da interação química entre o sólido e a substância adsorvida. O processo pode ser reversível ou irreversível. Na quimiossorção as forças de interação adsorvato-adsorvente são relativamente superiores quando comparadas às forças observadas na adsorção física. Na quimiossorção há a formação de uma ligação química (covalente, iônica) entre a molécula do adsorvato e a superfície do adsorvente. A descoloração do efluente é o resultado de dois mecanismos, a adsorção e a troca iônica (sítios com cargas no

adsorvente) e é influenciada por fatores físico-químicos, tais como a interação entre adsorvato e o adsorvente, área superficial do adsorvente, tamanho de partícula, tamanho de poros do adsorvente, temperatura, acidez da solução do adsorvato (pH) e tempo de contato entre adsorvente e adsorvato [43, 44].

A adsorção tem sido considerada superior a outros processos de descontaminação para reutilização de águas. Em alguns casos, o adsorvente pode ser no final do processo regenerado. Contudo, o primeiro passo para um processo de adsorção eficiente é a escolha de um adsorvente com alta capacidade de adsorção e elevada eficiência para a remoção do adsorvato.

Nos últimos anos, existe uma procura no desenvolvimento de novos materiais capazes de remover poluentes de água contaminada. Dentre muitos adsorventes, neste trabalho serão utilizados os sólidos cristalinos lamelares magadeíta, keniaíta e RUB-18 é um produto da família de silicato em camadas, como matrizes para os processos de adsorção utilizados para remoção dos corantes Azul de Metileno (AM), Laranja Reativo 16 (LR16) e Preto Reativo 5 (RB5) de efluentes sintéticos contaminados.

3 MATERIAIS E MÉTODOS

3.1 Síntese dos materiais

3.1.1 Síntese dos materiais sódicos

Os silicatos sódicos hidratados keniaíta sódica (Na-ken), magadeíta sódica (Na-mag) e Na-RUB-18 foram sintetizados utilizando tratamentos hidrotérmicos em autoclave de teflon [19, 26, 29, 30, 45-47, 48]. A uma suspensão de sílica gel foi adicionado hidróxido de sódio em solução aquosa nas seguintes proporções:

Na-ken → 4 SiO_2 : 2 NaOH : 35 H_2O

Na-mag → 9 SiO_2 : 1 NaOH : 75 H_2O

Na-RUB -18→ SiO_2 : 0,5 NaOH : 7 H_2O

O adsorvente Na-ken foi aquecido a 423K por 7 dias [19, 30, 47], o Na-mag a 420 K por 72h [29, 48] e o Na-RUB-18 a 378K por 9 dias [26, 49]. Os produtos foram lavados com água deionizada até atingir pH 7,0. Foram centrifugados e o Na-ken foi secado

a 333 K por 48h [19, 30, 47], o Na-mag a 320 K por 24h [29,48] e o Na-RUB-18 a 323K por 24h [26, 49].

3.1.2 Síntese dos materiais ácidos de keniaíta e magadeíta

Amostras de Na-ken e de Na-mag foram imersas em ácido clorídrico (0,10 mol.dm^{-3} e 0,20 mol.dm^{-3} respectivamente) com pH próximo a 2,0 e a suspensão foi agitada por 5 dias. Os produtos keniaíta ácida (H-ken) e magadeíta ácida (H-mag), foram filtrados, lavados com água deionizada até atingir pH 7,0 e secos por 333 K por 48 h e 320 K por 24 h, respectivamente [19, 29, 30, 47, 48].

3.1.3 Síntese do CTA-RUB-18

Uma amostra de 2,0 g de Na-RUB-18 foi disperso em 200cm^3 de 0,10 mol. dm^{-3} de uma solução aquosa de brometo de cetiltrimetilamônio (CTAB). A mistura foi agitada durante 3 dias à temperatura ambiente. O procedimento foi repetido 3 vezes até se completar o processo de intercalação, o qual foi acompanhado por difração de raios-X. O sólido obtido (CTA-RUB-18) foi centrifugado, lavado com etanol e seco a 323 K durante 24 h [26, 49].

3.1.4 Reação de organofuncionalização para o H-ken

Uma amostra do material H-ken foi suspenso em 15,0 cm^3 de DMS (dimetilsulfóxido) sob fluxo de N_2 a 298K por 1h.

A seguir adicionou-se o agente silante, 3-N-trimetóxisililpropiletilenodiamina à suspensão, sob agitação de 1h, em atmosfera de N_2 a 363K por 72h [46]. O sólido obtido foi filtrado, lavado com DMS e acetona em um sistema Soxleth para remover o solvente e em seguida seco sob linha de vácuo para produzir o composto organofuncionalizado denominado 2N-ken [27,46].

3.1.5 Reação de organofuncionalização para o CTA-RUB-18

Uma amostra de 2,0 g de CTA-RUB-18 pré-sintetizado foi suspenso em 100cm^3 de tolueno, sob fluxo de nitrogênio a 343K durante 1 h. A seguir, 2,0cm^3 do agente sililante trimethoxisilil propil uréia- (TPU – $(CH_3O)3Si(CH_2)3NHCONH_2$) foi adicionado ao meio reacional e foi mantido por mais 96h. O produto obtido (C-CHF-

U), foi filtrado, lavado com etanol (Synth), e seco sob vácuo a 343K durante 24 h [1, 24, 26].

3.2 Soluções e reagentes

Água deionizada foi utilizada em todos os experimentos, no preparo de todas soluções.

Testes preliminares foram realizados com diferentes corantes para avaliar o desempenho destes no processo de adsorção utilizando os diferentes adsorventes. Foram escolhidos três corantes para o estudo de adsorção, os quais foram os que apresentaram melhores resultados nos testes preliminares.

Os corantes utilizados nos experimentos foram o corante catiônico Azul de Metileno (AM) obtido da Sigma (CI 52030, azul básico 9, $C_{16}H_{18}N_3SCl$, apresentado na Figura 5) para os materiais magadeíta, o corante Laranja Reativo 16 (LR16) obtido da Sigma (Reactive Orange 16, CI 17757, $C_{20}H_{17}N_3O_{10}S_3Na_2$, apresentado na Figura 6) para os materiais keniaíta e o corante Preto Reativo 5 (PR5) obtido da Sigma (Reactive Black 5, CI 20505, $C_{26}H_{21}N_5O_{19}S_6Na_4$, apresentado na Figura 7) para o RUB-18.

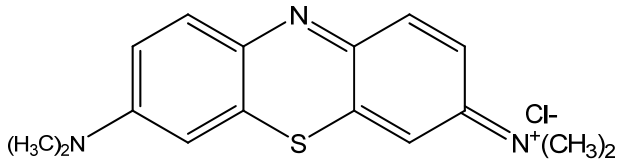

Figura 5 – Representação esquemática da estrutura molecular do corante catiônico Azul de Metileno (AM).

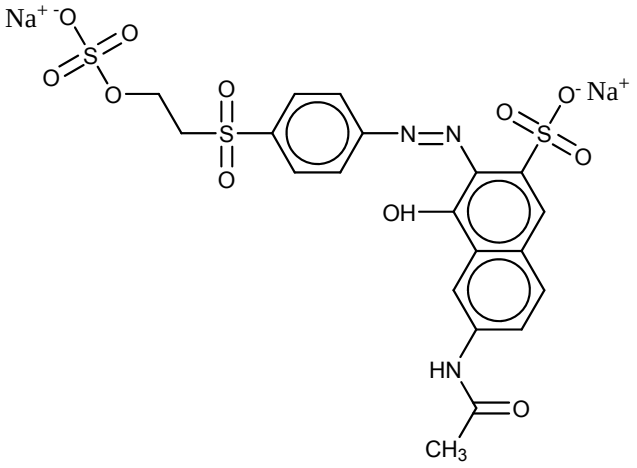

Figura 6 – Representação esquemática da estrutura molecular do corante reativo Laranja Reativo 16 (LR16).

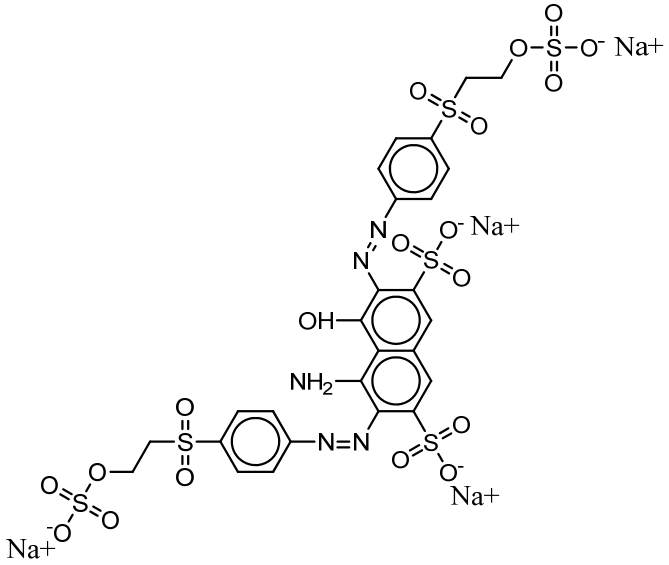

Figura 7 – Representação esquemática da estrutura molecular do corante reativo Preto Reativo 5 (PR5).

As soluções estoque foram preparadas pela dissolução dos respectivos corantes em água deionizada, rigorosamente pesados para obter a concentração de 5000 $mg.dm^{-3}$.

As soluções de trabalho foram obtidas por diluição da solução estoque dos corantes para as concentrações necessárias de trabalho.

Para o ajuste do pH de todas soluções, foram utilizadas soluções de hidróxido de sódio ou ácido clorídrico 0,10 mol.dm^{-3}. O pH das soluções foi medido utilizando um pHmetro Hanna modelo HI 255.

3.3 Técnicas de caracterização

3.3.1 Espectroscopia vibracional na região do infravermelho

Esta técnica é muito importante para a avaliação qualitativa do material, uma vez que a estrutura inorgânica lamelar exibe características que propiciam o acompanhamento vibracional através do aparecimento de bandas típicas. Por exemplo, na região interlamelar ocorre a interação das espécies convidadas com os sítios ativos presentes na superfície do sólido, sendo possível acompanhar por infravermelho esses efeitos que afetam a estrutura original [51].

Quando o composto cristalino lamelar sofre modificação devido à troca iônica, intercalação ou organofuncionalização, a integridade estrutural das lamelas é essencialmente mantida durante o processo e pode-se observar as vibrações características das moléculas orgânicas modificantes no material[28,29].

Os materiais foram caracterizados quanto à presença de grupos funcionais utilizando-se um espectrofotômetro vibracional na região do infravermelho com transformada de Fourier (FTIR), marca Bomem, modelo MB-Series.

A análise por FTIR consistiu em analisar pastilhas contendo as amostras pressionadas com KBr previamente seco e os espectros foram obtidos com uma resolução de 4 cm^{-1} com 32 varreduras acumuladas na região de 4000-400 cm^{-1}.

3.3.2 Isoterma de adsorção e dessorção de gás nitrogênio

As áreas superficiais específicas e a porosidade dos adsorventes magedeíta sódica e ácida e keniaíta sódica e ácida foram determinadas utilizando um analisador de volume de adsorção, ASAP 2010, fornecido pela Micromeritrics, em 77 K (ponto de ebulição do nitrogênio). As amostras foram pré-tratadas em 373 K por 24 h sob atmosfera de nitrogênio, a fim de eliminar umidade adsorvida na superfície das amostras sólidas. Depois disso, as amostras foram submetidas a 298 K sob vácuo. Para os cálculos de área e volume de poros foram utilizados os métodos de BET e BJH.

3.3.3 Análise Elementar

A análise elementar é uma técnica útil que possibilita quantificar os grupos imobilizados nos suportes inorgânicos com o resultado do percentual dos elementos carbono, hidrogênio e nitrogênio, determinando dessa forma o grau de funcionalização dos materiais [28,29,51].

As medidas foram obtidas pelo menos em duplicata e realizadas em um analisador elementar de CHN da Perkin-Elmer, modelo 2400.

3.3.4 Difração de Raio-X

A técnica de difração de raios-X é importante para a caracterização de materiais lamelares, possibilitando determinar as posições relativas dos átomos existentes na rede cristalina de um sólido e assim determinar a cristalinidade, estrutura e distância interplanar dos materiais. É possível também, acompanhar a variação da distância basal quando o material sofre alguma reação, troca iônica, intercalação ou modificação química [51].

Para obtenção dos difratogramas de raios-X dos materiais foi utilizado um difratômetro Shimadzu, modelo XRD 7000, na faixa de 2θ = 1,4 a 50º, com radiação CuKα correspondente a 1,54 Å.

3.3.5 Microscopia eletrônica de varredura

A microscopia eletrônica de varredura (MEV) é utilizada para análises microestruturais de sólidos através de imagens representativas e de fácil interpretação. As micrografias mostram a morfologia dos materiais, a forma das partículas formadas e até uma estimativa do tamanho médio que apresentam [52].

Todos os materiais foram analisados em um microscópio JEOL modelo JSM-6360 LV, para o estudo da morfologia dos materiais, equipado com um acelerador de voltagem de 5 kV a 77K.

3.3.6 Ressonância magnética nuclear de ^{29}Si e ^{13}C

A ressonância magnética nuclear é uma técnica muito utilizada para caracterização de estruturas lamelares, pois indica o ambiente químico para cada tipo de interação de átomos no composto. Assim, é possível verificar a presença de estruturas orgânicas no material e observar o deslocamento dos sinais após a

reação e modificação da superfície lamelar, além de identificar as diferentes vizinhanças dos átomos de silício nas amostras [51].

Os espectros de RMN no estado sólido, com polarização cruzada e rotação do ângulo mágico (CP-MAS), foram obtidos por um espectrômetro de alta resolução Bruker AC300/P, 121 MHz, operando em freqüências de 59,6 até 100,6 MHz com rotações de 10 até 15 KHz, tempo de aquisição de 3,0 a 8,0 ms e tempo de contato de 5 ms para o núcleo de ^{29}Si. Os deslocamentos químicos (ppm) foram referenciados ao tetrametilsilano (TMS).

3.3.7 Termogravimetria

Conforme recomendações da ICTAC (International Confederation for Thermal Analysis and Calorimetry), análise térmica é um grupo de técnicas em que uma propriedade da amostra é monitorada em função do tempo ou temperatura, enquanto a temperatura da amostra, em uma específica atmosfera, é programada. O programa deve envolver aquecimento ou resfriamento em uma taxa fixa de variação de temperatura.

Mais especificamente, pode-se definir a termogravimetria (TGA) como uma técnica em que a massa da amostra é monitorada em função do tempo ou temperatura, enquanto é programada a temperatura da amostra, numa específica atmosfera[48] .

As curvas termogravimétricas foram obtidas em termobalança da TA instruments 5100, modelo TGA 2050, com razão de aquecimento de 0,17 $K.s^{-1}$, sob fluxo de 30 $cm^3.s^{-1}$ de nitrogênio, variando na faixa de temperatura ambiente até 1223 K, com massa de aproximadamente 10 mg do sólido.

3.4 Experimentos de adsorção

3.4.1 Experimentos de adsorção em batelada

Os estudos de adsorção para avaliar as formas dos adsorventes magedeíta e keniaíta sódicos (Na-mag e Na-ken) e ácidos (H-mag e H-ken), para remoção dos corantes AM (Azul de Metileno) e LR16 (Laranja Reativo 16) em soluções aquosas, foram realizados em triplicata, utilizando o processo adsorção em batelada.

Para estes experimentos, massas fixas dos adsorventes variando de 20,0 a 200,0 mg foram suspensas em uma série de 20 cm^3 de soluções dos corantes com concentrações que variavam de 2,00 a 1.000,0 $mg.dm^{-3}$ utilizando Erlenmeyers com volume de 50 cm^3. O contato entre os adsorventes e adsorvatos foi realizado em um agitador horizontal, TECNAL, com tempo de agitação que variando entre 5 a 360 minutos, com 150 rotações por minutos (rpm). As temperaturas foram fixadas, colocando esse agitador numa câmera climatizada fornecida pela Oxylab [51-54].

Os estudos de equilíbrio foram realizados sob condições otimizadas de 210 min a 298 ± 1K, com pH inicial das soluções dos corantes que variou de 2,0 a 10,0. Posteriormente, a fim de separar os adsorventes das soluções aquosas, os frascos foram centrifugados a 3600 rpm por 10 minutos e as alíquotas de 1,0 a 10,0 cm^3 do sobrenadante foram devidamente diluídas. As concentrações finais dos corantes que permaneceram na solução foram determinadas por espectrofotometria visível, utilizando um espectrofotômetro Femto 600S provido de cubetas de vidro óptico com caminho óptico de 1,0 cm [52-54].

Foram feitas medições de absorbância no comprimento de onda máximo do AM (Azul de Metileno) em λ = 660 nm, do LR16 (Laranja Reativo 16) em λ = 493 nm e do PR5 (Preto Reativo 5) em λ = 590 nm. O limite de detecção determinado de acordo com a IUPAC [55] foi de 0,09 $mg.dm^{-3}$ para o AM, de 0,15 $mg.dm^{-3}$ para o LR16 e de foi de 0,14mg. dm^{-3} para o PR5.

A quantidade dos corantes adsorvido e a porcentagem de remoção dos corantes pelos adsorventes foram calculadas mediante a aplicação das Equações (1) e (2), respectivamente:

$$q = \frac{(C_o - C_f)}{m}.V \qquad \textbf{(1)}$$

$$\%\text{Remoção} = 100.\frac{(C_o - C_f)}{C_o} \qquad \textbf{(2)}$$

onde q é a quantidade do corante adsorvido ($mg.g^{-1}$); C_o é a concentração inicial do corante colocado em contato com os adsorventes ($mg.dm^{-3}$), C_f é a concentração

dos corantes ($mg.dm^{-3}$) após o processo de adsorção, V é o volume de solução dos corantes (dm^3) colocado em contato com os adsorventes e m é a massa (g) dos adsorventes.

3.4.2 Modelos cinéticos de adsorção

O estudo cinético de adsorção é importante no tratamento de efluentes aquosos porque ele fornece informações valiosas a respeito do mecanismo de adsorção [56].

Vários modelos foram desenvolvidos para encontrar as constantes intrínsecas das taxas cinéticas de adsorção. Tradicionalmente, as cinéticas de adsorção dos adsorvatos são descritas pelas expressões originalmente desenvolvidas por Lagergren [57]. Uma cinética de adsorção simples é a equação de pseudo-primeira ordem, dada abaixo:

$$\frac{dq}{dt} = k_f.(q_e - q_t) \qquad \textbf{(3)}$$

Na qual q_t é a quantidade de adsorvato sorvida em qualquer tempo t ($mg\ g^{-1}$), q_e é a quantidade adsorvida no equilíbrio ($mg\ g^{-1}$), k_f é a constante da taxa de pseudo-primeira ordem (min^{-1}), e t é o tempo de contato (min) entre o adsorvente e o adsorvato. A integração da equação (3) nas condições de contorno, $q_t = 0$ em t= 0, e qt= qt em t=t origina:

$$Ln\ (q_e - q_t) = Ln(q_e) - k_f.t \qquad \textbf{(4)}$$

Após rearranjar essa equação numa forma não linear, a equação cinética de pseudo-primeira ordem [57] torna-se:

$$q_t = q_e.[1 - exp(-k_f.t)] \qquad \textbf{(5)}$$

A cinética de adsorção de pseudo-segunda ordem [58] baseia-se em:

$$\frac{dq_t}{dt} = k_s.(q_e-q_t)^2 \quad \textbf{(6)}$$

Na qual, k_s é a constante da taxa de pseudo-segunda ordem (g mg^{-1} min^{-1}). A integração da equação (6) com as condições de contorno, $q_t = 0$ em t = 0, e qt = qt em t = t dá origem a:

$$q_t = \frac{k_s.q_e^2.t}{1+q_e.k_s.t} \quad \textbf{(7)}$$

A taxa inicia de adsorção (h_o, expressa em mg g^{-1} min^{-1}) pode ser obtida quando t aproxima-se a zero.

$$h_o = k_s.q_e^2 \quad \textbf{(8)}$$

A equação de Elovich é aplicada para cinética de quimissorção [59]. Essa equação tem sido aplicada satisfatoriamente em alguns processos de quimissorção e tem sido aplicada com sucesso em processos de cinética de adsorção lenta [60]. A equação cinética é válida para sistemas nos quais a superfície do adsorvente é heterogênea e é formulada como:

$$\frac{dq_t}{dt} = \alpha.\exp(-\beta q_t) \quad \textbf{(9)}$$

Integrando essa equação nas condições de contorno, qt = 0 em t =0 e qt = qt para t = t, origina-se:

$$q_t = \frac{1}{\beta}\text{Ln}\,(t + t_o) - \frac{1}{\beta}\text{Ln}(t_o) \quad \textbf{(10)}$$

Na qual α é a taxa inicial de adsorção (mg g^{-1} min^{-1}) e β é uma constante relacionada ao grau de cobertura e a energia de ativação envolvida no processo de quimissorção (g mg^{-1}) e $t_o = 1/\alpha\beta$.

Se t for muito maior que to, a equação cinética pode ser simplificada como:

$$qt = \frac{1}{\beta} Ln(\alpha.\beta) + \frac{1}{\beta} Ln(t) \quad \textbf{(11)}$$

Apesar dos modelos cinéticos de pseudo-primeira ordem e pseudo-segunda ordem serem os modelos cinéticos de adsorção mais comumente empregados nos trabalhos de cinética de adsorção, a determinação de alguns parâmetros cinéticos tais como, as possíveis mudanças das taxas de adsorção em função da concentração inicial do adsorvato e do tempo de contato entre adsorvente e adsorvato, como também a determinação de modelos cinéticos de ordem fracionária ainda precisam ser melhores explorados na literatura. Dessa forma, uma equação cinética alternativa de ordem fracionária foi proposta, na qual se fez uma adaptação à função exponencial de Avrami, utilizada para estudar cinética de decomposição térmica [56]

$$\alpha = 1- \exp[-(k_{AV}.t)]^n \quad \textbf{(12)}$$

Na qual α é a fração de adsorção (q_t/q_e) no tempo t, e k_{AV} é a constante cinética de Avrami (min^{-1}), e n a ordem fracionária do processo de adsorção que está associada as mudanças de ordem de adsorção de acordo com o tempo de contato entre o adsorvente e o adsorvato [59]

Inserindo-se α na equação 12, a equação cinética de adsorção de Avrami pode ser descrita como:

$$q_t= q_e.\{1- \exp[-(k_{AV}.t)]^n\} \quad \textbf{(13)}$$

A possibilidade da resistência da difusão intra-partícula afetar a cinética do processo de adsorção é geralmente avaliado pelo modelo de difusão intra-partícula [61]:

$$q_t = k_{id}.\sqrt{t} + C \quad \textbf{(14)}$$

Na qual k_{id} é a taxa de difusão intra-partícula (mg g^{-1} $min^{-0.5}$), e C é a constante relacionada com a espessura da camada de difusão (mg g^{-1}).

Quando se constrói um gráfico de q_t versus $\sqrt{t}$ espera-se um comportamento linear. Entretanto, às vezes o processo é regido por múltiplas etapas e taxas de adsorção, originando múltiplas retas.

3.4.3 Isotermas de adsorção

As isotermas de adsorção são requisitos básicos para o planejamento de qualquer sistema de adsorção. As isotermas expressam a relação existente entre a quantidade de adsorvato removido da fase aquosa e a quantidade de adsorvato remanescente na solução a uma temperatura constante [62].

A descrição matemática precisa da capacidade de adsorção no equilíbrio é indispensável para previsões fidedignas de parâmetros e comparações quantitativas do comportamento de adsorção para diferentes sistemas. Esses parâmetros de isotermas frequentemente podem fornecer informações sobre mecanismos de adsorção, propriedades da superfície e afinidades do adsorvente [62].

O modelo de isoterma de Langmuir é baseado nas seguintes pressupostos [63]:

- Os adsorvatos são quimicamente adsorvidos em um número fixo bem definido de sítios;
- um sítio ativo somente interage com uma espécie de adsorvato;
- todos os sítios são energeticamente equivalentes;
- não ocorrem interações entre as espécies de adsorvatos.

A isoterma de Langmuir é dada pela equação:

$$q_e = \frac{Q_{max}.K_L.C_e}{1 + K_L.C_e} \qquad \textbf{(15)}$$

Na qual, C_e (mg dm^{-3}) é a concentração do sobrenadante após o sistema ter entrado em equilíbrio, K_L é a constante de equilíbrio do processo de adsorção (dm^3 mg^{-1}) e Q_{max} é a capacidade máxima de adsorção do adsorvente (mg g^{-1}) assumindo a formação de uma monocamada de adsorvato sobre o adsorvente.

O modelo de isoterma de Freundlich[64] assume que a concentração do adsorvato na superfície do adsorvente aumenta infinitamente com a concentração do adsorvato. Teoricamente, esse comportamento é amplamente aplicado a sistemas heterogêneos.

Esse modelo segue um comportamento exponencial dado pela equação:

$$q_e = K_F.C_e^{1/n_F} \quad \textbf{(16)}$$

Na qual K_F é a constante relacionada com a capacidade de adsorção [mg g^{-1}(mg dm^{-3})$^{-1/n}$] e n_F é o expoente de Freundlich (adimensional).

Outro modelo de isotermas de adsorção é o modelo empírico Sips 6[5], que é uma combinação matemática dos modelos de isotermas de Langmuir e Freundlich. O modelo de Sips segue a equação:

$$q_e = \frac{Q_{max}.K_S.C_e^{1/n_S}}{1+K_S.C_e^{1/n_S}} \quad \textbf{(17)}$$

Na qual K_S é a constante de equilíbrio de adsorção de Sips (mg dm^{-3})$^{-1/n_S}$ e Q_{max} é a capacidade máxima de adsorção (mg g^{-1}), e n_S é o expoente de Sips (adimensional). Em baixas concentrações de adsorvato esse modelo assume a forma de Freundlich, enquanto que em altas concentrações assume a forma de adsorção de Langmuir em monocamadas.

O modelo de isoterma de Redlich-Peterson [66] é estabelecido pela equação empírica:

$$q_e = \frac{K_{RP}.C_e}{1+a_{RP}.C_e^{g}} \quad \text{na qual} \quad 0 < g \leq 1 \quad \textbf{(18)}$$

Na qual, K_{RP} e a_{RP} são as constantes de Redlich-Peterson, dadas em (dm^3 g^{-1}) e (mg dm^{-3})$^{-g}$, respectivamente, e g é um número adimensional denominado por expoente de Redlich-Peterson, cujo valor deve ser entre zero e um. Essa equação é reduzida para uma forma linear de isoterma, caso ocorra baixa área de cobertura (g = 0), ou à isoterma de Langmuir com g = 1.

4 CONCLUSÕES

Os silicatos cristalinos lamelares, magadeíta sódica e ácida (Na-mag e H-mag), keniaíta sódica e ácida (Na-ken e H-ken) e o octossilicato sintético Na-RUB-18 representaram uma boa alternativa como adsorventes para remoção dos corantes Azul de Metileno (AM), Laranja Reativo 16 (LR16) e Preto Reativo 5 (PR5), respectivamente.

Além disso, observou-se a eficiência do enxerto de moléculas orgânicas nas lamelas livres do H-ken transformando-se em 2N-ken e do Na-RUB-18 em CTA-RUB-18 e C-RUB-U. O sucesso é devido primeiramente a expansão do espaço basal pela inserção dos agentes sililantes no processo de interação eletrostática.

Todas as matrizes inorgânicas apresentaram capacidade de intercalar os corantes nas lamelas livres da matriz na superfície sólido/líquido quando as amostras estavam em soluções aquosas, considerando sempre a otimização de cada processo com relação ao ajuste de pH, tempo de agitação, dosagem do adsorvente e tempo necessário para saturar os centros disponíveis localizados na superfície do trocador iônico.

Pelos resultados texturiais dos adsorventes de área superficial específica pelo método BET e porosidade pelo método BJH, pode-se confirmar que os adsorventes H-ken e Na-ken, H-mag e Na-mag, apresentam características de materiais cristalinos lamelares com predominância de mesoporos (do tipo H3 pelo método BJH) o que explica a cinética de adsorção ser lenta para todos adsorventes.

Os resultados obtidos de cristalinidade por difração de raio-X e morfologia por microscopia eletrônica de varredura, possibilitaram determinar parâmetros estruturais importantes, como a distância basal e a presença de grupos na superfície, respectivamente, para todos os adsorventes caracterizados neste trabalho. Para os compostos organomodificados, adiciona-se ainda a análise elementar, que permitiu determinar o grau de imobilização obtido.

Quatro modelos cinéticos foram utilizados para ajustar os dados experimentais, ordem fracionária de Avrami, pseudo-primeira ordem, pseudo-segunda ordem e quimissorção de Elovich. Dos resultados de aplicação dos modelos, obteve-se que para o adsorvente keniaíta os melhores ajustes foram obtidos pelos modelos de ordem fracionária de Avrami e de quimiossorção. Para o adsorvente magadeíta, o melhor ajuste foi o do modelo cinético de ordem fracionária

de Avrami, bem como para o adsorvente RUB-18. Isso possibilitou a aplicação do modelo de difusão intrapartícula que permite avaliar a resistência de transferência de massa por difusão pelas partículas do corante nos poros dos adsorventes sugerindo que o mecanismo pode seguir taxas múltiplas de adsorção.

Os dados de adsorção do corante LR16 no adsorvente keniaíta foram ajustados ao modelo de isoterma de Sips, obtendo-se uma capacidade máxima de adsorção de 70,7 $mg.g^{-1}$. Com base nestes resultados supõe-se que o corante têxtil usa mais de um centro da molécula da base diamina que foi enxertada na superfície quando estas interagem com os nitrogênios básicos disponíveis. Isso é esperado, uma vez que o corante possui um grupo sulfonato e um grupo sulfona na superfície, os quais tem cargas negativas capazes de interagir com os grupos diamina com cargas positivas do material organomodificado.

Para o adsorvente magadeíta, os dados de adsorção do corante Azul de Metileno foram ajustados a todos os modelos de isotermas, com exceção ao modelo de Freundlich, onde os valores de q_e foram coincidentes para os modelos de Langmuir, Sips e Redlich-Peterson. As capacidades máximas de adsorção foram 331 e 173 $mg.g^{-1}$ para magadeíta sódica e ácida, respectivamente. Devido a quantidade adsorvida para o adsorvente na forma sódica ser superior ao da forma ácida, o mecanismo de adsorção é facilitado pelo processo de troca iônica com o corante, não só devido à ligação iônica característica do Azul de metileno, mas também por que o processo ocorre com uma expansão favorável do espaço basal entre as lamelas.

Para o adsorvente RUB-18, dos modelos de isoterma de adsorção, obteve-se melhor ajuste dos dados experimentais, ao se aplicar o modelo de isoterma de Sips. A capacidade máxima de adsorção foi de 76.77 $mg.g^{-1}$ (0.0774 $mmol.g^{-1}$). Com base nestes resultados, supõe-se que o corante têxtil utiliza mais de um centro básico da molécula de uréia que interage com os nitrogênios básicos disponíveis na superfície do adsorvente. Isto é esperado, uma vez que o corante tem dois grupos sulfonato e dois grupos sulfato-etil-sulfona, todos com cargas negativas que interagem com os grupos amina do material organomodificado positivo.

Conclui-se então, que esses adsorventes podem ser aplicados para remoção de corantes têxteis de efluentes contaminados, uma vez que os resultados obtidos favoreceram a adsorção dos corantes mesmo em processos com mais de um ou dois estágios, porém com características importantes para a elucidação dos

possíveis mecanismos de adsorção destes silicatos cristalinos lamelares, magadeíta, keniaíta e RUB-18.

5 REFERÊNCIAS BIBLIOGRÁFICAS

1. Fonseca,M.G., Airoldi,C., *Química Nova*, 26, 699, 2003.
2. Greenwood, N.N., Eamshaw,A., *Chemistry of the Elements*, 2ª ed., Butterworth-Heinemann, Oxford, 2002.
3. Santos,P.S., *Tecnologia das Argilas*, Ed. USP / Edgard Blucher Ltda., SP, vol 1, 1975.
4. Visconti,Y.S., *Argilas e Minerais Afins*, INT, Rio de Janeiro, 1951.
5. Lee, J.D. *Química Inorgânica não tão concisa*, Ed. Edgard Blucher, 5ª Ed., 2003.
6. www.ige.unicamp.brsiteaulas30filo-silicatos.pdf (acessado em agosto de 2012)
7. www.cesnors.ufsm.br/professores/vanderlei/geologia/pdf (acessado em agosto de 2012)
8. Soler-Illia,G.J.A.A., Sanchez,C., Lebeer,B., Patarin,J., *Chem.Rev.,* 102,4093,2002.
9. Pinnavaia,T.J., *Acs Adv.Chem.Ser.*, 245, 283, 1995.
10. Eypert-Blaison,C.,Michot,L.J.,Humbert,B.,Pelletier,M.,Villieras,F.,Caillerie,J.B.D.J., *Phys.Chem.B*, 102,730, 2002.
11. Eypert-Blaison,C.,Michot,L.J.,Humbert,B.,Pelletier,M.,Villieras,F.,Caillerie,J.B.D.J., *Phys.Chem.B*, 13,1480, 2001.
12. Van der Voot, P., Vansant, E. F., *J. Liq. Chrom. Rel. Technol.*, 19, 2723, 1996.
13. Pastore,H.O., Munsignatti,M., Mascarenhas,A.J.S., *Clays Clay Miner.,*48, 224, 2000.
14. Flanigen, E. M., Lok, B. M., Patton, R. L., Wilson, S. T., *Pure Appl. Chem.*, 58, 1351,1986.
15. Ilisz, I., Dombi, A., Mogyorósi, K., Dékány,I., *Coll. Surf. A*, 230, 89,2004.
16. Occelli, M.L., Auroux,A., Ray,G.J., *Microporous Mesoporous Mater.,* 39, 43, 2000.
17. Kosuge, K., Singh, P.S., *Chem. Mater.,* 12, 421, 2000.
18. Almond, G.G., Harris, R.K., Franklin, K.R., *J. Mater. Chem.*, 7, 681, 1997.
19. Schwieger, W., Heidemann, D., Bergk, K.H., *Rev. Chim. Miner.*, 22, 639, 1985.
20. Zhang, Z., Saengkerdsub, S., Dai, S., *Chem. Mater.,* 15, 2921, 2003
21. Wang, Z., Pinnavaia, T.J., *J. Mater. Chem.*, 13, 2127, 2003.
22. Watton, S.P., Taylor, C.M., Kloster, G.M., Bowman, S.C., *Progr. Inorg. Chem.*,51, 333, 2003.

23. Thiesen, P.H., Beneke, K., Lagaly, G., *J. Mater. Chem.,* 12, 3010, 2002.

24. Borowski,M., Kovalev,O., Gies,H., *Microporous Mesoporous Mater.*, 107, 71 (2008).

25. Iler, R.K., *J. Colloid Sci.* 19, 648 (1964).

26. Schwieger,W., Lagaly,G., *Handbook of layered materials*, CRC Press, Cap. 11, Alemanha (2004).

27. Kooli, F., Mianhui,L., Alshahateet, S.F., Chen, F., Yinghuai,Z., *J.Phys.Chem. Solids,* 67,926, 2006.

28. Petrucelli, G.C., *"Síntese, caracterização e termoquímica de materiais lamelares nanoestruturados derivados de magadeíta"*, Tese de Doutorado, IQ-UNICAMP,Campinas, 2008.

29. Ruiz, V.S.O., Petrucelli, G.C., Airoldi, C., *J. Mater. Chem.*, 16, 2338 (2006). 30. Royer, B., Cardoso, N.F., Lima, E.C., Ruiz, V.S.O., Macedo, T.R., Airoldi, C., *J. Colloid Interface Sci.*, 336, 398, 2009.

31. Petrucelli, G.C., Meirinho, M.A., Macedo, T.R., Airoldi, C., *Thermochim. Acta,* 450, 16, 2006.

32. Guaratini, C.C.I.; Zanoni, M.V.B.; *Química Nova*, 23, 71-78, 2000.

33. Index Colour (© Society of Dyers and Colourists and American Association of Textile Chemists and Colourists), 2002.

34. Costa, A.M.A., *Química*, 105,31-35, 2007.

35. Asku,Z. , *Process Biochemistry*, 40, 997-1026, 2005.

36. Matyjas, E., Rybicki, E., *Autex Research Journal,* 3, 90-95, 2003.

37. www.abiquim.org.br/corantes/corclassificação.asp, (acessado em agosto de 2012).

38. EPA, Textile Processing Industry, U.S. Environmental Protection Agency, Washington, EPA-625/7-78-002, 1978. Last revised: 2005.

39. Bae, J.S., Freeman, H.S., *Dyes and Pigments*, 73,81-85, 2007.

40. Sponza, D.T.; *Journal of Hazardous Materials*, 138, 438 – 447, 2006.

41. Pavan, F.A., Gushikem, Y., Mazzocato, A.S., Dias, S.L.P., Lima, E.C., *Dyes and Pigments*, 72, 256-266, 2007.

42. Gupta, V., Suhas,I., *Journal Enviromental. Managment,* 90, 2313, 2009.

43. Ruthven,D.M., *Principles of Adsorption and Adsorption Process,* John Wiley & Sons, NY, 1984.

44. Atkins, P.W., De Paula, J., *Físico-Química*, Rio de Janeiro, 8ª Ed. , LTC, 2008.

45. Kosuge, K., Tsunashima, A., *J. Chem. Soc., Chem. Commun.*, 2427, 1995.

46. Leu, C.-M., Wu,Z.-M., Wei,K.-H., *Chem.Mater.,* 14, 3016, 2002.

47. Ogawa, M., *J. Mater. Chem.*, 12, 3304, 2002.

48. Royer, B., Cardoso, N.F., Lima, E.C., Macedo, T.R., Airoldi, C., *Separation Science and Tech.,* 45, 129, 2010.

49. Thiesen,P.H., Beneke,K., Lagaly. G, *J. Mater. Chem.* 12, 3010 (2002).

50. Pavan, F.A., Gushikem, Y., Mazzocato, J., Dias, S.L.P., Lima, E.C., *Dyes and Pigm.,* 72, 256, 2007.

51. Price,P.M., Clark,J.H., D. J. Macquarrie. J., *Dalton Trans.* 101 (2000).

52. Butruille,J.R., Pinnavaia, T.J., Eds. *Comprehensive Supramolecular Chemistry*, vol 7, 1st Ed, Chap. 7, USA (1996).

53. Lima, E.C., Royer, B., Vaghetti,J.C.P., Simon, N.M., da Cunha, B.M., Pavan, F.A., Benvenutti, E. V., Veses, R.C., Airoldi, C., *J.Hazard. Mat.,*155, 536, 2008.

54. Pavan, F.A., Lima, E.C., Dias, S.L.P., Mazzocato, J., *J. Hazard. Mater.,* 150, 703, 2008.

55. Lima, E.C., Krug, F.J., Nóbrega, J.A., Nogueira, A.R.A., *Talanta*, 47, 613, 1998.

56. Lopes, E., Anjos, F., Vieira, E., Cestari, A., *J. Colloid Interface Sci.,* 263, 542, 2003.

57. Largegren, S., *Kungliga Suensk Vetenskapsakademiens Handlingar*, 241, vol.1, 1989.

58. Ho, Y., Mckay, G., *Proc. Biochem*., 34, 451, 1999.

59. Jacques, R., Lima, E.C., Dias, S.L.P., Mazzocato, J., Pavan, F.A., *Sep. Purif. Technol*., 57, 193, 2007.

60. Weber, W., Morris, J., *J. Sanit. Eng. Div. Am. Soc. Civil Eng.*, 89, 31, 1963.

61. Demir, H., Top, A., Balkose, D., Ulku, S., *J. Hazard. Mater*., 153, 389, 2008.

62. Kumar, Y., King, P., Prasad, V., *J. Hazard. Mater*., 137, 367, 2006.

63. Langmuir, I., *Journal Am. Chem. Soc*., 40, 1361, 1981.

64. Freundlich, H., Z*. Phys. Chem*., 57, 385, 1906.

65. Sips, R., *J. Chem. Phys*.,16, 490,1948.

66. Redlich, O., Peterson, D., *J. Phys. Chem*., 63, 1024, 1959.

Anexo 1

Journal of Colloid and Interface Science 336 (2009) 398–405

Contents lists available at ScienceDirect

Journal of Colloid and Interface Science

www.elsevier.com/locate/jcis

Organofunctionalized kenyaite for dye removal from aqueous solution

Betina Royer [a], Natali F. Cardoso [a], Eder C. Lima [a,*], Vanusa S.O. Ruiz [b], Thaís R. Macedo [b], Claudio Airoldi [b]

[a] Institute of Chemistry, Federal University of Rio Grande do Sul, UFRGS, Av. Bento Gonçalves 9500, P.O. Box 15003, 91501-970 Porto Alegre, Rio Grande do Sul, Brazil
[b] Institute of Chemistry, University of Campinas, UNICAMP, P.O. Box 6154, 13084-971 Campinas, São Paulo, Brazil

ARTICLE INFO

Article history:
Received 24 January 2009
Accepted 1 April 2009
Available online 14 April 2009

Keywords:
Layered material
Kenyaite
Adsorbent
Dye
Sumifix Brilliant Orange 3R

ABSTRACT

Crystalline layered sodium kenyaite was exchanged to proton kenyaite when reacted with hydrochloric acid solution, providing a new surface with available silanol groups that are able to couple with *N*-3-trimethoxysilylpropylethylenediamine silylating agent, after prior expansion of the basal distance with the polar organic solvent dimethyl sulfoxide. The resulting organofunctionalized nanomaterial (2N-Ken) was characterized by elemental analysis, infrared spectroscopy, X-ray diffraction, carbon and silicon nuclear magnetic resonances in the solid state, surface analysis, porosity, thermogravimetry, and electron scanning microscopy. The quantity of silylating agent incorporated into the nanospace, calculated from the nitrogen elemental analysis, was determined as 0.48 mmol g^{-1}, after expanding of the acidic precursor basal distance from 1.62 to 1.99 nm. The presence of a covalent silicon–carbon bond of the organosilyl moiety on the inorganic layered structure was confirmed through nuclear magnetic resonance. This new nanomaterial has the ability to extract the Sumifix Brilliant Orange 3R textile dye from aqueous solution, using a batchwise process. The effects of stirring time, adsorbent dosage, and pH on the adsorption capacity demonstrated that 4 h is enough to reach equilibrium at 298 ± 1 K under pH 4.0. Based on error function values (F_{error}) the data were best fitted to fractional-order and chemisorption kinetic models when compared to pseudo-first-order and pseudo-second-order kinetic models. The equilibrium data were better fitted to the Sips isotherm model.

1. Introduction

Kenyaite is a member of the family of hydrous layered silicates, which is also constituted by makatite, kanemite, RUB-18, and magadiite [1]. With the exception of RUB-18, all other materials were first found in nature, magadiite and kenyaite being discovered at Magadi Lake, Kenya, in 1967 [2]. From a synthetic point of view, the compounds are generally obtained in the sodium form, as found for the pristine materials. The kenyaite chemical composition $Na_2O{\cdot}22SiO_2{\cdot}10H_2O$ presents an interlayer distance on the order of 2.00 nm. Its structural details were first elucidated through nuclear magnetic resonance of sodium and silicon nuclei; however, its refined structure remains unknown [1,3]. The other members of the family, makatite [4], kanemite [5], and RUB-18 [3], have already had their structures determined, where charge neutrality is maintained through the hydrated sodium counterion distributed inside the layered framework. These arrangements of hydrated sodium ions and silanol surface groups are also observed for both magadiite and kenyaite [1,2].

In general, the available silanol groups disposed on any layered surface, such as seen with the proposed kenyaite structure, enable the attachment of organic molecules onto the inorganic polymeric structure, as already observed in the case of natural talc [6], synthetic phillosilicate [7], and mesoporous silica [8]. This behavior suggests that a great variety of novel synthesized materials can be obtained through chemical modification of the surface using different methodologies, such as the sol–gel process, solvent evaporation, and the conventional reflux method. It is possible to design molecules grafted to nanomaterials with established functionalities and different possibilities of practical applications [9].

Recently, the interlayer space of kenyaite has been modified by different alkyl methoxysilanes and the synthesized materials obtained were used as supports to evaluate the possibility of surface modification [1], as a convenient material to obtain new polymer-layered nanocomposites with thermal, mechanical, and moisture absorption retardation properties [10]. Also, the modified nanocomposites show great ability to remove divalent cations and heavy metals from aqueous solution [11].

Interest in the adsorption of dyes from aqueous solution is growing, due to their wide applicability for coloring different industrial materials. However, these activities are responsible for generating large volumes of hazardous species in their wastewater effluents [12–14]. In this context, there is a growing interest in finding new adsorbents for dye removal from aqueous solution. Among these, are natural zeolite [15], fly ash [16], red mud [16],

* Corresponding author. Fax: +55 51 3308 7304.
E-mail addresses: eder.lima@ufrgs.br, profederlima@gmail.com (E.C. Lima).

0021-9797/$ - see front matter © 2009 Elsevier Inc. All rights reserved.
doi:10.1016/j.jcis.2009.04.025

nonactivated unburned carbon [17,18], organofuncionalized silica gel [19], and also layered silicates [20,21]. Considering the last class of adsorbents, magadiite was used as an adsorbent for dye removal from aqueous solutions and normally the adsorption process was carried out by conventional ion exchange processes [20,21]. The possibility of an organomodification reaction prior to dye adsorption would increase the capacity of adsorption by the organofunctionalized material. For this purpose kenyaite was chosen as a source of layered silicate, since its surface contains a high degree of regularly distributed silanol groups that favor organomodification reactions. Also its structure maintains its structural features in the final process, due to a layer thickness of 1.77 nm [1].

The present investigation deals with grafting of a diaminepropylsilane moiety between the layers of kenyaite, which was further employed for removal of Sumifix Brilliant Orange 3R textile dye (SBO) from aqueous solution. This dye is widely employed for dyeing silk and cotton textiles. Therefore there is a great interest in removing Sumifix Brilliant Orange 3R from textile wastewater industries. Structural and chemical features associated with the silane grafted on the layered structure are presented, as well as the kinetics and equilibrium parameters of the batch dye adsorption method.

2. Materials and methods

2.1. Synthesis of Na-kenyaite

The hydrated sodium silicate kenyaite was synthesized by hydrothermal treatment in a Teflon autoclave with autogenous pressure. A suspension of silica gel (Fluka) was added to a 0.10 mol dm^{-3} sodium hydroxide (Nuclear) solution in the molar ratio $4SiO_2$:2NaOH:$35H_2O$, corresponding to 20.0 g of silica, 6.68 g of sodium hydroxide, and 100 cm^3 of deionized water. The gel obtained was transferred to the autoclave and treated at 423 K for 7 days. The synthesized Na-kenyaite (Na-Ken) was filtered, washed with deionized water to pH 7, and dried at 333 K for 48 h [10,22].

2.2. Synthesis of H-kenyaite

A sample of 3.0 g of Na-Ken was immersed in 0.10 mol dm^{-3} hydrochloric acid (Nuclear), the pH was maintained near 2, and the suspension was stirred for 5 days. The resulting layered silicic acid (H-Ken) was filtered, washed with deionized water to pH 7, and dried at 333 K for 48 h [10].

2.3. Organomodification reaction

A sample of 3.0 g of H-Ken was suspended in 15.0 cm^3 of dimethyl sulfoxide (Quimis) under a nitrogen flow at 298 K for 1 h. The silanol groups from the inorganic layers of H-Ken are not easily reached due to the narrow interlayer distance. Therefore, to overcome this hindrance, prior treatment with organic solvents, such as dimethyl sulfoxide, *N*-methylformamide, or *N*, *N*-dimethylformamide, is necessary, in order to enlarge the original distance, favoring the organofunctionalization reaction [11]. Then, 2.0 cm^3 of the silylating agent *N*-3-trimethoxysilylpropylethylenediamine ($(CH_3O)_3Si(CH_2)_3NHCH_2CH_2NH_2$, Aldrich) was added to the suspension and stirred for 1 h. After that, the suspension was stirred under a nitrogen purge at 363 K for 72 h. The solid obtained was filtered, washed with dimethyl sulfoxide and with acetone (Synth) in a Soxhlet system, to remove the pillaring solvent, and then dried on a vacuum line to yield the immobilized compound, denoted as 2N-Ken [11].

2.4. Characterization

Carbon, nitrogen, and hydrogen contents were determined on a Perkin–Elmer 2400 Series II microelemental analyzer, and at least two independent determinations were performed.

The X-ray diffraction patterns were obtained with a Shimadzu Model XD3A diffractometer with 2θ in the 1.4–50° range, using Cu Kα 1.54060 Å radiation.

The infrared spectra were performed on a Bomem Model MB FTIR spectrophotometer, using KBr pellets, in the 4000 and 400 cm^{-1} region, with resolution of 4 cm^{-1}, by accumulating 32 scans.

The nuclear magnetic resonance spectra were recorded with a Bruker AC300/P solid state high-resolution spectrometer, by using cross-polarization and magic angle spinning (CP-MAS). The frequencies were 59.6 and 75.5 MHz, with rotational frequencies of 15 and 26 kHz, and acquisition times of 3.0 ms and 0.8 s for the ^{29}Si and ^{13}C nuclei, respectively. Chemical shifts were referenced to tetramethylsilane.

The surface analyses and porosity were carried out with a volumetric adsorption analyzer, ASAP 2010, from Micromeritrics, at 77 K (boiling point of nitrogen). The samples were pretreated at 373 K for 24 h under a nitrogen atmosphere, in order to eliminate moisture adsorbed on the solid sample surface. After that, the samples were submitted to 298 K in vacuum, reaching the residual pressure of 10^{-4} Pa. For area and pore calculations the DBET and BJH methods were evaluated.

The thermogravimetric curves were obtained on a TA Instruments 5100, with a heating rate of 0.167 K s^{-1}, under 1.67 cm^3 s^{-1} of an argon flow, varying from room temperature to 1273 K, with an initial mass of approximately 10.0 mg of solid.

A Jeol 6360-LV scanning electron microscope was used for studying the morphology of the materials, previously suspended in acetone and then sputter-coated with a thin conducting layer of gold for 400 s.

2.5. Solutions and reagents

Deionized water was used throughout the experiments for all solution preparations.

The reactive dye Sumifix Brilliant Orange 3R textile dye also know as Reactive Orange 16 (C.I. 17757; $C_{20}H_{17}N_3O_{10}S_3Na_2$, 601.54 g mol^{-1}, λ_{max} = 493 nm; see Scheme 1) was obtained from Sigma with a dye content of 50%. It was used without further purification. SBO has one sulfonate group and one sulfato-ethyl-sulfone group; both have negative charges even in highly acidic solutions, because their pK_a values are lower than zero [13,23].

The stock solution was prepared by dissolving accurately weighed dye in distilled water to a concentration of 5000 mg dm^{-3}. The working solutions were obtained by diluting the dye stock

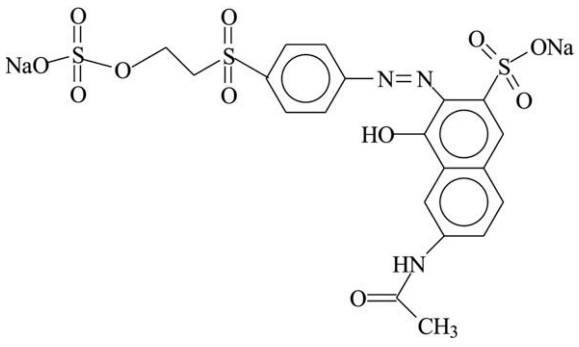

Scheme 1. Molecular structure of Sumifix Brilliant Orange 3R (SBO).

solution to the required concentrations. In order to adjust the pH of the solutions, 0.10 mol dm^{-3} sodium hydroxide or hydrochloric acid solutions were used, using a Hanna (HI 255) pHmeter.

2.6. Batchwise adsorption procedure

The adsorption studies to evaluate the 2N-Ken for SBO dye removal from aqueous solutions were carried out in triplicate using a batch adsorption procedure. For these experiments, fixed amounts of adsorbent varying from 20.0 to 200.0 mg were suspended in a series of 50 cm^3 glass flasks containing 20.0 cm^3 of dye solution with concentrations that varied from 2.00 to 1000.0 mg dm^{-3}. These suspensions were stirred for suitable times from 5 to 360 min. The isotherms clearly demonstrated that a well-established plateau was obtained and the equilibrium studies determined in these optimized conditions were 4 h at 298 ± 1 K, with the initial pH of the dye solutions ranging from 3.0 to 8.0. Subsequently, in order to separate the adsorbents from the aqueous solutions, the flasks were centrifuged at 3600 rpm for 10 min, as already described in other works [12–14,19], and aliquots of 1.0–10.0 cm^3 of the supernatant were properly diluted. The final concentrations of the dye remaining in solution were determined by visible spectrophotometry, using a Femto spectrophotometer provided with 1.0 cm path-length optical-glass cells. Absorbance measurements were made at the maximum wavelength of SBO dye 493 nm. The SBO detection limit using the spectrophotometric method, determined according to IUPAC [24], was 0.15 mg dm^{-3}. The amount of the dye uptake and percentage of dye removal by the adsorbent were calculated by applying Eqs. (1) and (2), respectively,

$$q = \frac{(C_o - C_f)}{m} \cdot V, \tag{1}$$

$$\%\ \text{Removal} = 100 \cdot \frac{(C_o - C_f)}{C_o}, \tag{2}$$

where q is the amount of dye uptake by the adsorbent (mg g^{-1}); C_o is the initial SBO concentration in contact with the adsorbent (mg dm^{-3}), C_f is the dye concentration (mg dm^{-3}) after the batch adsorption procedure, V is the volume of dye solution (dm^3) in contact with the adsorbent, and m is the mass (g) of adsorbent.

2.7. Kinetic and equilibrium models

The kinetic equations corresponding to Avrami, pseudo-first-order, pseudo-second-order, Elovich, and intraparticle diffusion models [25] are given in Table 1. The isotherm equations corresponding to Langmuir, Freundlich, Sips, and Redlich–Peterson models [25] are listed in Table 2.

2.8. Statistical evaluation of the kinetic and isotherm parameters

The kinetic and equilibrium models were fitted by employing a nonlinear method, using the nonlinear fitting facilities of the software Microcal Origin 7.0. In addition, the models were also evaluated by an error function, which measures the differences in the amount of dye uptake by the adsorbent predicted by the models and the actual q measured experimentally [26].

$$F_{\text{error}} = \sqrt{\sum_{i}^{p} \left(\frac{q_{\text{i model}} - q_{\text{i experimental}}}{q_{\text{i experimental}}} \right)^2 \cdot \left(\frac{1}{p-1} \right)}, \tag{3}$$

where $q_{\text{i model}}$ is the value of q predicted by the fitted model for each point, $q_{\text{i experimental}}$ is the value of q measured experimentally for the same point, and p is the number of experiments performed.

Table 1
Kinetic adsorption models.

Kinetic model	Nonlinear equation
Avrami	$q_t = q_e \cdot \{1 - \exp[-(k_{AV} \cdot t)]^{nAV}\}$
Pseudo-first-order	$q_t = q_e \cdot [1 - \exp(-k_f \cdot t)]$
Pseudo-second-order	$q_t = \frac{k_s \cdot q_e^2 \cdot t}{1 + q_e \cdot k_s \cdot t}$
	$h_o = k_s \cdot q_e^2$ Initial sorption rate
Elovich	$q_t = \frac{1}{\beta}\ln(\alpha \cdot \beta) + \frac{1}{\beta}\ln(t)$
Intraparticle diffusion	$q_t = k_{id} \cdot \sqrt{t} + C$

Table 2
Isotherm models.

Isotherm model	Equation
Langmuir	$q_e = \frac{Q_{max} \cdot K_L \cdot C_e}{1 + K_L \cdot C_e}$
Freundlich	$q_e = K_F \cdot C_e^{1/n_F}$
Sips	$q_e = \frac{Q_{max} \cdot K_S \cdot C_e^{1/n_S}}{1 + K_S \cdot C_e^{1/n_S}}$
Redlich–Peterson	$q_e = \frac{K_{RP} \cdot C_e}{1 + a_{RP} \cdot C_e^g}$, where $0 \leqslant g \leqslant 1$

3. Results and discussion

3.1. Adsorbent characterization

The X-ray diffraction pattern of sodium and acidic kenyaites, Na-Ken and H-Ken, shown in Fig. 1 (curves a and b), reveals peaks at 2θ values of 4.51° and 5.45°, respectively, related to the diffraction of the (0 0 1) crystal surface of the layered silicate [27]. These values are in agreement with a layered structure with average lamellar distances of 1.96 and 1.62 nm, in agreement with published results [27]. The decrease in the basal spacing is expected, in agreement with the loss of solvated sodium ions in the exchange process, due to the smaller solvated proton size. Grafting of *N*-3-trimethoxysilylpropylethylenediamine to the H-Ken surface causes a swelling of silicate layers to 1.99 nm, clearly viewed by the shift in the d_{001} reflection to lower 2θ value of 4.43° (Fig. 1c).

As the exchange process takes place, the silanol groups distributed on the inorganic layers are able to form covalent bonds in the organofunctionalization, giving 2N-Ken. Under these conditions the immobilized agent offers pendant organic chains with attached

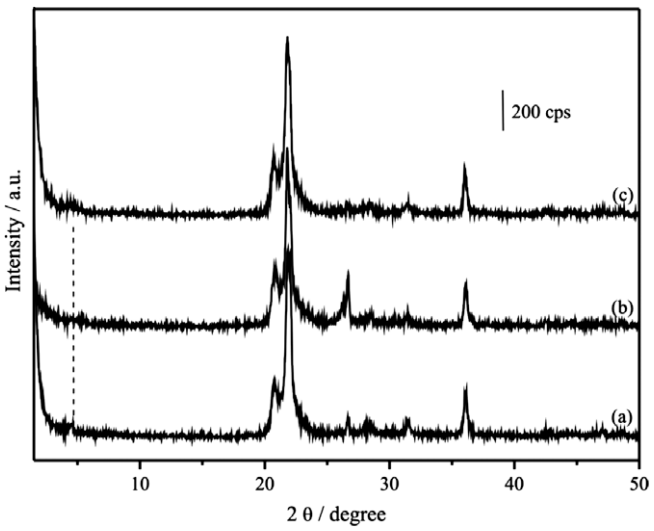

Fig. 1. X-ray diffraction patterns of sodium kenyaite (a), acidic kenyaite (b), and organomodified material 2N-Ken.

basic centers, which are potentially protonated in acidic aqueous solution, to be used in applications, for example, of adsorption with appropriate dyes. As the pristine silicic acid does not favor the entrance of the reagent inside the interlayer nanospace to perform the anchoring process, the polar organic solvent dimethyl sulfoxide was used to expand the original basal distance sufficiently to accommodate the anchoring agent, as previously reported [10,11]. From the elemental analysis of the immobilized material, giving the results C, 4.28%; H, 0.58%; and N, 1.34%, the amount of agent incorporated inside the inorganic support was calculated, based on the amount of nitrogen, to give 0.48 mmol g^{-1}.

Organofunctionalization of the silica gel surface normally utilizes two of the alkoxide groups for each covalently bonded molecule, while the remaining free group can be hydrolyzed during the washing process [28]. As the silicic acid surface has an amount of 2.0 mmol g^{-1} of silanol groups free for reactions [11], then 2N-Ken may use three groups for this attachment. The XRD pattern obtained demonstrates an increase of expansion of 0.37 nm in relation to the H-Ken starting material. The maximum length of the diamine pendant group was estimated with the software ACD/LABS version 11.0, to be 0.957 nm, with the layer thickness for kenyaite structure of 1.77 nm [1], and consequently a basal distance of 2.73 nm is expected. Based on this structural arrangement it was possible to estimate a molecular orientation of 46.9° inside the layers. This angle was calculated through Eq. (4), where d_{exp} is the value obtained from XRD, assuming that d_{calc} is 2.73 nm for a perpendicular orientation of 90° and α represents a vetorial superposition:

$$\alpha = \text{arcsen}(d_{exp}/d_{calc}). \quad (4)$$

The scanning electron microscopy results of pristine sodium kenyaite and chemically modified kenyaite are shown in Fig. 2, demonstrating lamellar morphology domains. The common plates of typical particles of sodium kenyaite are observed. In the case of the chemically modified surface, the presence of spherical nodules suggests the effectiveness of silylating agent attachment [11].

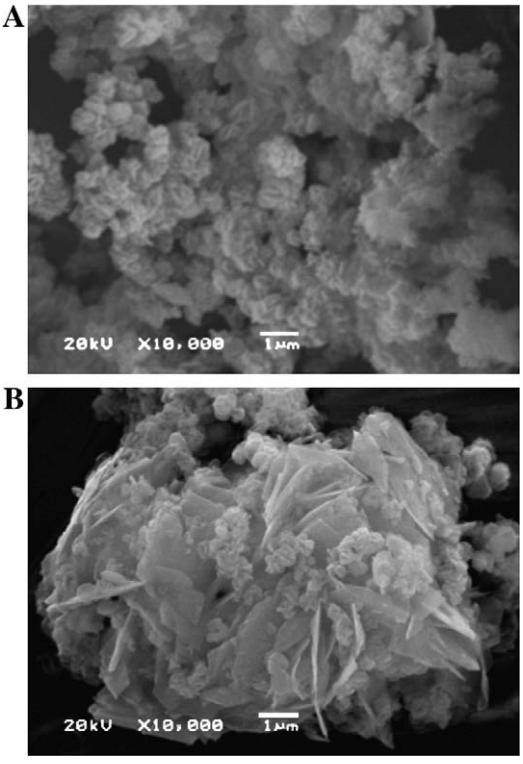

Fig. 2. Scanning electron microscopy of Na-Ken (A) and 2N-Ken (B) samples.

The infrared spectrum of the as-synthesized sodium kenyaite presents typical bands due to the physisorbed water in the inorganic framework, shown by the stretching frequency ν(OH) at 3470 cm^{-1} and the bending band δ(OH) at 1632 cm^{-1} [11,30]. The weak band at 3738 cm^{-1} is attributed to free silanol groups of the silicate surface [29], the shoulder at 1250 cm^{-1} can be attributed to the asymmetric stretching mode of the Si–O–Si [29] bond, and the bands at 1090 and 1055 cm^{-1} are assigned to ν(Si–O) stretching vibrations [29]. The bands corresponding to the water vibrations decreased in intensity in the acidic form of the material, since the water of hydration is removed, in agreement with the increase in the silanol stretching frequency [29]. The organofunctionalized kenyaite showed bands in the 2967–2824 cm^{-1} region, due to ν(C–H) stretching vibrations [10], from the silylating agent attached to the surface [10].

The surface areas obtained for sodium and acidic kenyaite were 12 ± 1 and 11 ± 1 $m^2 g^{-1}$, with pore diameters of 15 ± 1 and 30 ± 2 nm, respectively, and the organomodified surface gave an area of 13 ± 1 $m^2 g^{-1}$ with a pore diameter of 22 ± 1 nm. As observed, the surface areas for the pristine form, the acidic form, and the material after the organofunctionalization reaction are relatively low, with pore diameter values in agreement with those found for typical mesoporous materials, with nitrogen adsorption isotherms that correspond to H3 type IV [30]. Despite the reduced surface area, the diamine sites should still be accessible for dye adsorption, since the material retains an appreciable pore size.

The ^{29}Si NMR spectra give additional information about structural features of these proposed silicates. The spectrum for sodium kenyaite has two signals, at −97.0 and −107.0 ppm, due to the presence of Q^3, $(SiO)_3Si–O^-$, and Q^4, $(SiO)_4Si$, units, respectively, which are associated with the connectivity between the layers [31], as shown in Fig. 3A (curve a). For the acidic form the surface silanol groups change the silicon environment and a displacement of Q^3 and Q^4 signals is observed to give the peaks at −107.0 and −113.0 ppm [31], as shown in Fig. 3A (curve b).

The organofunctionalized compound, with the organic pendant chain covalently bonded to the surface of the silicate layer, maintained the inorganic framework structure, as expected, with a little displacement of the Q^3 and Q^4 signals in relation to the starting precursor at −101.0 and −110.0 ppm, respectively, as shown in Fig. 3A (curve c). In addition, on grafting of the diamine groups, the appearance of two new signals is observed, due to T^2 and T^3 environments [10], at −58.0 and −67.0 ppm, respectively. The T^2 signal is obtained through replacement of alkoxide by silanol groups, and the presence of T^3 species may determine condensation between adjacent alkylsilyl groups to tetrahedral coordination of organosilicate units. A reduction of the Q^3 (−107.0 ppm) signal intensity was also observed with an increase in the signal intensity of the Q^4 (−113.0 ppm) peak. This confirms the attachment of the diamine groups to the silanol groups of the interlamellar silicate surface.

Evidence of the alkylsilyl groups grafted at the interlamellar surface of the layered polysilicate kenyiate is given through ^{13}C NMR, as shown in Fig. 3B. The long pendant chain covalently bonded in 2N-Ken showed a complex spectrum, by presenting C1 and C2 carbon atoms from the silane coupling reagent nearest to the silicon atom that appeared at 10 and 22 ppm, respectively. The peaks at 52 and 57 ppm are assigned to the third and fourth carbon atoms directly bonded to the NH group, followed by a peak at 39 ppm, from the fifth carbon atom bonded to the terminal NH_2 group [11] (see Fig. 3B).

3.2. Effects of acidity on adsorption

One of the most important factors in adsorption studies is the effect of the acidity of the medium [32]. Different species being ad-

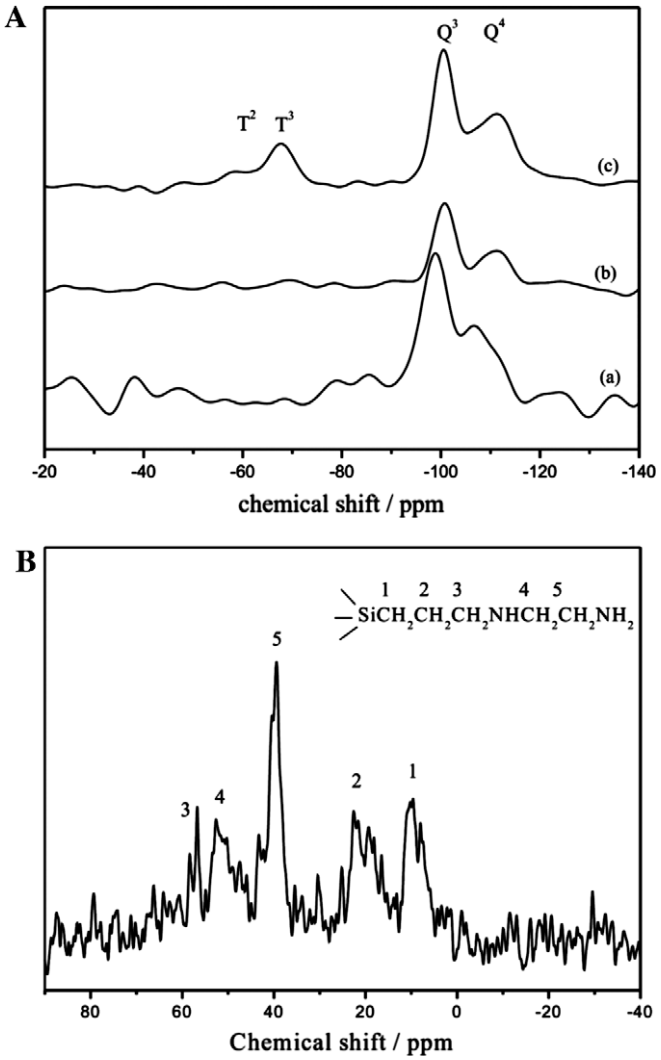

Fig. 3. (A) ^{29}Si MAS NMR of Na-Ken (a), H-Ken (b), and 2N-Ken (c) crystalline layered compounds. (B) ^{13}C NMR of the organomodified derivative 2N-Ken.

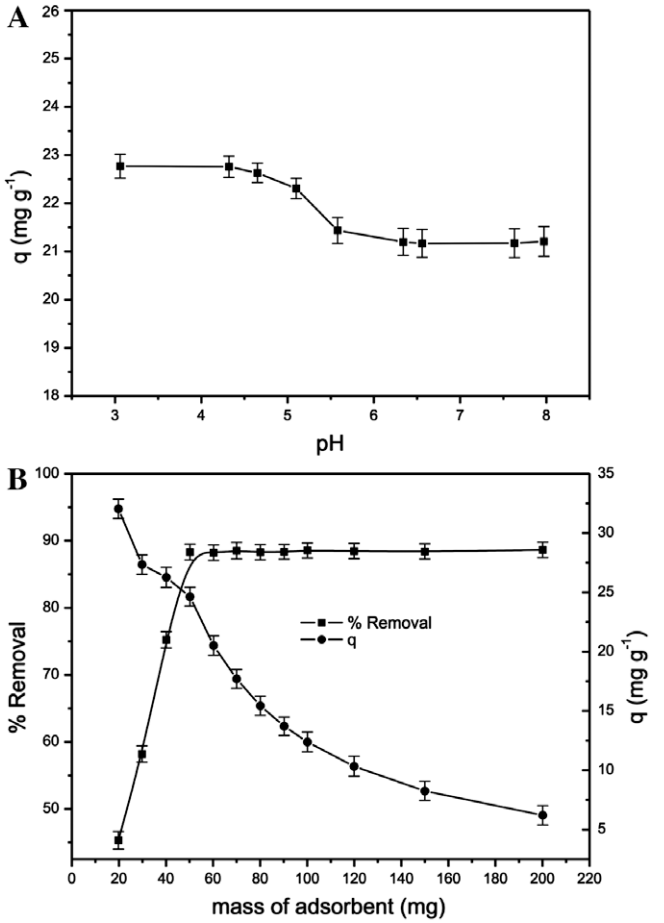

Fig. 4. (A) Effect of pH on the adsorption. (B) Effect of mass of adsorbent on the percentage of removal and amount of SBO dye adsorbed.

sorbed on diverse adsorbents will present divergent ranges of suitable pH regions for adsorption. The effects of initial pH on SBO dye adsorption capacity using 2N-Ken adsorbent were evaluated within the pH range from 3.0 to 8.0, as shown in Fig. 4A. The amount of dye adsorbed (q) was constant for pH ranging from 3.0 to 4.5. Taking into account that industrial effluents containing dyes present pH values of about 4.0–5.0, the pH of the dye solution was kept at 4.0 for all remaining experiments. It should be noted that the final pH of the dye solutions after the adsorption procedure decreased by approximately 0.5.

3.3. Adsorbent mass

The investigation of the mass of adsorbent for dye removal from aqueous solution was carried out using adsorbent masses ranging from 20.0 to 200.0 mg, by fixing the initial concentration and volume of SBO solutions at 70.0 mg dm^{-3} and 20.0 cm^3, respectively. The highest amount of dye removal was attained for adsorbent masses of at least 50.0 mg of adsorbent, as shown in Fig. 4B (at left). For adsorbent masses higher than these values, the dye removal remained almost constant. The increase in the percentage of dye removal with adsorbent masses can be attributed to increases in the adsorbent surface areas, augmenting the number of adsorption sites available for adsorption [33]. On the other hand, the increase in the adsorbent mass promotes a remarkable decrease in the amount of dye uptake per gram of adsorbent (q), as shown in Fig. 4B (at right), an effect that can be mathematically explained by combining Eqs. (1) and (2):

$$q = \frac{\%\ \text{Removal} \cdot C_o.V}{100 \cdot m}. \tag{5}$$

As observed from Eq. (5), the amount of dye uptake (q) and the mass of adsorbent (m) are inversely proportional. For a fixed dye percentage removal, the increase of adsorbent mass leads to a decrease in q values, since the volume (V) and initial dye concentrations (C_o) are always fixed. These values clearly indicate that the adsorbent mass must be fixed at 50.0 mg, the mass that corresponds to the minimum amount of adsorbent that leads to constant dye removal.

3.4. Kinetic studies

Studies of adsorption kinetics are an important feature to be considered in aqueous effluent treatments as it provides valuable information on the mechanism of adsorption processes [13]. In attempting to describe the SBO dye adsorption by the adsorbent, four kinetic models were tried, as shown in Fig. 5A. The kinetic parameters for the best models are listed in Table 3. Thus, only the Avrami fractionary kinetic order and Elovich chemisorption models are depicted in Table 3. The pseudo-first-order and pseudo-second-order kinetic models are not shown in this table because they presented F_{error} values at least five times higher than the Avrami fractionary kinetic model.

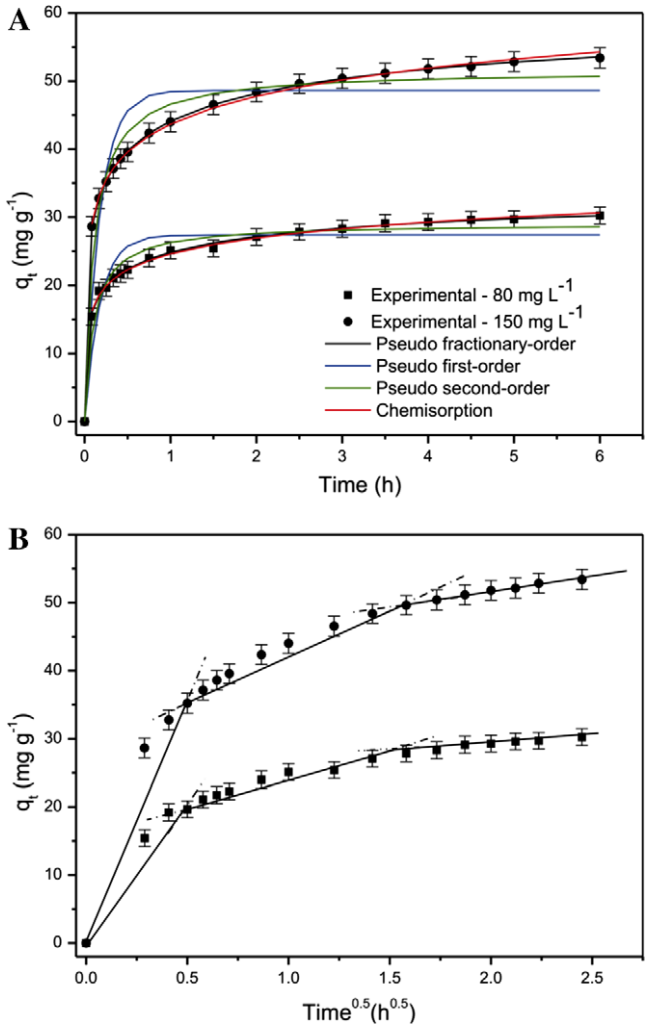

Fig. 5. Kinetic curves. Conditions: temperature 298 K; pH 4.0; mass of adsorbent 50.0 mg; initial SBO concentration 80.0 mg dm^{-3}.

The fractional and chemisorption kinetic models were suitably fitted, presenting low error function values and also high R^2 values. The lower the error function, the lower the difference of the q calculated by the model from the experimentally measured q [25,33,34]. It should be stressed that only analysis of R^2 values for the establishment of a given model is not enough. The error function evaluates the differences associated with each individual point fitted by the model, in relation to each measured experimental point. On the other hand, R^2 measures the differences associated with each individual point in relation to the average fitted curve [25,33,34].

Additionally, it was verified that the q_e values found in the fractional order were in good agreement with the experimental data. For pseudo-first-order and pseudo-second-order models, the q_e fitted values were not coincident with the q_e experimental value. This result indicates that the fractional-order and chemisorption kinetic models better explain the adsorption process of SBO uptake by 2N-Ken adsorbent.

Analysis of the values of the kinetic parameters represented in Table 3 indicates that the k_{AV} values showed a variation lower than 3.8%, when the initial concentration of the adsorbate increased from 80.0 to 150.0 mg dm^{-3}. On the other hand, the percentage of variation of α (initial adsorption rate) was 87.9%, when the initial concentration level of the SBO was increased from 80.0 to 150.0 mg dm^{-3}. Therefore, the fractional kinetic model provides a constant rate parameter which is much better for comparison of different kinetic constants, using several adsorbates and adsorbents, as already observed in other publications [13,25,34].

Table 3
Kinetic parameters for SBO removal using 2N-Ken as adsorbent.

Fractional order	80.0 mg dm^{-3}	150.0 mg dm^{-3}
k_{AV} (h^{-1})	2.61	2.71
q_e (mg g^{-1})	33.9	59.8
n_{AV}	0.291	0.292
R^2	0.9979	0.9999
F_{error}	1.65×10^{-2}	2.72×10^{-3}
Chemisorption		
α (mg g^{-1} h^{-1})	5037	9465
β (g mg^{-1})	0.297	0.169
R^2	0.9975	0.9991
F_{error}	1.81×10^{-2}	8.53×10^{-3}
Intraparticle diffusion		
$k_{i,2}$ (mg g^{-1} h$^{-0.5}$)[a]	6.56	7.07

Conditions: temperature fixed at 298 K; pH 4.0; adsorbent mass: 50.0 mg.
[a] Second stage.

Taking into account that the kinetic results fit very well into the Avrami fractional kinetic model, listed in Table 3 and Fig. 5A, the intraparticle diffusion model was plotted in order to verify the influence of mass transfer resistance on the binding of SBO to 2N-Ken adsorbent, as indicated by the values listed in Table 3 and shown in Fig. 5B.

The possibility of intraparticle diffusion resistance affecting adsorption was explored using the appropriate intraparticle diffusion model [34]. Thus, the diffusion constant, k_{id} (mg g^{-1} h$^{-0.5}$, see Table 1), can be obtained from the slope of the plot of q_t (uptake at any time, mg g^{-1}) versus the square root of time. Fig. 5B shows the plot of q_t versus $t^{1/2}$, with multilinearity for the dye using 2N-Ken adsorbent. This result implies that the adsorption processes involve more than a single kinetic stage or sorption rate [34]. The adsorbent exhibits three stages, which can be attributed to three linear parts, as shown in Fig. 5B. The first linear portion was attributed to the diffusional process of SBO to the adsorbent surface [34]; hence, was the fastest sorption stage. The second linear portion is attributed to intraparticle diffusion, which was a delayed process [35]. The third stage may be regarded as the diffusion through smaller pores, which is followed by establishment of equilibrium [34], which was obtained within 4 h for all systems studied.

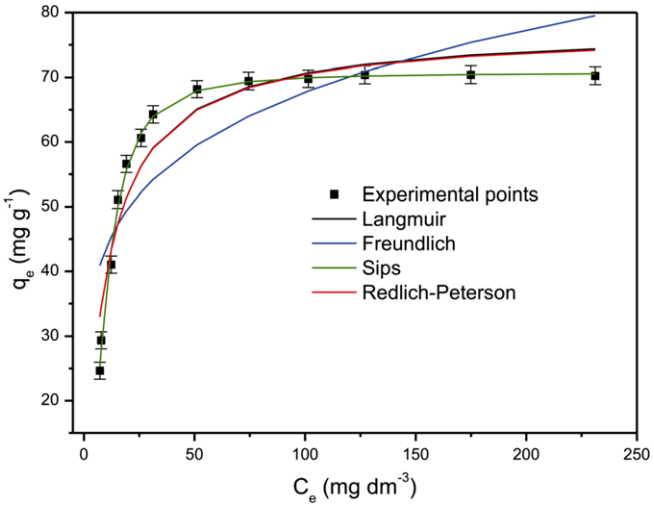

Fig. 6. Equilibrium models. Conditions: temperature 298 K; pH 4.0; mass of adsorbent 50.0 mg; contact time 300 min.

Table 4
Isotherm parameters for SBO adsorption, using 2N-Ken as adsorbent.

	2N-Ken
Langmuir	
Q_{max} (mg g^{-1})	77.5
K_L (dm^3 mg^{-1})	0.103
R^2	0.9285
F_{error}	0.122
Freudlich	
K_F (mg g^{-1}(mg dm^{-3})$^{-1/n_F}$)	28.0
n_F	5.22
R^2	0.7176
F_{error}	0.246
Sips	
Q_{max} (mg g^{-1})	70.7
K_S ((mg dm^{-3})$^{-1/n_S}$)	0.0124
n_S	0.518
R^2	0.9966
F_{error}	0.0249
Redlich–Peterson	
K_{RP} (dm^3 g^{-1})	7.97
a_{RP} (mg dm^{-3})$^{-g}$	0.103
g	1.00
R^2	0.9288
F_{error}	0.122

Conditions: temperature 298 ± 1 K, contact time 240 min, at pH 4.0, and mass of adsorbent 50.0 mg.

3.5. Equilibrium studies

The adsorption isotherm describes the amount of adsorbate uptake by the adsorbent and the adsorbate concentration that should remain in solution [35]. Therefore, a lot of equations for analyzing experimental adsorption equilibrium data are available. The equation parameters of these equilibrium models often provide some insight into the adsorption mechanism, the surface properties, and the affinity of the adsorbent. For this purpose the Langmuir, Freundlich, Sips, and Redlich–Peterson isotherm models [35] were assayed.

The isotherms of SBO adsorption on 2N-Ken adsorbent were obtained, by using the best experimental conditions, as shown in Fig. 6, and the data of the fitted models are presented in Table 4. Based on the F_{error}, the equilibrium data only fit the Sips isotherm model well when using this adsorbent for sorption of this dye. On the other hand, all other tested models failed in fitting the isotherm curve, as shown by the low R^2 as well as high F_{error} values, indicating that for this specific case the Langmuir, Freundlich, and Redlich–Peterson isotherm models were not suitably fitted. The lower the error function (F_{error}), the smaller the difference of the q calculated by the model from the experimentally measured q [25,33,34]. As noted earlier, only analysis of R^2 values for the establishment of a given model is not enough; use of the error function that evaluates the differences associated with each individual point fitted by the model is also necessary [25,33,34].

Taking into account the Sips isotherm, the maximum amount of the dye uptake was 70.7 mg g^{-1} that corresponds to 0.12 mmol g^{-1}. From the point of view of the exchanger process at the solid/liquid interface, the SBO has sulfonate and sulfate-ethyl-sulfonate groups (negative charges) to ionically interact with the protonated nitrogens attached to the pendant chain covalently grafted on the silicate layer (see Scheme 2). This interactive process is favored at pH < 4 (see Fig. 4A), when the basic nitrogen atoms are easily protonated to acquire a positive charge. In general for the adsorption process, the degree of adsorption depends on both the active sites

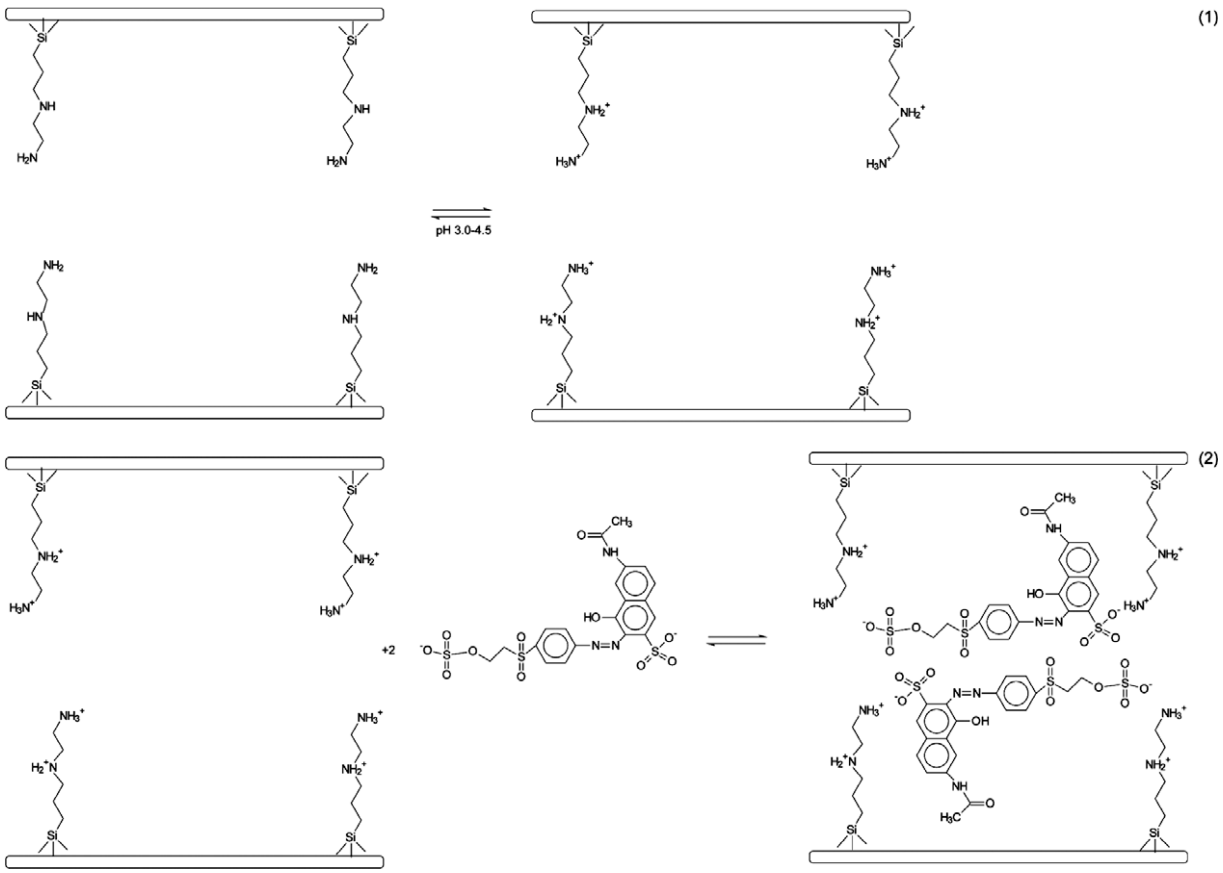

Scheme 2. Mechanism of adsorption of SBO by 2N-Ken adsorbent.

of the adsorbent and the adsorbate properties. The results obtained suggest that the textile dye uses more than one basic center of the grafted trimethoxysilylpropylethylenediamine molecule, during the interactive process [11], as it might be expected for a favorable adjustment of its size inside the pores of the adsorbent to counteract the opposing charges when saturated an amount of 0.48 mmol g^{-1} is retained.

4. Summary

When as-synthesized sodium kenyaite was transformed to the corresponding acidic form, the available silanol groups demonstrated efficiency in coupling a silylating agent into the free interlayer cavity. The success of the grafting of the organic molecules depends first on prior basal distance expansion through the polar solvent dimethyl sulfoxide. Structural features related to silicon nuclear magnetic resonance in the solid state showed carbon–silicon covalent bond formation, supporting the attachment of the pendant organic chains to the inorganic layer, by reaching the final interlayer distance of 1.99 nm. The available protonated basic atoms extract the Sumifix Brilliant Orange 3R textile dye from aqueous solution using the batchwise process. The dye adsorption data were adjusted to the Sips isotherms model and the kinetic data were fitted to fractional-order and chemisorption kinetic models. For this interactive process the basic protonated nitrogen atoms were saturated to give plateaus represented by the maximum number of moles adsorbed, for example, 70.7 mg g^{-1} (0.12 mmol g^{-1}), given by the Sips isotherm. Based on these results, it is supposed that the textile dye uses more than one basic center of the grafted diamine molecule when interacting with the available basic nitrogens to reach 0.48 mmol g^{-1}. This is expected, since the dye has one sulfonate group and one sulfatoethyl-sulfone group, both of which have negative charges to interact with the positive diamine groups of the organomodified material. However, this interaction may happen with different protonated diamine groups. It is also necessary to consider the size of the dye molecules, despite the large pore size of the host.

5. Notations

5.1. Greek letters

α	the initial adsorption rate (mg g^{-1} h^{-1}) of the Elovich equation
β	Elovich constant related to the extent of surface coverage and also to the activation energy involved in chemisorption (g mg^{-1})
a_{RP}	Redlich–Peterson constant (mg $dm^{-3})^{-g}$
C	constant related with the thickness of the boundary layer (mg g^{-1})
C_f	dye concentration at the end of the adsorption (mg dm^{-3})
C_e	dye concentration at equilibrium (mg dm^{-3})
C_o	initial dye concentration put in contact with the adsorbent (mg dm^{-3})
g	dimensionless exponent of Redlich–Peterson equation
h_o	the initial sorption rate (mg g^{-1} h^{-1}) of the pseudo-second-order equation
k_{AV}	Avrami kinetic constant (h^{-1})
k_f	pseudo-first-order rate constant (h^{-1})
K_F	the Freundlich constant related to adsorption capacity ([mg g^{-1}(mg $dm^{-3})^{-1/n_F}$])
k_{id}	intraparticle diffusion rate constant (mg g^{-1} $h^{-0.5}$)
K_L	Langmuir affinity constant (dm^3 mg^{-1})
K_{RP}	Redlich–Peterson constant (dm^3 g^{-1})
K_S	the Sips constant related to the affinity constant (mg $dm^{-3})^{-1/n_s}$
k_s	the pseudo-second-order rate constant (g mg^{-1} h^{-1})
m	mass of adsorbent (g)
n_{AV}	a fractional reaction order (Avrami) which can be related to the adsorption mechanism
n_F	dimensionless exponent of the Freundlich equation
n_S	dimensionless exponent of the Sips equation
q	amount of the dye adsorbed by the adsorbent (mg g^{-1})
q_e	amount of adsorbate adsorbed at the equilibrium (mg g^{-1})
Q_{max}	the maximum adsorption capacity of the adsorbent (mg g^{-1})
q_t	amount of adsorbate adsorbed at time t (mg g^{-1})
t	time of contact (h)
V	volume of dye put in contact with the adsorbent (dm^3)

Acknowledgments

The authors are grateful to FAPESP, MCT, CNPq, and CAPES for financial support and fellowships. We also acknowledge Dr. Carol Hollingworth Collins for language improvements.

References

[1] P.H. Thiesen, K. Beneke, G. Lagaly, J. Mater. Chem. 12 (2002) 3010.
[2] F. Feng, K.J. Balkus Jr., J. Porous Mater. 10 (2003) 5.
[3] M. Borowski, O. Kovalev, H. Gies, Micropor. Mesopor. Mater. 107 (2008) 71.
[4] H. Annehed, L. Falth, F.J. Lincoln, Z. Kristallogr. 159 (1982) 203.
[5] L.A.J. Garvie, B. Devouard, T.L. Groy, F. Camara, P.R. Buseck, Am. Miner. 84 (1999) 1170.
[6] M.G. Fonseca, C.R. Silva, J.S. Barone, C. Airoldi, Chem. Mater. 14 (2002) 2810.
[7] J.-C. Gallégo, M. Jaber, J. Miehé-Brendlé, C. Marichal, New J. Chem. 32 (2008) 407.
[8] J.A.A. Sales, A.G.S. Prado, C. Airoldi, Surf. Sci. 590 (2005) 51.
[9] P.M. Price, J.H. Clark, D.J. Macquarrie, J. Chem. Soc., Dalton Trans. (2000) 101.
[10] C.-M. Leu, Z.-W. Wu, K.-H. Wei, Chem. Mater. 14 (2002) 3016.
[11] V.S.O. Ruiz, G.C. Petrucelli, C. Airoldi, J. Mater. Chem. 16 (2006) 2338.
[12] F.A. Pavan, Y. Gushikem, A.S. Mazzocato, S.L.P. Dias, E.C. Lima, Dyes Pigments 72 (2007) 256.
[13] E.C. Lima, B. Royer, J.C.P. Vaghetti, N.M. Simon, B.M. da Cunha, F.A. Pavan, E.V. Benvenutti, R.C. Veses, C. Airoldi, J. Hazard. Mater. 155 (2008) 536.
[14] F.A. Pavan, E.C. Lima, S.L.P. Dias, A.C. Mazzocato, J. Hazard. Mater. 150 (2008) 703.
[15] S. Wang, Z.H. Zhu, J. Hazard. Mat. 136 (2006) 946.
[16] S. Wang, Y. Boyjoo, A. Choueib, Z.H. Zhu, Water Res. 39 (2005) 129.
[17] S. Wang, L. Li, H. Wu, Z.H. Zhu, J. Colloid Interface Sci. 292 (2005) 336.
[18] S. Wang, H.T. Li, Dyes Pigments 72 (2007) 308.
[19] F.A. Pavan, S.L.P. Dias, E.C. Lima, E.V. Benvenutti, Dyes Pigments 76 (2008) 64.
[20] M. Ogawa, J. Mater. Chem. 12 (2002) 3304.
[21] N. Miyamoto, R. Kawai, K. Kuroda, M. Ogawa, Appl. Clay Sci. 19 (2001) 39.
[22] W. Schwieger, D. Heidemann, K.-H. Bergk, Rev. Chim. Miner. 22 (1985) 639.
[23] S.W. Won, H.J. Yun, Y.S. Yun, J. Colloid Interface Sci. 331 (2009) 83.
[24] E.C. Lima, F.J. Krug, J.A. Nóbrega, A.R.A. Nogueira, Talanta 47 (1998) 613.
[25] J.C.P. Vaghetti, E.C. Lima, B. Royer, B.M. da Cunha, N.F. Cardoso, J.L. Brasil, S.L.P. Dias, J. Hazard. Mater. 162 (2009) 270.
[26] E.C. Lima, B. Royer, J.C.P. Vaghetti, J.L. Brasil, N.M. Simon, A.A. dos Santos Jr., F.A. Pavan, S.L.P. Dias, E.V. Benvenutti, E.A. da Silva, J. Hazard. Mater. 140 (2007) 211.
[27] M.E. Landis, B.A. Aufdembrink, P. Chu, I.D. Johnson, G.W. Kirker, M.K. Rubin, J. Am. Chem. Soc. 113 (1991) 3189.
[28] P.K. Jal, S. Patel, B. Mishra, Talanta 62 (2004) 1005.
[29] Y. Huang, Z. Jiang, W. Schwieger, Chem. Mater. 11 (1999) 1210.
[30] S. Hamoudi, S. Kaliaguine, Micropor. Mesopor. Mater. 59 (2003) 195.
[31] G.G. Almond, R.K. Harris, K.R. Franklin, J. Mater. Chem. 7 (1997) 681.
[32] J.L. Brasil, R.R. Ev, C.D. Milcharek, L.C. Martins, F.A. Pavan, A.A. dos Santos Jr, S.L.P. Dias, J. Dupont, C.P.Z. Noreña, E.C. Lima, J. Hazard. Mater. 133 (2006) 143.
[33] J.C.P. Vaghetti, E.C. Lima, B. Royer, J.L. Brasil, B.M. da Cunha, N.M. Simon, N.F. Cardoso, C.P.Z. Noreña, Biochem. Eng. J. 42 (2008) 67.
[34] J.C.P. Vaghetti, E.C. Lima, B. Royer, N.F. Cardoso, B. Martins, T. Calvete, Sep. Sci. Technol. 44 (2009) 615.
[35] B. Royer, N.F. Cardoso, E.C. Lima, J.C.P. Vaghetti, N.M. Simon, T. Calvete, R.C. Veses, J. Hazard. Mater. 164 (2009) 1213.

Anexo 2

Separation Science and Technology, 45: 129–141, 2010

ISSN: 0149-6395 print/1520-5754 online
DOI: 10.1080/01496390903256257

Taylor & Francis
Taylor & Francis Group

Sodic and Acidic Crystalline Lamellar Magadiite Adsorbents for the Removal of Methylene Blue from Aqueous Solutions: Kinetic and Equilibrium Studies

Betina Royer,[1] Natali F. Cardoso,[1] Eder C. Lima,[1] Thais R. Macedo,[2] and Claudio Airoldi[2]

[1]*Institute of Chemistry, Federal University of Rio Grande do Sul, Porto Alegre, RS, Brazil*
[2]*Institute of Chemistry, University of Campinas, Campinas, SP, Brazil*

The present study reports the feasibility of two synthetic crystalline lamellar nano-silicates, sodic magadiite (Na-mag) and its converted acidic form (H-mag), as alternative adsorbents for the removal of the dye methylene blue (MB) from aqueous solutions. The ability of these adsorbents for removing the dye was explored through the batch adsorption procedure. Effects such as the pH and the adsorbent dosage on the adsorption capacities were explored. Four kinetic models were applied, the adsorption being best fitted to a fractionary-order kinetic model. The kinetic data were also adjusted to an intra-particle diffusion model to give two linear regions, indicating that the kinetics of adsorption follows multiple sorption rates. The equilibrium data were fitted to Langmuir, Freundlich, Sips, and Redlich-Peterson isotherm models. The maxima adsorption capacities for MB of Na-mag and H-mag were 331 and 173 mg g^{-1}, respectively.

Keywords adsorption; magadiite; methylene blue; nanomaterial; phyllosilicate

INTRODUCTION

Industrial activities are responsible for generating large volumes of hazardous species in their wastewater effluents (1). Among those species, dyes represent an undesirable class of compounds that inevitably require special treatment, due to the fact that the simple presence of these compounds in water reduces light penetration, precluding photosynthesis of aqueous flora (2). In addition, other features associated with many dyes are those that affect humans, such as allergies, dermatitis, skin irritations, cancers, and mutagenicity (3–5). On the other hand, colored waters are aesthetically objectionable for drinking and other normal purposes (6). As expected, when industrial effluents contain traces of dyes, a purification operation before being released to the environment is required (2,6).

Several methods have been developed for synthetic dye removal from waters and wastewaters in order to decrease their impact on the environment. The most inexpensive and efficient procedure for such operations is related to adsorption (7–11), because the dye species are transferred from the water effluent to a solid phase, with a consequent decrease in the effluent concentration to reach as close as possible to a minimum amount (7–11). Subsequently, the adsorbent could be regenerated or kept in a dry place without direct contact with the environment (7–11).

From a series of inorganic natural (8,9) and synthetic materials (10–12), layered silicates and silicic acids have aroused enormous interest due to their exceptional adsorptions, cation-exchange properties, intercalations, and organofunctionalization abilities (12). All these properties infer the use of these materials for valuable potential applications as adsorbents, ion exchangers, catalysts, and molecular sieves.

The layered silicic acid families constituted of kenyaite, makatite, kanemite, octosilicate, and magadiite and comprise a defined class of compounds with distinct layered arrangements. All these pure crystalline layered materials are successfully synthesized in the laboratory by hydrothermal treatment, through controlled conditions of time, temperature, pressure, stoichiometry, and reagent ratio, to obtain these compounds principally in the sodic form, which is the preferred operational procedure. With the exception of octosilicate, all other polysilicates are also found naturally, for example, in highly alkaline lakes (13).

Despite the great importance of this class of layered compounds, the correct structure of magadiite still remains unknown. Some studies consider it to be built up of regular sheets of SiO_4 tetrahedra, with terminal oxygen atoms neutralized by sodium ions (14). To obtain crystalline magadiite in the acidic form, the original sodium cations must be ion-exchanged with hydrochloric acid (15).

Received 3 March 2009; accepted 15 July 2009.
Address correspondence to Eder C. Lima, Institute of Chemistry, Federal University of Rio Grande do Sul, UFRGS, Av. Bento Gonçalves 9500, Porto Alegre, RGS 91501-970, Brazil. Tel & Fax: +55 51 3308 7175. E-mail: profederlima@gmail.com or eder.lima@ufrgs.br

Similarly, to derivatize the silica surfaces (16), a large number of silanol groups are available, which hydrogen bond to a large number of organic polar basic compounds (17) to aid the adsorptive process or favor interaction as intercalation reactions take place (18).

The present investigation deals with the crystalline lamellar silicate sodic magadiite (Na-mag) and its converted acidic form (H-mag), as alternative adsorbents for removal of methylene blue (MB) from aqueous solutions, using a batch adsorption procedure. Methylene blue is an organic dye belonging to the phenothiazine family. It is mainly used for coloring bast (soft vegetable fibers such as jute, flax, and hemp), paper, leather, mordant cotton, silk, and wool (19). Due to its large application for coloring different industrial materials, there is a constant interest in removing it from aqueous solutions.

MATERIALS AND METHODS

Synthesis of Magadiite Material

Sodium magadiite (Na-mag) was synthesized using hydrothermal conditions as described previously (20). Briefly, a suspension of silica gel (Merck) and sodium hydroxide (Vetec) in an aqueous solution, with a molar ratio of SiO_2:NaOH:H_2O equal to 9:1:75, was heated at 420 K for 72 h in a sealed Teflon-lined vessel. The white product was then washed with water until the pH reached near neutral conditions, in order to remove the excess of hydroxide. The solid was centrifuged and dried at 320 K for 24 h. The acidic form (H-mag) was prepared at room temperature, over 24 h, by suspending the precursor Na-mag in 0.20 mol dm^{-3} hydrochloric acid (20).

Characterization

The X-ray diffraction patterns were obtained on a Shimadzu model XD3A diffractometer, with 2θ varying from 1.4 to 55°, using nickel filtered Cu K_α (1.54 nm) radiation. Infrared vibrational spectra were obtained on a MB-Bomem FTIR spectrometer, after pressing with KBr, accumulating 32 scans in the 4000 to 400 cm^{-1} region at a resolution of 4 cm^{-1}(21).

The NMR spectra were obtained on a Bruker AC300/P solid-state high-resolution spectrometer, using cross-polarization and magic angle spinning (CPMAS), at a frequency of 59.6 MHz with a rotational frequency of 15 kHz, acquisition time of 6 ms, and contact time of 5 ms for the ^{29}Si nucleus. Chemical shifts were referenced to tetramethylsilane.

SEM images were recorded using a Jeol model JSM-6360 LV scanning electron microscope, equipped with a field emission electron gun operated at 77 K and 5 kV. The samples were deposited under a thin layer of a vitreous support and dried with an acetone solution, sputter deposited prior to SEM analyses, and the resolution achieved was <5 nm.

The specific surface areas for the samples were determined by the BET (Brunauer, Emmett, Teller) multipoint technique using a volumetric apparatus (22) with a nitrogen probe. Pore size distribution was obtained by nitrogen adsorption–desorption isotherms, determined at the liquid nitrogen boiling point, using a volumetric apparatus connected to a turbo Edwards vacuum line system, employing a mercury capillary barometer (22). The data analyses were made by the BJH (Barret, Joyer, Halenda) method.

Thermogravimetric curves were obtained with a thermobalance from TA instruments 5100, TGA 2050 model, under a flow of dry nitrogen 30 $cm^3\,s^{-1}$ and at heating rate of 0.17 $K\,s^{-1}$.

The point of zero charge (pH_{pzc}) for both adsorbents was measured through mass titration (23) methods.

Solutions and Reagents

Deionized water was used throughout the experiments for all solution preparations.

The analytical grade cationic dye, methylene blue (MB) (C.I. 52030, basic blue 9, $C_{16}H_{18}N_3SCl$, as shown in Scheme 1) was obtained from Sigma and was used without further purification. The stock solution was prepared by dissolving accurately weighed dye in deionized water to obtain a concentration of 5000 mg dm^{-3}. Other solutions were obtained by diluting the stock dye solution to the required concentration. To adjust the pH of the solutions, 0.10 mol dm^{-3} sodium hydroxide or hydrochloric acid solutions were used. The pH of the solutions was measured using a Hanna (HI 255) pH meter.

Batchwise Procedure

The adsorption studies to evaluate the magadiite adsorbents in sodic (Na-mag) and acidic (H-mag) forms for MB dye removal from aqueous solutions were carried-out in triplicate using the batch adsorption procedure. For these experiments, fixed amounts of adsorbents varying from 20.0 to 200.0 mg were suspended in a series of 20.0 cm^3 of dye solution with concentrations that varied from 2.00 to 1000.0 mg dm^{-3} using 50 cm^3 glass flasks. These suspensions were stirred for suitable times from 5 to 360 min for kinetic experiments. The isotherms clearly demonstrated that a well-established plateau was obtained. The equilibrium studies were carried out using the optimized condition of 210 min at 298 ± 1 K. The pH of the dye solutions ranged from 2.0 to 10.0. Subsequently, in order to separate the adsorbents from the aqueous solutions, the flasks were centrifuged at 3600 rpm for 10 min, and aliquots of 1.0 to

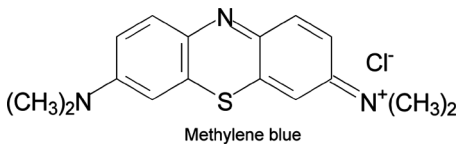

SCH. 1. Structural formula of methylene blue.

$10.0\,cm^3$ of the supernatant were properly diluted. The final concentrations of the dye that remained in the solution were determined by visible spectrophotometry, using a Femto spectrophotometer provided with 1.0 cm path length optical-glass cells. Absorbance measurements were made at the maximum wavelength of MB dye of 660 nm. The MB detection limit using the spectrophotometric method, determined according to IUPAC (24), was $0.09\,mg\,dm^{-3}$.

Batch desorption studies were carried out by agitating $20.0\,cm^3$ of $200.0\,mg\,dm^{-3}$ MB solutions (pH 8.5) with 60.0 mg of Na-mag and H-mag adsorbents for 60 min. The remaining liquid phase was separated from the solid phase, and the dye loaded adsorbents, were first washed with water for removing the non-adsorbed dye. Then, the dye loaded adsorbents were agitated with 25.0 ml of aqueous solutions (0.01–0.25 mol dm^{-3} NaOH; 0.01–0.50 mol dm^{-3} KCl; and 0.01–0.25 mol dm^{-3} HCl) up to 1 h. The desorbed dye was separated and estimated as described above.

The amount of dye uptake by and the percentage of dye removal from the adsorbents were calculated by applying Eqs. (1) and (2), respectively:

$$q = [(C_o - C_f) \cdot V]/m \tag{1}$$

$$\%Removal = [100 \cdot (C_o - C_f)/(C_o)] \tag{2}$$

where q is the amount of dye uptake by the adsorbents ($mg\,g^{-1}$); C_o is the initial MB concentration in contact with the adsorbent ($mg\,dm^{-3}$), C_f is the dye concentration ($mg\,dm^{-3}$) after the batch adsorption procedure, V is the volume of dye solution (dm^3) in contact with the adsorbent, and m is the mass (g) of adsorbent.

Kinetic and Equilibrium Models

Kinetic equations corresponding to Avrami (25), pseudo first-order (26), pseudo second-order (27), Elovich (28), and the intra-particle diffusion model (29) are given in Table 1.

TABLE 1
Kinetic adsorption models

Kinetic model	Non-linear equation	Ref.
Avrami	$q_t = q_e\{1 - \exp[-(k_{AV}t)]^{nAV}\}$	(25)
Pseudo-first order	$q_t = q_e[1 - \exp(-k_f t)]$	(26)
Pseudo second order	$q_t = (k_s \cdot q_e^2 \cdot t)/(1 + q_e \cdot k_s \cdot t)$ $ho = k_s q_e^2$ initial sorption rate	(27)
Elovich	$q_t = (1/\beta)\mathrm{Ln}(\alpha\beta) + (1/\beta)\mathrm{Ln}(t)$	(28)
Intra-particle diffusion	$qt = k_{id} \cdot \sqrt{t} + C$	(29)

TABLE 2
Isotherm models

Isotherm model	Equation	Ref.
Langmuir	$q_e = (Q_{max} \cdot K_L \cdot C_e/1 + K_L \cdot C_e)$	(30)
Freundlich	$q_e = K_F \cdot C_e^{1/nF}$	(31)
Sips	$q_e = (Q_{max} \cdot K_S \cdot C_e^{1/n_s}/1 + K_S \cdot C_e^{1/n_s})$	(32)
Redlich-Peterson	$q_e = (K_{RP} \cdot C_e/1 + aRP \cdot C_e^g)$ where $0 \le g \le 1$	(33)

The isotherm equations corresponding to Langmuir (30), Freundlich (31), Sips (32), and Redlich-Peterson models (33) are listed in Table 2.

Statistical Evaluation of the Kinetic and Isotherm Parameters

The kinetic and equilibrium models were fitted by employing the nonlinear method, using the nonlinear fitting facilities of the software Microcal Origin 7.0. In addition, the models were also evaluated by an error function, which measures the differences in the amount of dye uptake by the adsorbent predicted by the models and the actual q measured experimentally (34).

$$F_{error} = \sqrt{\sum_{i}^{p} (q_{i\,model} - q_{i\,experimental}/q_{i\,experimental})^2 \cdot (1/p - 1)} \tag{3}$$

where $q_{i\ model}$ is the value of q predicted by the fitted model, $q_{i\ experimental}$ is the value of q measured experimentally and p is the number of experiments performed.

RESULTS AND DISCUSSION

Adsorbent Characterization

The synthesized crystalline compounds Na-mag and H-mag (20) were characterized through X-ray diffraction (XRD) patterns, as shown in Fig. 1a. The expected lamellar structure for Na-mag is in agreement with the signals at 2θ 5.7, 11.4 and 17.1°, to give 1.55, 0.78, and 0.52 nm, which correspond to the indexed (001), (002), and (003) diffraction planes, respectively (13). Additional signals at 2θ of 23 to 30° to give the 3.83 to 2.94 nm range are also characteristic features related to the crystalline layered compound. When the precursor material is acidified to prepare H-mag, the corresponding signal due to the interlayer distance changes to 2θ 7.3° that corresponds to 1.17 nm, as shown in Fig. 1a, clearly indicating a decrease of the interlayer distance, as the sodium cation is exchanged by a proton, not only due to the difference in size, but also to the large hydration of the sodium ion (12).

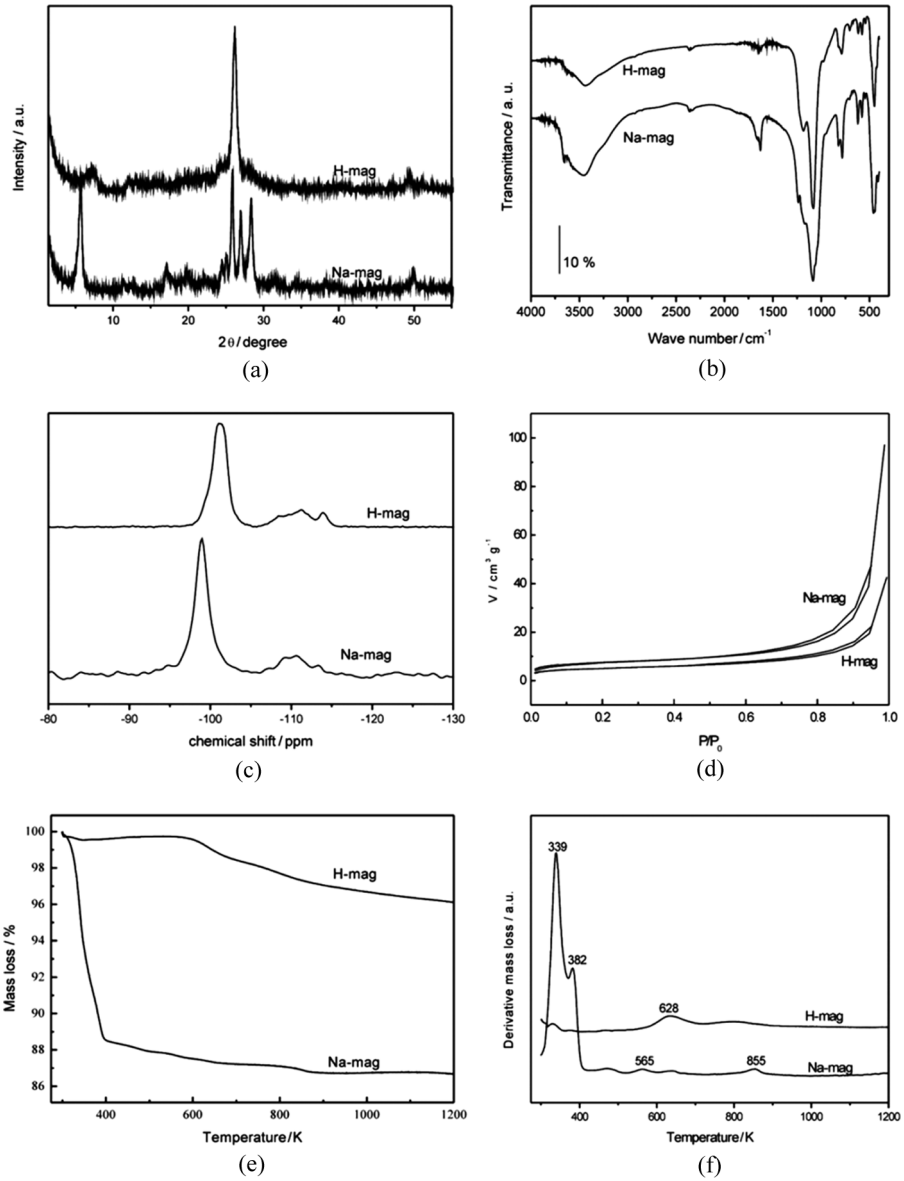

FIG. 1. A- X-ray diffraction patterns (XRD); B- IR spectroscopy; C- ^{29}Si NMR; D- N_2 adsorption/desorption isotherms; E- thermogravimetric curves, F- derivative thermogravimetric curves, for Na-mag and H-mag.

The infrared spectrum of Na-mag presents a wide band due to O−H stretching vibrations, which is attributed to the interlayer water bonded to the acidic centers on the inorganic layers and reinforced by the silanol groups in the 3640 to 3590 cm^{-1} range, followed by the out of plane vibration in the 1660 to 1628 cm^{-1} interval (15) as shown in Fig. 1b. The absorption bands of the layered silicate framework are located in the 1400 to 500 cm^{-1} region. The bands at 1000 to 1250 cm^{-1} are attributed to SiO_4 group vibrations with strong asymmetric stretching at 1075 cm^{-1}, assigned to Si-O-Si (υ_{as} Si−O−Si) and also to the terminal Si−O− (υ Si−O−) bonds. The symmetric Si−O−Si (υ_s Si−O−Si) stretching vibrations are located in the 700 to 950 cm^{-1} region and the corresponding deformation bands for Si−O−Si and O−Si−O (δ SiO) are sited in the 400 to 700 cm^{-1} interval (35). When sodium ions are exchanged by protons, the same bands for the inorganic framework are maintained, with a highly intense peak at 701 cm^{-1} in agreement with sodium replacement. Pronounced bands related to silanol groups occurred in the 3200 to 3750 cm^{-1} range (12,35), as shown in Fig. 1b.

^{29}Si NMR spectra in the solid state for sodic and acidic magadiites are shown in Fig. 1c. Through the distribution of groups containing silicon atoms on the surface it is

possible to understand the characteristic structure of the inorganic layered matrices. For the sodium magadiite (Na-mag) spectrum a Q_3 signal at -99.2 ppm was observed, which is related to the $HOSi(OSi)_3$ species in the silicate sheet; however, the strongly hydrogen bonded water molecules result in a broad peak, and for the acidic form (H-mag) this signal is located at -101.1 ppm. For Q_4 signal, $Si(OSi)_4$, three peaks are observed in sodium magadiites at -109.2, -111.2, and -114.3 ppm respectively (15), while for acidic magadiite, those Q^4 signals were located at 110.9, -113.5, and -114.1 ppm. Each magadiite layer presented equal numbers of sodium cations or protons to counter the negative charge on the oxygen atoms, being as a result, neutral structures. For acidic magadiite distinguishable siloxane and silanol groups can be defined (12), which were identified by the signal displacement of the peaks.

The BET surface area results for sodic and acidic magadiites were 25.1 ± 0.1 and $16.9 \pm 0.1\ m^2\ g^{-1}$, respectively. Those crystalline layered materials present a smooth hysteresis that corresponds to the H3 type, which are associated with split-shape pores between parallel plaques. From the BJH method average pore diameters for sodic and acidic magadiites of 25 ± 1 and 19 ± 1 nm were obtained, respectively, showing a non-homogeneous pore distribution. After matrix acidification, the lamella are going to be closer together as was confirmed by X-ray diffraction patterns and, consequently, a decrease in surface area and average pore diameter for acidic magadiite is expected (20). These adsorption/desorption isotherms are shown in Fig. 1d for sodic and acidic magadiites.

The thermogravimetric and derivative curves for sodium and acidic forms for both magadiites are shown in Figs. 1e and 1f, respectively. When sodic and acidic magadiites are heated distinct masses are lost, as clearly demonstrated through the derivative curves. Thus, from the curve for Na-mag (Fig. 1e), the highest loss, shown through the derivative curve (Fig. 1f), presents two peaks at 339 and 382 K. These inflections could be interpreted as related to loss of water molecules bonded through hydrogen bonds to other similar molecules, as well as those bonded to inorganic silanol groups on the surface and finally to those bonded to the sodium ions located in the interlayer cavity, to give a total of 15.6% that corresponds to 9.2 moles of water (20). Although the general appearance of the thermogravimetric curves is similar, differences in the amount of water and in the temperatures of water release could be related to measurement conditions, when compared with other reports (15,36). Two other not well-defined mass losses were also observed for the sodium matrix at 565 and 855 K, which were attributed to inorganic framework silanol dehydroxylations to form siloxane bonds. The replacement of sodium by proton ions causes a modification of hydration capability of the sample. The thermogravimetric curves present a much lower mass loss for H-mag, as shown in Fig. 1e, which reflects in the respective derivative curve, as shown in Fig. 1f, by presenting a value of 1.6%, to give only 0.80 moles of water, as expected from the absence of Na^+ ions in the interlayer space. Very weak signals are present at 628 K, as was also previously observed (20).

The micrographs for sodic and acidic matrices are shown in Fig. 2. By comparing these images, it is possible to observe that the general morphology of the precursor Na-mag matrix is maintained even after acidic treatment to obtain H-mag. The existence of plaques (12) is clearly viewed, as expected for such layered materials.

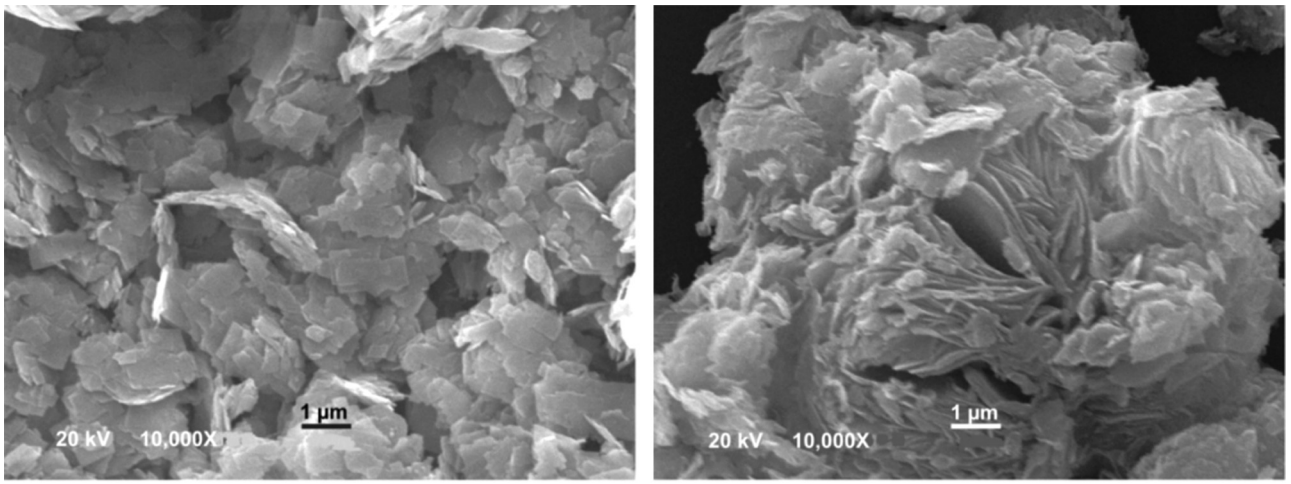

(a) (b)

FIG. 2. SEM for Na-mag (A) and H-mag (B).

Effects of Acidity on Adsorption

One of the most important factors in adsorption studies is the effect of the acidity of the medium (37). Different species will present divergent ranges of suitable pH depending on which adsorbent is used. The effects of initial pH on MB dye adsorption capacity using sodic and acidic magadiite were evaluated within the pH range of 2 to 10, as shown in Fig. 3a. Dye removal increased significantly with the pH, ranging from 2.0 to 8.0 and 2.0 to 8.5 for sodic and acidic magadiites, respectively. For Na-mag, the variation of the amount of MB removal was lower than 0.3% for pH values ranging from 8.0 to 10.0. For H-mag in the pH 8.5 to 10.0 interval the variation in the percentage of removal was lower than 0.8%. Therefore, the best pH interval for MB adsorption on both sodic and acidic magadiite was from 8.5 to 10.0.

The point of zero charge (pH_{PZC}) obtained for Na-mag and H-mag were 4.5 and 3.7, respectively. For pH values higher than pH_{PZC} the adsorbent presents a negative surface charge. The higher amount of MB dye adsorbed by the two adsorbents at pH values higher than 8.5 can be explained by considering the electrostatic interactions between the surface charge of the adsorbents, which became negatively charged at $pH > 4.5$ and >3.7, for Na-mag and H-mag, respectively ($pH > pH_{PZC}$), with the positively charged MB dye. Based on these data, for both adsorbents, the pH value was fixed at 8.5.

Adsorbent Dosage

The adsorbent dosage investigation for dye removal from aqueous solution was carried out using masses of both adsorbents ranging from 20.0 to 200.0 mg, by fixing the initial concentration and volume of MB solutions at 500.0 mg dm^{-3} and 20.0 cm^3, respectively. It was observed that higher amounts of dye removal were attained for adsorbent masses of at least 60.0 mg of each adsorbent, as shown in Fig. 3b. For adsorbent masses higher than these values, the dye removal remained almost constant. The increase in the percentage of dye removal with the adsorbent mass can be attributed to the increase in the adsorbent surface areas, augmenting the number of adsorption sites available for adsorption (6,21,34). On the other hand, the increase in the adsorbent mass promotes a remarkable decrease in the amount of dye uptake per gram of adsorbent (q), as shown in Fig. 3c, an effect that

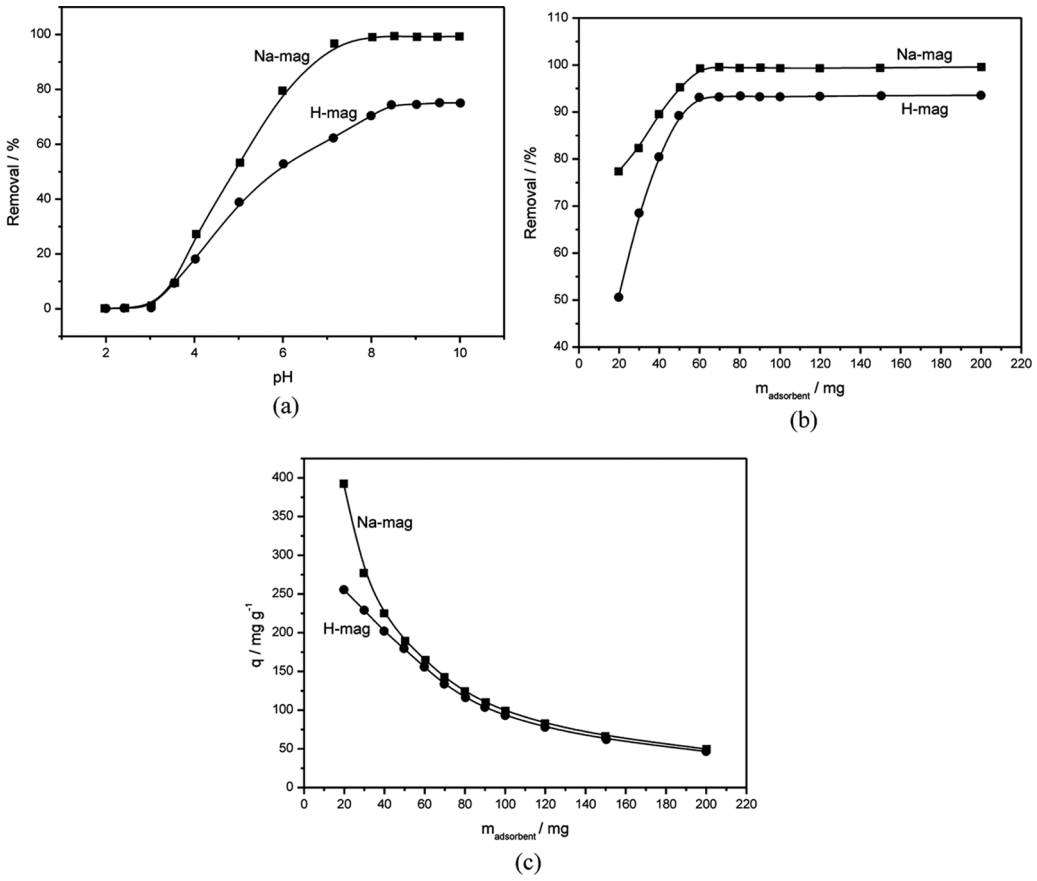

FIG. 3. Effect of pH on MB adsorption (200 mg dm^{-3}); B- Effect of adsorbent mass on the percentage of MB removal (500 mg dm^{-3}) from aqueous effluents; C- Effect of adsorbent mass on the amount of dye adsorbed. Contact time was fixed at 240 min.

can be mathematically explained by combining Eqs. (1) and (2) to give:

$$q = (\%\text{Removal} \cdot Co \cdot V)/(100 \cdot m) \quad (4)$$

As observed from Eq. (4), the amount of dye uptake (q) and the mass of adsorbent (m) are inversely proportional. For a fixed dye percentage removal, the increase of adsorbent mass leads to a decrease in q values, since the volume (V) and initial dye concentrations (C_o) are always fixed. These values clearly indicate that the adsorbent masses must be fixed at 60.0 mg for both sodic and acidic magadiites, masses that correspond to the minimum amount of adsorbent that leads to constant dye removal.

Kinetic Studies

Studies of adsorption kinetics are an important feature to be considered in aqueous effluent treatments as they provide valuable information on the mechanism of adsorption processes (21,34). In attempting to describe the dye adsorption by both adsorbents, four kinetic models were fitted, as shown in Figs. 4a and 4b. The kinetic parameters for the fitted models are listed in Table 3.

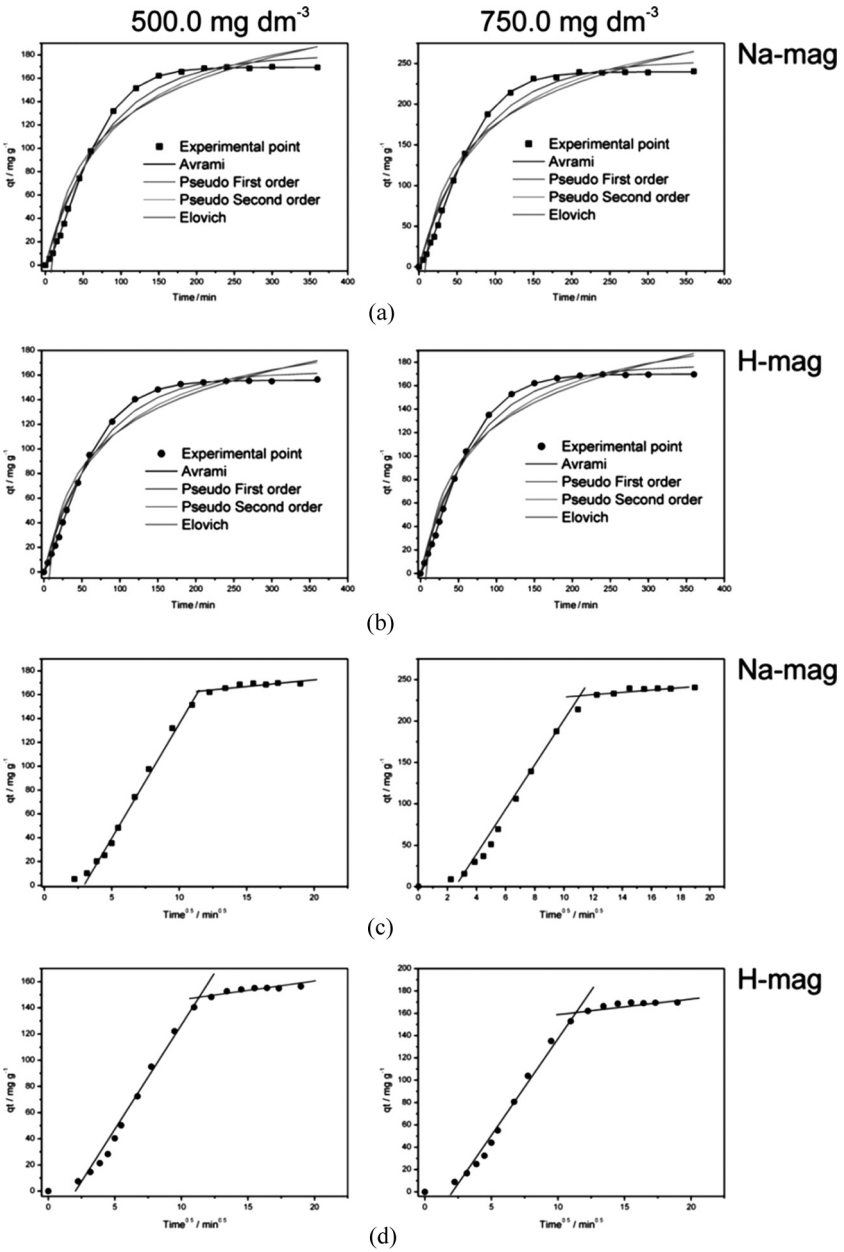

FIG. 4. Kinetic models for MB adsorption.

TABLE 3
Kinetic parameters for MB removal using Na-mag and H-mag adsorbents. Conditions: temperature 298 ± 1 K at pH 8.5 and mass of adsorbent 60.0 mg

	Na-mag		H-mag	
	$500\ mg\ dm^{-3}$	$750\ mg\ dm^{-3}$	$500\ mg\ dm^{-3}$	$750\ mg\ dm^{-3}$
Avrami				
k_{AV} (min^{-1})	0.0149	0.0151	0.0157	0.0159
q_e ($mg\ g^{-1}$)	169	240	156	170
n_{AV}	1.42	1.41	1.30	1.29
R^2	0.9998	0.9997	0.9997	0.9998
F_{error}	0.0685	0.0810	0.0721	0.0780
Pseudo-first order				
k_f (min^{-1})	0.0125	0.0127	0.0137	0.0140
q_e ($mg\ g^{-1}$)	180	254	163	177
R^2	0.9852	0.9858	0.9911	0.9917
F_{error}	0.424	0.366	0.216	0.185
Pseudo-second order				
k_s ($g\ mg^{-1}\ min^{-1}$)	$5.00 \cdot 10^{-5}$	$3.00 \cdot 10^{-5}$	$6.00 \cdot 10^{-5}$	$6.00 \cdot 10^{-5}$
q_e ($mg\ g^{-1}$)	234	330	208	225
h_o ($mg\ g^{-1}\ min^{-1}$)	2.75	3.27	2.59	3.04
R^2	0.9704	0.9709	0.9770	0.9773
F_{error}	0.515	0.453	0.298	0.265
Elovich				
α ($mg\ g^{-1}\ min^{-1}$)	6.02	8.64	6.06	6.74
β ($g\ mg^{-1}$)	0.0202	0.0143	0.0227	0.0210
R^2	0.9564	0.9563	0.9618	0.9615
F_{error}	1.41	1.23	0.829	0.745
Intra-particle diffusion				
ki ($mg\ g^{-1}\ min^{-0.5}$)	19.3	25.9	16.5	18.0

*First stage.

The Avrami fractionary kinetic order was suitably fitted, presenting low error function values and also high R^2 values, for the two initial concentration levels of the dye with both adsorbents. The lowest error function is followed by similar differences in calculated q values, by considering the experimentally measured model (34). It should be stressed that only the analysis of R^2 values for the establishment of a given model is not enough, because the error function evaluates the differences associated with each individual point fitted by the model, in relation to each measured experimental point. On the other hand, the R^2 value measures the differences associated with each individual point in relation to the average fitted curve (34).

Additionally, it was verified that the q_e values found in the fractionary-order were in good agreement with the experimental data. For all other models, the q values were not coincident with the q_e experimental values. These results indicate that the fractionary-order kinetic model best explains the adsorption process of MB uptake by Na-mag and H-mag adsorbents.

By analyzing the values of the kinetic parameters depicted in Table 3, it should be mentioned that the k_{AV} values showed a variation lower than 1.3%, when the initial concentration of the adsorbate increased from 500 to $750\ mg\ dm^{-3}$.

The Avrami kinetic equation has been successfully employed to explain several kinetic processes of different adsorbents and adsorbates. The Avrami exponent (n_{AV}) is a fractionary number related with the possible changes of the adsorption mechanism that take place during the adsorption process (6,21,25,28,38–43). If the mechanism of adsorption follows only an integer-kinetic order, the adsorption could follow multiple kinetic orders that are changed during the contact of the adsorbate with the adsorbent (38–43). The n_{AV} is a result of multiple kinetic orders for the adsorption procedure.

Taking into account that the kinetic results fit very well into the Avrami fractionary kinetic model for the dye using Na-mag and H-mag adsorbents, listed in Table 3 and Figs. 4a and 4b, the intra-particle diffusion model (29),

was plotted in order to verify the influence of mass transfer resistance on the binding of MB to both adsorbents, as indicated by the values listed in Table 3 and shown in Figs. 4c and 4d.

The possibility of intra-particle diffusion resistance affecting adsorption was explored using the appropriate model (29). Thus, the diffusion constant, ki ($mg\,g^{-1}\,min^{-0.5}$), can be obtained from the slope of the plot of qt (uptake at any time, $mg\,g^{-1}$) versus the square root of time. Figures 4c and 4d show the plots of qt versus $t^{1/2}$, with multi-linearity for the dye using Na-mag and H-mag adsorbents. These results imply that the adsorption processes involve more than a single kinetic stage or sorption rate (43). The adsorbents exhibited two stages, which can be attributed to two linear parts, involving Figs. 4c and 4d. The first linear part can be attributed to intra-particle diffusion, which caused delay in the process. However, the second stage may be regarded as the diffusion through smaller pores, which is followed by the establishment of equilibrium (43).

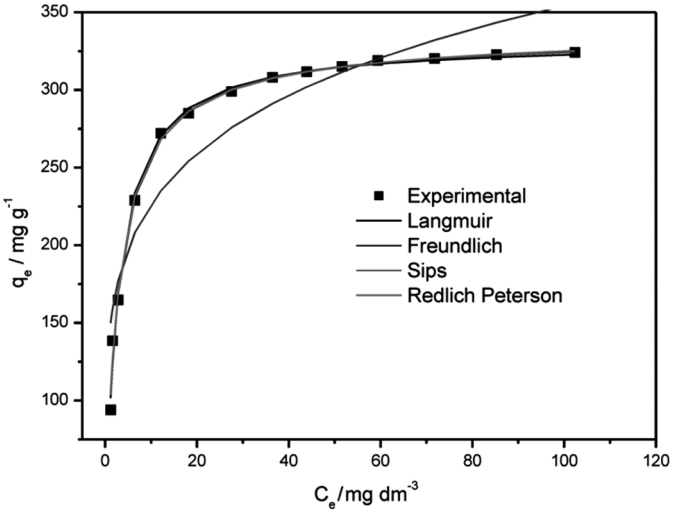

(a)

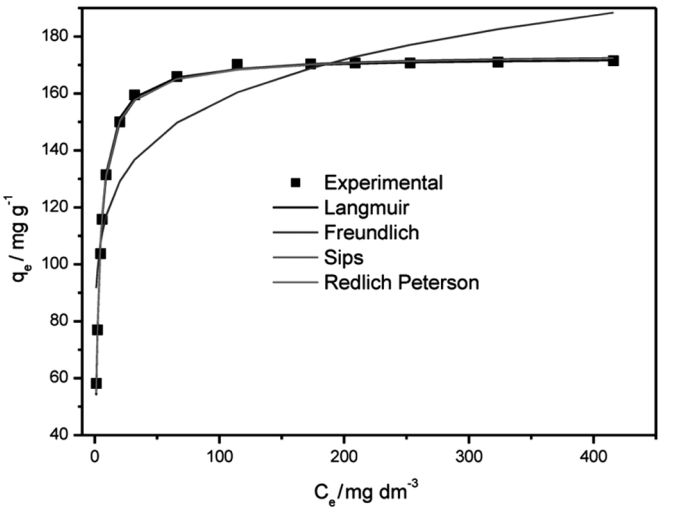

(b)

FIG. 5. Isotherm models for MB adsorption from aqueous solutions on Na-mag and H-mag adsorbents using the batch adsorption procedure at 298 ± 1 K, adsorbent mass of 60 mg; pH fixed at 8.5 for contact time of 210 min. A- Na-mag and B- H-mag.

Equilibrium Studies

The adsorption isotherm describes the amount of adsorbate uptake by the adsorbent and the adsorbate concentration that should remain in solution. Therefore, a lot of equations for analyzing experimental adsorption equilibrium data are available. The equation parameters of these equilibrium models often provide some insight into the adsorption mechanism, the surface properties and the affinity of the adsorbent. For this purpose the Langmuir (30), the Freundlich (31), the Sips (32), and the Redlich-Peterson (33) isotherm models were assayed.

The isotherms of MB adsorption on both adsorbents were performed, by using the best experimental conditions, as shown in Fig. 5, and the data of the fitted models are presented in Table 4. Based on the F_{error}, the equilibrium

TABLE 4
Isotherm parameters for MB adsorption using Na-mag and H-mag as adsorbents. Conditions: Temperature 298 ± 1 K, contact time 210 min, at pH 8.5 and mass of adsorbent 60.0 mg

	Na-mag	H-mag
Langmuir		
Q_{max} ($mg\,g^{-1}$)	331	173
K_L ($dm^3\,mg^{-1}$)	0.369	0.352
R^2	0.9952	0.9978
F_{error}	0.0401	0.0236
Freudlich		
K_F($mg\,g^{-1}$($mg\,dm^{-3}$)$^{-1/n_F}$)	145	88.7
n_F	5.14	8.01
R^2	0.8848	0.8153
F_{error}	0.185	0.194
Sips		
Q_{max}($mg\,g^{-1}$)	335	174
K_S (($mg\,dm^{-3}$)$^{-1/n_s}$)	0.381	0.379
n_S	1.06	1.08
R^2	0.9956	0.9988
F_{error}	0.0421	0.0129
Redlich-Peterson		
K_{RP} ($dm^3\,g^{-1}$)	129	62.8
a_{RP} ($mg\,dm^{-3}$)$^{-g}$	0.410	0.373
g	0.987	0.995
R^2	0.9956	0.9980
F_{error}	0.0410	0.0203

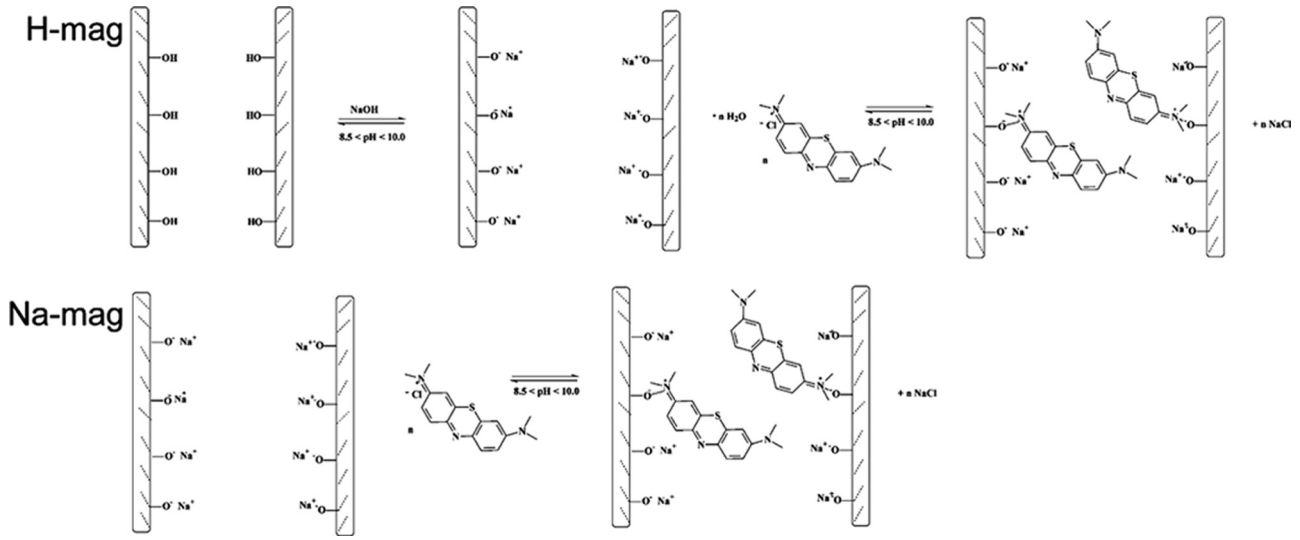

SCH. 2. Mechanism of adsorption of methylene blue on Na-mag and H-mag.

data fit very well all the isotherm models for both adsorbents, with the exception of the Freundlich model. For Na-mag, the results fit slightly better to the Langmuir isotherm model and for H-mag to the Sips isotherm model, whose results were corroborated by the R^2 value.

Taking into account that the equilibrium results were practically coincident for the Langmuir, the Sips, and the Redlich-Peterson isotherm models, the maximum amounts of MB uptake were 331 and 173 mg g^{-1} for Na-mag and H-mag, respectively. From the viewpoint of the interacting exchanger process at the solid/liquid interface, the adsorption of MB by the adsorbents should follow the mechanism depicted in Scheme 2. For H-mag the adsorption follows two steps and for Na-mag only one step is required. For H-mag, in the first step, the lamellar silicate is equilibrated with the aqueous solution ($8.5 < pH < 10.0$), where the available silanol groups loose protons, to form interchangeable sodium silicate. In the second step for both H-mag and for Na-mag the MB is intercalated inside the lamella of the silicate, with an ion-exchange process between the positively charge of dye (MB) with the sodium cation originally bound to the silicate matrix. The ion-exchange of the dye with the lamellar silicate occurs with an expansion of the basal space, as previously observed (44). Taking into account that Na-mag presents cationic sodium ions already bonded to the layered surface, the ion-exchange mechanism is facilitated by the entrance of the guest (MB), a fact that explains its higher adsorption capacity for MB.

Desorption Experiments

Desorption experiments were carried-out in order to verify the possible ion-exchange mechanism of adsorption

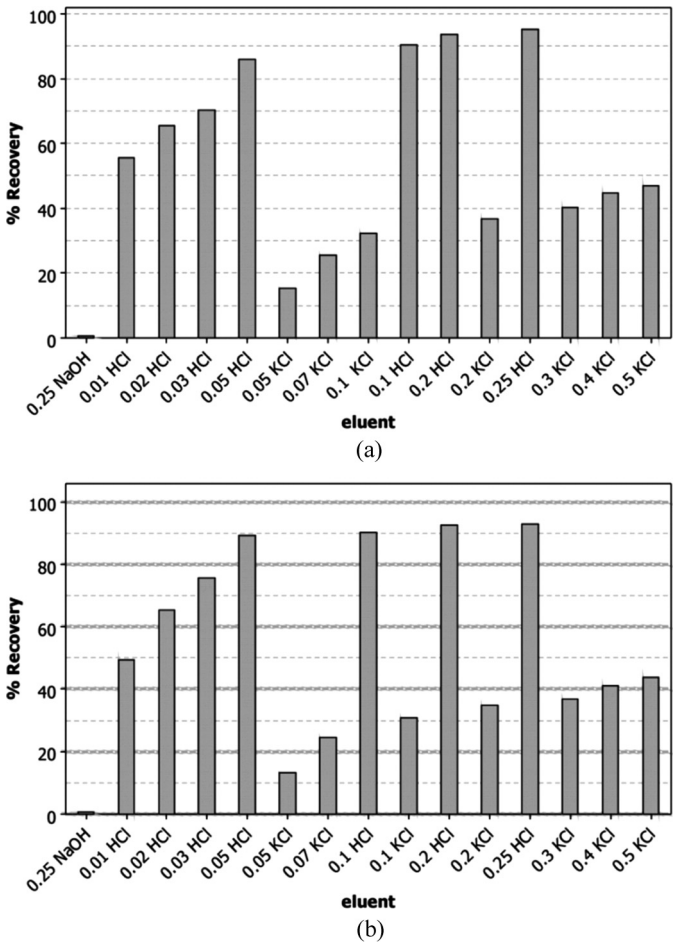

FIG. 6. Desorption of MB loaded on Na-mag (a) and on H-mag (b) adsorbents with solutions expressed by concentration in mol dm^{-3}. Desorption experiments were carried out at 298 K during 1 h.

of MB on Na-mag and H-mag adsorbents, as well as to test the reusability of the adsorbents in industrial applications (see Fig. 5). It was observed that NaOH did not lead to any removal of the MB dye loaded adsorbents after 1 h of contact time (see Fig. 6). The desorption experiments carried-out with KCl promoted a fair regeneration of the MB loaded Na-mag (<47%) and MB loaded H-mag adsorbents (<44%) after 1 h of contact (see Fig. 5). The immediate desorption (<10 min) of MB from Na-mag and H-mag was achieved by using HCl solutions (see Fig. 5). These results reinforce the ion-exchange mechanism of adsorption of MB on Na-mag and H-mag adsorbents, already explained above. The recuperated adsorbents were again employed for MB dye adsorption, after regeneration of the adsorbents with 0.25 mol dm^{-3} of sodium hydroxide. No significant losses of adsorption capacity (<1.5%), were observed during the 5 cycles of adsorption/desorption using both adsorbents.

These results are important from the economic point of view, since industrial effluents contaminated with MB (19) could be treated with the Na-mag and H-mag adsorbents, using stirred tank reactors that were simulated by the batch adsorption procedure described in this work.

Comparison of Different Inorganic Adsorbents for MB Adsorption

A comparison of several inorganic adsorbents employed for MB adsorption is listed in Table 5 (8,45–54). As observed, the Na-mag and H-mag adsorbents employed in this investigation present very high adsorption capacities for the dye when compared with several other inorganic adsorbents. By considering a set of eighteen adsorbents, Na-mag presented higher sorption capacity than fifteen of them (8,45–54), and H-mag showed to be more efficient than eleven of this same series of adsorbents (8,45–54). These outstanding sorption capacities place Na-mag as one of the best adsorbents and H-mag in an intermediate position in relation to the adsorption capacity for MB dye removal from aqueous solutions.

TABLE 5
Comparison of maxima adsorption capacities (MAC) of MB on different inorganic adsorbents (Ads)

Ads	MAC (mg g^{-1})	Ref.
Natural zeolite	25	8
Pyrolyzed petrified sediment	2.39	45
Activated carbon	298	46
Activated carbon	345	46
Activated carbon	385	46
Activated carbon	588	46
Acid treated diatomite	126.6	47
Palygorskite clay	51.0	48
Ordered mesoporous carbon	100.0	49
Titania-silica mesoporous materials	96	50
Activated carbo-aluminosilicate	117.9	51
Activated carbo-aluminosilicate	212.5	51
Activated carbo-aluminosilicate	325.2	51
Activated spent diatomaceous earth	56.2	52
Titania nanotubes	290	53
Natural zeolite	18.3	54
Geopolymeric adsorbents from fly ash	32.0	54
H-mag	173	This work
Na-mag	331	This work

CONCLUSION

The synthesized crystalline layered silicic sodic magadiite and its converted acidic form represent good alternative adsorbents for methylene blue removal from aqueous solutions. Both inorganic matrices have the ability to intercalate the dye inside the free cavities of the matrix at the solid/liquid interface, when the samples are suspended in water, after establishing the best conditions of pH, in the 8.5 to 10.0 range, with a minimum shaking time of 210 min, a time necessary to saturate the available centers located on the exchanger surface and to provide a well-defined isotherm. Good regenerations of the MB loaded Na-mag (95%) and H-mag (93%) adsorbents were achieved using a 0.25 mol dm^{-3} hydrochloric acid solution, reinforcing the ion-exchange mechanism. Four defined kinetic models were used to adjust the adsorption and the best fit was the Avrami (fractionary-order) model. However, the intra-particle diffusion model gave two linear regions, which suggested that the adsorption can be also followed by multiple adsorption rates. The maximum adsorption capacities were 331 and 173 mg g^{-1} for sodic and acidic magadiite, respectively. The proposed mechanism for this process can be related to the highest value obtained for the sodic form, that is caused by the facility of the dye to exchange, not only due to the ionic bonding character of this cation, but also because the process occurred in a favorable expanded basal space.

ACKNOWLEDGEMENTS

The authors are grateful to MCT, CNPq, FAPESP, and CAPES for financial support and fellowships. Prof. Carol Collins is also acknowledged for valuable language improvements.

NOTATIONS

α the initial adsorption rate (mg g^{-1} min^{-1}) of the Elovich equation.

β Elovich constant related to the extent of surface coverage and also to the activation energy involved in chemisorption (g mg^{-1}).

a_{RP} the Redlich-Peterson constant $(mg\,dm^{-3})^{-g}$.
C constant related with the thickness of boundary layer $(mg\,g^{-1})$.
C_f dye concentration at the end of the adsorption $(mg\,dm^{-3})$.
C_e dye concentration at equilibrium $(mg\,dm^{-3})$.
C_o initial dye concentration in contact with the adsorbent $(mg\,dm^{-3})$.
dq differential of q.
g dimensionless exponent of the Redlich-Peterson equation.
h_o the initial sorption rate $(mg\,g^{-1}\,min^{-1})$ of the pseudo-second order equation.
k_{AV} the Avrami kinetic constant (min^{-1}).
k_f pseudo-first order rate constant (min^{-1}).
K_F the Freundlich constant related to adsorption capacity $[mg\,g^{-1}\,(mg\,dm^{-3})^{-1/nF}]$.
k_{id} intra-particle diffusion rate constant $(mg\,g^{-1}\,min^{-0.5})$.
K_L Langmuir affinity constant $(dm^3\,mg^{-1})$.
K_{RP} Redlich-Peterson constant $(dm^3\,g^{-1})$.
K_S the Sips constant related to the affinity constant $(mg\,dm^{-3})^{-1/ns}$.
k_s the pseudo-second order rate constant $(g\,mg^{-1}\,min^{-1})$.
m mass of adsorbent (g).
n_{AV} fractionary reaction order (Avrami) which is related to the adsorption mechanism.
n_F dimensionless exponent of Freundlich equation.
n_S dimensionless exponent of Sips equation.
q amount of the dye adsorbed by the adsorbent $(mg\,g^{-1})$.
q_e amount of dye adsorbed at the equilibrium $(mg\,g^{-1})$.
Q_{max} the maximum adsorption capacity of the adsorbent $(mg\,g^{-1})$.
q_t amount of adsorbate adsorbed at time t $(mg\,g^{-1})$.
t time of contact (min).
V volume of dye in contact with the adsorbent (dm^3).

REFERENCES

1. Pavan, F.A.; Gushikem, Y.; Mazzocato, A.C.; Dias, S.L.P.; Lima, E.C. (2007) Statistical design of experiments as a tool for optimizing the batch conditions to methylene blue biosorption on yellow passion fruit and mandarin peels. *Dyes Pigm.*, *72*: 256.
2. Pavan, F.A.; Lima, E.C.; Dias, S.L.P.; Mazzocato, A.C. (2008) Methylene blue biosorption from aqueous solutions by yellow passion fruit waste. *J. Hazard. Mater.*, *150*: 703.
3. de Lima, R.O.A.; Bazo, A.P.; Salvadori, D.M.F.; Rech, C.M.; Oliveira, D.P.; Umbuzeiro, G.A. (2007) Mutagenic and carcinogenic potential of a textile azo dye processing plant effluent that impacts a drinking water source. *Mutat. Res.*, *626*: 53.
4. Tsuboy, M.S.; Angeli, J.P.F.; Mantovani, M.S.; Knasmüller, S.; Umbuzeiro, G.A.; Ribeiro, L.R. (2007) Genotoxic, mutagenic and cytotoxic effects of the commercial dye CI Disperse Blue 291 in the human hepatic cell line HepG2. *Toxicol. in Vitro*, *21*: 1650.
5. Caritá, R.; Marin-Morales, M.A. (2008) Induction of chromosome aberrations in the Allium cepa test system caused by the exposure of seeds to industrial effluents contaminated with azo dyes. *Chemosphere*, *72*: 722.
6. Lima, E.C.; Royer, B.; Vaghetti, J.C.P.; Simon, N.M.; da Cunha, B.M.; Pavan, F.A.; Benvenutti, E.V.; Veses, R.C.; Airoldi, C. (2008) Application of Brazilian-pine fruit coat as a biosorbent to removal of reactive red 194 textile dye from aqueous solution. Kinetics and equilibrium study. *J. Hazard. Mater.*, *155*: 536.
7. Kavitha, D.; Namasivayam, C. (2008) Capacity of activated carbon in the removal of acid brilliant blue: Determination of equilibrium and kinetic model parameters. *Chem. Eng. J.*, *139*: 453.
8. Wang, S.; Zhub, Z.H. (2006) Characterisation and environmental application of an Australian natural zeolite for basic dye removal from aqueous solution. *J. Hazard. Mater.*, *136*: 946.
9. Gupta, V.K.; Mohan, D.; Saini, V.K. (2006) Studies on the interaction of some azo dyes (naphthol red-J and direct orange) with nontronite mineral. *J. Colloid Interface Sci.*, *298*: 79.
10. Pavan, F.A.; Dias, S.L.P.; Lima, E.C.; Benvenutti, E.V. (2008) Removal of Congo red from aqueous solution by anilinepropylsilica xerogel. *Dyes Pigm.*, *76*: 64.
11. Wang, S.; Li, H. (2006) Structure directed reversible adsorption of organic dye on mesoporous silica in aqueous solution. *Microporous Mesoporous Mater.*, *97*: 21.
12. Thiesen, P.H.; Beneke, K.; Lagaly, G. (2002) Silylation of a crystalline silicic acid: An MAS, NMR and porosity study. *J. Mater. Chem.*, *12*: 3010.
13. Fujita, I.; Kuroda, K.; Ogawa, M. (2003) Synthesis of interlamellar silylated derivatives of magadiite and the adsorption behavior for aliphatic alcohols. *Chem. Mater.*, *15*: 3134.
14. Almond, G.G.; Harris, R.K.; Franklin, K.R. (1997) A structural consideration of kanemite, octosilicate, magadiite and kenyaite. *J. Mater. Chem.*, *7*: 681.
15. Eypert-Blaison, C.; Sauzéat, E.; Pelletier, M.; Michot, L.J.; Villiéras, F.; Humbert, B. (2001) Hydration mechanisms and swelling behavior of Na-magadiite. *Chem. Mater.*, *13*: 1480.
16. Fonseca, M.G.; Silva, C.R.; Barone, J.S.; Airoldi, C. (2000) Layered hybrid nickel phyllosilicates and reactivity of the gallery space. *J. Mater. Chem.*, *10*: 789.
17. Wang, Z.; Pinnavaia, T.J. (2003) Intercalation of poly(propyleneoxide) amines (Jeffamines) in synthetic layered silicas derived from ilerite, magadiite, and kenyaite. *J. Mater. Chem.*, *13*: 2127.
18. Miyamoto, N.; Kawai, R.; Kuroda, K.; Ogawa, M. (2001) Intercalation of a cationic cyanine dye into the layer silicate magadiite. *Appl. Clay Sci.*, *19*: 39.
19. Uses of methylene blue http://www.britannica.com/EBchecked/topic/378634/methylene-blue#. Accessed on March 3rd, 2009.
20. Macedo, T.R.; Airoldi, C. (2006) Host lamellar silicic acid magadiite for some heterocyclic amine inclusions and quantitative calorimetric data. *Microporous Mesoporous Mater.*, *94*: 81.
21. Vaghetti, J.C.P.; Lima, E.C.; Royer, B.; Cardoso, N.F.; Martins, B.; Calvete, T. (2009) Pecan nutshell as biosorbent to remove toxic metals from aqueous solution. *Sep. Sci. Technol.*, *44*: 615.
22. Arenas, L.T.; Vaghetti, J.C.P.; Moro, C.C.; Lima, E.C.; Benvenutti, E.V.; Costa, T.M.H. (2004) Dabco/silica sol-gel hybrid material. The influence of the morphology on the $CdCl_2$ adsorption capacity. *Mater. Lett.*, *58*: 895.
23. Ofomaja, A.E.; Ho, Y.S. (2007) Effect of pH on cadmium biosorption by coconut copra meal. *J. Hazard. Mater.*, *139*: 356.
24. Lima, E.C.; Brasil, J.L.; Santos, A.H.D.P. (2003) Evaluation of Rh, Ir, Ru, W-Rh, W-Ir and W-Ru as permanent modifiers for the determination of lead in ashes, coals, sediments, sludges, soils, and

freshwaters by electrothermal atomic absorption spectrometry. *Anal. Chim. Acta*, *484*: 233.
25. Lopes, E.C.N.; dos Anjos, F.S.C.; Vieira, E.F.S.; Cestari, A.R. (2003) An alternative Avrami equation to evaluate kinetic parameters of the interaction of Hg(II) with thin chitosan membranes. *J. Colloid Interface Sci.*, *263*: 542.
26. Largegren, S. (1898) About the theory of so-called adsorption of soluble substances. *Kungliga Suensk Vetenskapsakademiens Handlingar*, *241*: 1.
27. Ho, Y.S.; Mckay, G.M. (1999) Pseudo-second order model for sorption process. *Proc. Biochem.*, *34*: 451.
28. Vaghetti, J.C.P.; Lima, E.C.; Royer, B.; da Cunha, B.M.; Cardoso, N.F.; Brasil, J.L.; Dias, S.L.P. (2009) Pecan nutshell as biosorbent to remove Cu(II), Mn(II) and Pb(II) from aqueous solutions. *J. Hazard. Mater.*, *162*: 270.
29. Weber-Jr., W.J.; Morris, J.C. (1963) Kinetics of adsorption on carbon from solution. *J. Sanit. Eng. Div. Am. Soc. Civil Eng.*, *89*: 31.
30. Langmuir, I. (1918) The adsorption of gases on plane surfaces of glass, mica and platinum. *J. Am. Chem. Soc.*, *40*: 1361.
31. Freundlich, H.M.F. (1906) Über die adsorption in lösungen. *Z. Phys. Chemie*, *57A*: 385.
32. Sips, R. (1948) On the structure of a catalyst surface. *J. Chem. Phys.*, *16*: 490.
33. Redlich, O.; Peterson, D.L. (1959) A useful adsorption isotherm. *J. Phys. Chem.*, *63*: 1024.
34. Vaghetti, J.C.P.; Lima, E.C.; Royer, B.; Brasil, J.L.; da Cunha, B.M.; Simon, N.M.; Cardoso, N.F.; Noreña, C.P.Z. (2008) Application of Brazilian-pine fruit coat as a biosorbent to removal of Cr(VI) from aqueous solution. Kinetics and equilibrium study. *Biochem. Eng. J.*, *42*: 67.
35. Jacques, R.A.; Bernardi, R.; Caovila, M.; Lima, E.C.; Pavan, F.A.; Vaghetti, J.C.P.; Airoldi, C. (2007) Removal of Cu(II), Fe(III) and Cr(III) from aqueous solution by aniline grafted silica gel. *Sep. Sci. Technol.*, *42*: 591.
36. Superti, G.B.; Oliveira, E.C.; Pastore, H.O.; Bordo, A.; Bisio, C.; Marchese, L. (2007) Aluminum magadiite: an acid solid layered material. *Chem. Mater.*, *19*: 4300.
37. Lima, E.C.; Royer, B.; Vaghetti, J.C.P.; Brasil, J.L.; Simon, N.M.; dos Santos-Junior, A.A.; Pavan, F.A.; Dias, S.L.P.; Benvenutti, E.V.; da Silva, E.A. (2007) Adsorption of Cu(II) on Araucaria angustifolia wastes: Determination of the optimal conditions by statistic design of experiments. *J.Hazard. Mater.*, *140*: 211.
38. Cestari, A.R.; Vieira, E.F.S.; Matos, J.D.S.; dos Anjos, D.S.C. (2005) Determination of kinetic parameters of Cu(II) interaction with chemically modified thin chitosan membranes. *J. Colloid Interface Sci.*, *285*: 288.
39. Cestari, A.R.; Vieira, E.F.S.; Pinto, A.A.; Lopes, E.C.N. (2005) Multistep adsorption of anionic dyes on silica/chitosan hybrid 1. Comparative kinetic data from liquid- and solid-phase models. *J. Colloid Interface Sci.*, *292*: 363.
40. Cestari, A.R.; Vieira, E.F.S.; Vieira, G.S.; Almeida, L.E. (2006) The removal of anionic dyes from aqueous solutions in the presence of anionic surfactant using aminopropylsilica. -A kinetic study. *J. Hazard. Mater.*, *138*: 133.
41. Vieira, E.F.S.; Cestari, A.R.; Lopes, E.C.N.; Barreto, L.S.; Lázaro, G.S.; Almeida, L.E. (2007) Determination of kinetic parameters from isothermal calorimetry for interaction processes of pyrimethamine with chitosan derivatives. *React. Funct. Polym.*, *67*: 820.
42. Zubieta, C.E.; Messina, P.V.; Luengo, C.; Dennehy, M.; Pieroni, O.; Schulz, P.C. (2008) Reactive dyes remotion by porous TiO_2-chitosan materials. *J. Hazard. Mater.*, *152*: 765.
43. Royer, B.; Cardoso, N.F.; Lima, E.C.; Vaghetti, J.C.P.; Simon, N.M.; Calvete, T.; Veses, R.C. (2009) Applications of Brazilian-pine fruit shell in natural and carbonized forms as adsorbents to removal of methylene blue from aqueous solutions – Kinetic and equilibrium study. *J. Hazard. Mater.*, *164*: 1213.
44. Lazarin, M.; Airoldi, C. (2004) Intercalation of methylene blue into barium phosphate – synthesis and electrochemical investigation. *Anal. Chim. Acta*, *523*: 89.
45. Aroguz, A.Z.; Gulen, J.; Evers, R.H. (2008) Adsorption of methylene blue from aqueous solution on pyrolyzed petrified sediment. *Bioresour. Technol.*, *99*: 1503.
46. El-Qada, E.N.; Allen, S.J.; Walker, G.M. (2008) Adsorption of basic dyes from aqueous solution onto activated carbons. *Chem. Eng. J.*, *135*: 174.
47. Al-Qodaha, Z.; Lafi, W.K.; Al-Anber, Z.; Al-Shannag, M.; Harahsheh, A. (2007) Adsorption of methylene blue by acid and heat treated diatomaceous silica. *Desalination*, *217*: 212.
48. Al-Futaisi, A.; Jamrah, A.; Al-Hanai, R. (2007) Aspects of cationic dye molecule adsorption to palygorskite. *Desalination*, *214*: 327.
49. Xun, Y.; Shu-Ping, Z.; Wei, X.; Hong-You, C.; Xiao-Dong, D.; Xin-Mei, L.; Zi-Feng, Y. (2007) Aqueous dye adsorption on ordered mesoporous carbons. *J. Colloid Interface Sci.*, *310*: 83.
50. Messina, P.V.; Schulz, P.C. (2006) Adsorption of reactive dyes on titania–silica mesoporous materials. *J. Colloid Interface Sci.*, *299*: 305.
51. Shawabkeh, R.A. (2004) Synthesis and characterization of activated carbo-aluminosilicate material from oil shale. *Microporous Mesoporous Mater.*, *75*: 107.
52. Tsai, W.T.; Hsien, K.J.; Yang, J.M. (2004) Silica adsorbent prepared from spent diatomaceous earth and its application to removal of dye from aqueous solution. *J. Colloid Interface Sci.*, *275*: 428.
53. Hsieh, C.T.; Fan, W.S.; Chen, W.Y. (2008) Impact of mesoporous pore distribution on adsorption of methylene blue onto titania nanotubes in aqueous solution. *Microporous Mesoporous Mater.*, *116*: 677.
54. Li, L.; Wang, S.; Zhu, Z. (2006) Geopolymeric adsorbents from fly ash for dye removal from aqueous solution. *J. Colloid Interface Sci.*, *300*: 52.

Anexo 3

Journal of Hazardous Materials 181 (2010) 366–374

Contents lists available at ScienceDirect

Journal of Hazardous Materials

journal homepage: www.elsevier.com/locate/jhazmat

A useful organofunctionalized layered silicate for textile dye removal

Betina Royer[a], Natali F. Cardoso[a], Eder C. Lima[a,*], Thaís R. Macedo[b], Claudio Airoldi[b]

[a] Institute of Chemistry, Federal University of Rio Grande do Sul, UFRGS, Av. Bento Gonçalves 9500, P.O. Box 15003, 91501-970 Porto Alegre, Rio Grande do Sul, Brazil
[b] Institute of Chemistry, University of Campinas, UNICAMP, P.O. Box 6154, 13084-971 Campinas, São Paulo, Brazil

ARTICLE INFO

Article history:
Received 16 March 2010
Received in revised form 13 April 2010
Accepted 5 May 2010
Available online 11 May 2010

Keywords:
Layered material
RUB-18
Organofunctionalization
Adsorbent
Textile dye
Reactive Black 5 dye

ABSTRACT

The octosilicate Na-RUB-18 has the ability to exchange its original sodium with cetyltrimethylammonium cations. This procedure leads to interlayer space expansion, with the aim of obtaining inorganic–organic nanostructured hybrids by chemical modification reactions. The silylating agent 3-trimethoxysilylpropylurea was attached to the inorganic layer using heterogeneous methodology. The new organofunctionalized material was characterized by elemental analysis, X-ray diffraction, ^{13}C and ^{29}Si nuclear magnetic resonances in the solid state, infrared spectroscopy, thermogravimetry and scanning electron microscopy. The amount of silylating agent immobilized on surface was 2.03 mmol g^{-1}, with a basal distance of 2.43 nm. Nuclear magnetic resonance of ^{13}C and ^{29}Si nuclei evidenced covalent bond formation between organosilyl and silanol groups at the surface. The new synthesized nanostructured layered material was able to remove the textile dye Reactive Black 5 from aqueous solution, followed through a batchwise process. The effects of stirring time, adsorbent dosage and pH on the adsorption capacity demonstrated that 150 min is enough to reach equilibrium at 298 ± 1 K at pH 3.0. Based on error function values the data were best fitted to fractional-order kinetic models and compared to pseudo-first-order, pseudo-second-order and chemisorption kinetic models. The equilibrium data were better fitted to the Sips isotherm models.

1. Introduction

Industrial activities are responsible for generating large volumes of hazardous species contaminating wastewater effluents [1]. Even more pronounced is the effluent contamination by colored rejects, which cause serious problems of environment pollution [2,3]. As a result, the interest in textile dye removal from aqueous solution has grown, as has the development of synthetic materials that could be used for this purpose [1–4]. These materials must have wide applicabilities, not only for discoloring different industrial wastewater, but also due to interesting structural aspects that lead to better results compared to natural and other commonly used sorbents [5,6].

Normally the sorption process was carried out by conventional ion exchange procedure [7]. The possibility of chemically modified different surfaces increases capability of dye sorption presented by those synthesized organofunctionalized materials, as previously assigned [2,4].

RUB-18 is a member of the hydrous layered silicate family, also composed of makatite, kanemite, kenyaite and magadiite [8]. With the exception of RUB-18, these silicates were first discovered in nature. From the synthetic point of view this set of silicates is also synthesized in the laboratory in the sodic form. For example, $Na_8Si_{32}O_{64}(OH)_8{\cdot}32H_2O$ with a basal distance of 1.10 nm, with structural lamella composed of four rings connected by other five silicon atoms [9]. The [5^4] cage model was first investigated with this layered silicate. Makatite and kanemite also had their structures determined, but those for the other members of the family, magadiite and kenyaite, remain unknown [8,10]. These silicates present charge neutrality maintained through the hydrated sodium counter ion distributed inside the layered framework [8,9].

The silanol groups disposed on the layered surface of the RUB-18 structure enable silylating agents bonding, after prior exchange of sodium with cethyltrimethylammonium cations, with the objective to expand the interlayer cavity to obtain a greater organophillic character, favoring by this procedure covalent bond formation between the silylating agent and the layered surface [11]. Examples of chemical organofuncionalization of surfaces are conventional procedures used for synthesis of natural talc phyllosilicates and other layered materials [3,12]. On the other hand, the organofunctionalized materials can be obtained by different methodologies, such as the sol–gel process, solvent evaporation and conventional reflux methodology [13]. The procedure leads to the design of chosen molecules to be grafted to nanostructured materials that

* Corresponding author. Tel.: +55 51 3308 7175; fax: +55 51 3308 7304.
E-mail addresses: eder.lima@ufrgs.br, profederlima@gmail.com (E.C. Lima).

0304-3894/$ – see front matter © 2010 Elsevier B.V. All rights reserved.
doi:10.1016/j.jhazmat.2010.05.019

Nomenclature

a_{RP}	Redlich–Peterson constant $(mg\,dm^{-3})^{-g}$
C	constant related with the thickness of the boundary layer $(mg\,g^{-1})$.
C_f	dye concentration at the end of the adsorption $(mg\,dm^{-3})$
C_e	dye concentration at equilibrium $(mg\,dm^{-3})$
C_o	initial dye concentration put in contact with the adsorbent $(mg\,dm^{-3})$
g	dimensionless exponent of Redlich–Peterson equation
h_o	the initial sorption rate $(mg\,g^{-1}\,min^{-1})$ of the pseudo-second-order equation
k_{AV}	Avrami kinetic constant (min^{-1})
k_f	pseudo-first-order rate constant (min^{-1}).
K_F	the Freundlich constant related to adsorption capacity $[mg\,g^{-1}(mg\,dm^{-3})^{-1/n_F}]$.
k_{id}	intra-particle diffusion rate constant $(mg\,g^{-1}\,min^{-0.5})$.
K_L	Langmuir affinity constant $(dm^3\,mg^{-1})$.
K_{RP}	Redlich–Peterson constant $(dm^3\,g^{-1})$
K_S	the Sips constant related to the affinity constant $((mg\,dm^{-3})^{-1/n_S})$
k_s	the pseudo-second-order rate constant $(g\,mg^{-1}\,min^{-1})$
m	mass of adsorbent (g)
n_{AV}	a fractional reaction order (Avrami) which can be related to the adsorption mechanism
n_F	dimensionless exponent of the Freundlich equation
n_S	dimensionless exponent of the Sips equation
q	amount of the dye absorbed by the adsorbent $(mg\,g^{-1})$
q_e	amount of adsorbate adsorbed at the equilibrium $(mg\,g^{-1})$
Q_{max}	the maximum adsorption capacity of the adsorbent $(mg\,g^{-1})$
q_t	amount of adsorbate adsorbed at time t $(mg\,g^{-1})$
t	time of contact (h)
V	volume of dye put in contact with the adsorbent (dm^3)

Greek letters

α	the initial adsorption rate $(mg\,g^{-1}\,min^{-1})$ of the Elovich equation
β	Elovich constant related to the extent of surface coverage and also to the activation energy involved in chemisorption $(g\,mg^{-1})$

present established functionalities and different practical applications.

The silicate RUB-18 presents a regular layered surface and high capacity for organofunctionalization reactions. Recently, the interlayer space of RUB-18 has been modified by different methoxy and chlorosilanes and the synthesized inorganic–organic nanostructured materials were successfully used for removal of divalent cation and heavy metal from aqueous solution [13,14].

The present investigation deals with a synthesized organofunctionalized RUB-18 for use as a sorbent for Reactive Black 5 textile dye removal. Consequently, the natural and chemical aspects related to the silylating agent grafted on the layers are presented, together with the application of this material as sorbent for dye removal from aqueous effluents.

2. Experimental

2.1. Synthesis of Na-RUB-18

The hydrated sodium silicate RUB-18 was synthesized by a hydrothermal procedure [14]. Briefly, suspension of silica gel (Fluka) and a sodium hydroxide (Nuclear) solution in the molar ratio of SiO_2:0.5NaOH:7.0H_2O, that corresponds to 25.0 g of amorphous silica gel, 8.32 g of sodium hydroxide and 53 cm^3 of deionised water was transferred to a Teflon-lined autoclave with autogeneous pressure and treated at 378 K for 9 days. The as-synthesized Na-RUB-18 was filtered, washed with deionised water until neutral pH and dried at 323 K for 24 h [14–16].

2.2. Synthesis of CTA-RUB-18

A sample of 2.0 g of Na-RUB-18 was dispersed in 200 cm^3 of 0.10 mol dm^{-3} of an aqueous solution of cetyltrimethylammonium bromide (CTAB). The mixture was stirred for 3 days at room temperature. The procedure was repeated 3 times until completing the intercalation process, which was followed by X-ray diffraction. Finally, the solid obtained (CTA-RUB-18) was centrifuged, washed with ethanol and dried at 323 K for 24 h [14,16].

2.3. Organofunctionalization

A sample of 2.0 g of the as-synthesized CTA-RUB-18 was suspended in 100 cm^3 of toluene under nitrogen flow at 343 K for 1 h. Then, 2.0 cm^3 of the silylating agent 3-trimethoxysilylpropylurea (TPU, $(CH_3O)_3Si(CH_2)_3NHCONH_2$) was added to the reaction medium, which remained for another 96 h. The obtained product (C-RUB-U) was filtered, washed with ethanol (Synth), dried under vacuum at 343 K for 24 h [4,14,15].

2.4. Characterization

Carbon, nitrogen and hydrogen amounts were determined on a Perkin-Elmer 2400 Series II microelemental analyzer and two independent determinations were performed. X-ray diffraction patterns were collected on a Shimadzu model XRD 7000 diffractometer, varying 2θ from 1.4 to 50°, with CuKα radiation (corresponding to 1.54 nm). Thermogravimetric curves were obtained on a TA Instruments 5100, with heating rate of 0.167 K s^{-1}, under 1.67 $cm^3\,s^{-1}$ of argon flow, from room temperature to 1273 K, and initial mass of at least 10.0 mg of the solid.

Nuclear magnetic resonance spectra were recorded with a Bruker AC300/P solid state high-resolution spectrometer, by cross-polarization and magic angle spinning (CP-MAS). The frequencies were 79.4 and 100.6 MHz, with rotational frequencies of 10 kHz and delay times of 6.0 ms and 8.0 ms for ^{29}Si and ^{13}C nuclei, respectively. Chemical shifts were referenced to tetramethylsilane. Infrared spectra were performed on a Bomem model MB FTIR spectrophotometer, with KBr pellets in the 4000–400 cm^{-1} region and resolution scan of 4 cm^{-1}, accumulating 32 scans. The micrographs were measured on a JEOL 6360-LV scanning electron microscope. The samples were first suspended in acetone and the micrograph was obtained after sputter coating a thin conducting layer of gold for 400 s.

2.5. Solutions and reagents

Deionised water was used throughout the experiments for all solution preparations.

The Reactive Black 5 textile dye (RB-5), (C.I. 20505; $C_{26}H_{21}N_5O_{19}S_6Na_4$, 991.82 g mol^{-1}, λ_{max} = 590 nm, as shown in Scheme 1) was obtained from Sigma with a dye content of 55%.

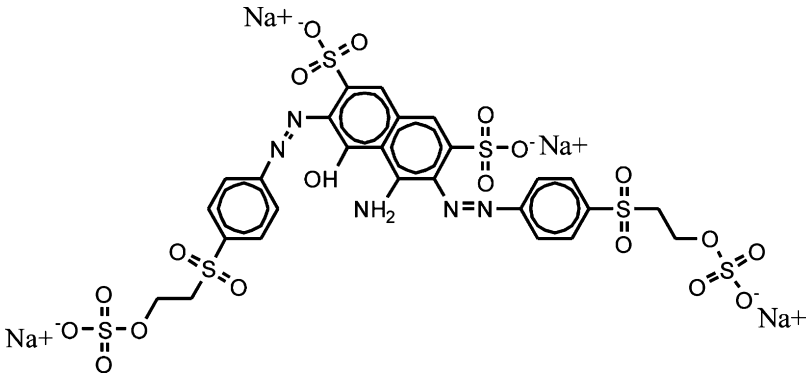

Scheme 1. Structural formula of Reactive Black 5 dye (RB-5).

It was used without further purification. The dye has two sulfonate groups and another two sulfato-ethyl-sulfone group, with negative charges even in highly acidic solutions, due to their pK_a values are lower than zero [17].

The stock solution was prepared by dissolving accurately weighed dye in distilled water at a concentration of 5000 mg dm^{-3}. The working solutions were obtained by diluting the dye stock solution to the required concentrations. In order to adjust the pH of the solutions, 0.10 mol dm^{-3} sodium hydroxide or hydrochloric acid solutions were used, using a Hanna (HI 255) pHmeter.

2.6. Batchwise adsorption procedure

The adsorption studies to evaluate the C-RUB-U for RB-5 dye removal from aqueous solutions were carried-out in triplicate using a batch adsorption procedure. For these experiments, fixed amounts of adsorbent varying from 20.0 to 200.0 mg were suspended in a series of 50 cm^3 glass flasks containing 20.0 cm^3 of dye solution with concentrations that varied from 2.00 to 1000.0 mg dm^{-3}. These suspensions were stirred for suitable times from 5 to 360 min. The isotherms clearly demonstrated that a well-established plateau was obtained and the equilibrium studies determined in these optimized conditions were 150 min at 298 ± 1 K, with the initial pH of the dye solutions ranging from 2.5 to 8.5. Subsequently, in order to separate the adsorbents from the aqueous solutions, the flasks were centrifuged at 3600 rpm for 10 min, as already described in other publications [17,18], and aliquots of 1.0–10.0 cm^3 of the supernatant were properly diluted. The final concentrations of the dye remaining in solution were determined by visible spectrophotometry, using a Femto spectrophotometer provided with 1.0 cm path length optical-glass cells. Absorbance measurements were made at the maximum wavelength of the dye, 590 nm, and the detection limit using the spectrophotometric method, determined according to IUPAC [19], was 0.14 mg dm^{-3}. The amount of the dye uptake and percentage of dye removal by the adsorbent were calculated by applying Eqs. (1) and (2), respectively:

$$q = \frac{(C_o - C_f)}{m} V \quad (1)$$

$$\%\text{Removal} = 100\frac{(C_o - C_f)}{C_o} \quad (2)$$

where q is the amount of dye uptake by the adsorbent (mg g^{-1}); C_o is the initial RB-5 concentration in contact with the adsorbent (mg dm^{-3}), C_f is the dye concentration (mg dm^{-3}) after the batch adsorption procedure, V is the volume of dye solution (dm^3) in contact with the adsorbent and m is the mass (g) of adsorbent.

2.7. Kinetic and equilibrium models

The kinetic equations corresponding to the Avrami, pseudo-first-order, pseudo-second-order, and Elovich models are given in Table 1 [20]. The isotherm equations corresponding to the Langmuir, Freundlich, and Sips models are listed in Table 2 [21].

2.8. Statistical evaluation of the kinetic and isotherm parameters

The kinetic and equilibrium models were fitted by employing a nonlinear method, with successive interactions calculated by the method of Levenberg–Marquardt and also interactions calculated by the Simplex method, using the nonlinear fitting facilities of the software Microcal Origin 7.0. In addition, the models were also evaluated by an error function, which measures the differences in the amount of dye uptake by the adsorbent predicted by the models and the actual q measured experimentally [22]

$$F_{\text{error}} = \sqrt{\left(\frac{1}{n-p}\right)\sum_{i}^{n}(q_{i,\text{exp}} - q_{i,\text{model}})^2} \quad (3)$$

where $q_{i,\text{exp}}$ is the value of q measured experimentally, $q_{i,\text{model}}$ is the value of q predicted by the fitted model, n is the number of experiments performed, and p is the number of parameter of the fitted model.

Table 1
Kinetic adsorption models.

Kinetic model	Nonlinear equation
Avrami	$q_t = q_e\{1 - \exp[-(k_{AV}t)]^{n_{AV}}\}$
Pseudo-first-order	$q_t = q_e[1 - \exp(-k_f t)]$
Pseudo-second-order	$q_t = \frac{k_s q_e^2 t}{1 + q_e k_s t}$
	$h_o = k_s q_e^2$
	Initial sorption rate
Elovich	$q_t = \frac{1}{\beta}\ln(\alpha\beta) + \frac{1}{\beta}\ln(t)$

Table 2
Isotherm models.

Isotherm model	Equation
Langmuir	$q_e = \frac{Q_{max} K_L C_e}{1 + K_L C_e}$
Freundlich	$q_e = K_F C_e^{1/n_F}$
Sips	$q_e = \frac{Q_{max} K_S C_e^{1/n_S}}{1 + K_S C_e^{1/n_S}}$

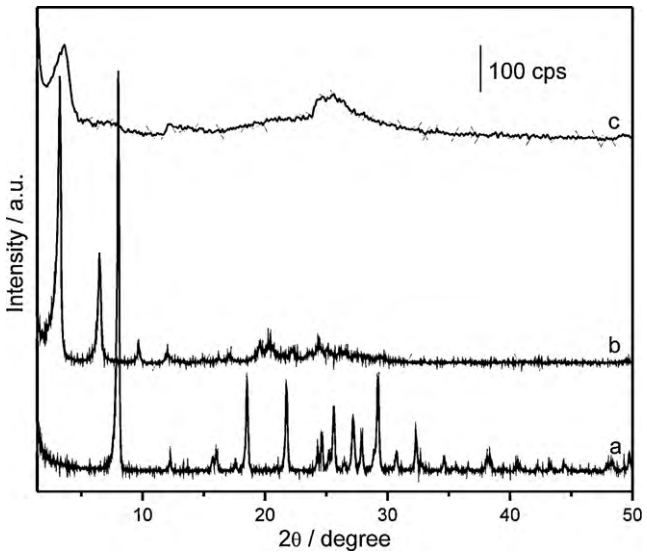

Fig. 1. X-ray diffraction patterns of Na-RUB-18 (a), CTA-RUB-18 (b) and of the organomodified C-RUB-U (c) materials.

3. Results and discussion

3.1. Sorbent characterization

X-ray diffraction pattern of the Na-RUB-18, intercalated CTA-RUB-18 and organofunctionalized C-RUB-U compounds are shown in Fig. 1. As observed at the curve a, Na-RUB-18 shows lamellar domains revealed by peaks for 2θ at 8.1 and 16.1°, related to the diffraction of the [0 0 1] and [0 0 2] planes of the solid surface, respectively [9,14]. The first peak is attributed to the basal distance of 1.09 nm and after exchanging the interlayered sodium ions by the cetyltrimethylammonium cations the basal distance increased 2.70 nm, 2θ being 3.3°, as expected, favoring the step of organofunctionalization [12,14]. The attachment of the silylating agent N-trimethoxysilylpropylurea to the layered RUB-18 surface causes a decrease of the precursor silicate basal distance, from 2.70 to 2.43 nm, easily viewed by the shift in the d_{001} reflection to greater 2θ value at 3.6°, showing also that the intercalated cation was removed after the attachment [14]. Covalent bond formation between silanol groups on the layered surface and the silylating agent in the organofunctionalization process, disposes attached pendant chains that could be protonated in aqueous solutions, adding potential capability for dye sorption [2]. The elemental analysis results for synthesized modified material gave: C, 9.84%; H, 2.12%; N, 5.68%, with the immobilized amount of pendant organic groups being 2.03 mmol g^{-1}, based on the amount of nitrogen obtained. This result reflects the amount of anchored organic groups able to interact with the RB-5 textile dye. The result obtained by elemental analysis is very near from that obtained through thermogravimetry, that gave an amount of 2.09 mmol g^{-1} of organic groups, which decomposed upon heating the sample. The agreement between elemental analysis and thermogravimetry shows a well behaved system [15].

Through ^{29}Si CP-MAS NMR it is possible to determine the connectivity of the layers [23]. The spectrum obtained for the Na-RUB-18 shows two signals, at −99.9 and −111.1 ppm, from the units Q^3, $(SiO)_3Si–O^-$, and Q^4, $(SiO)_4Si$, respectively, due to silanol and siloxane groups on the structure of the layered silicate, as shown in Fig. 2A (a). For the intercalated form CTA-RUB-18, the spectrum in Fig. 2A (b) gave the same set of signals, with little displacement to −101.4 and −112.3 ppm, due to Q^3 and Q^4 groups, respectively.

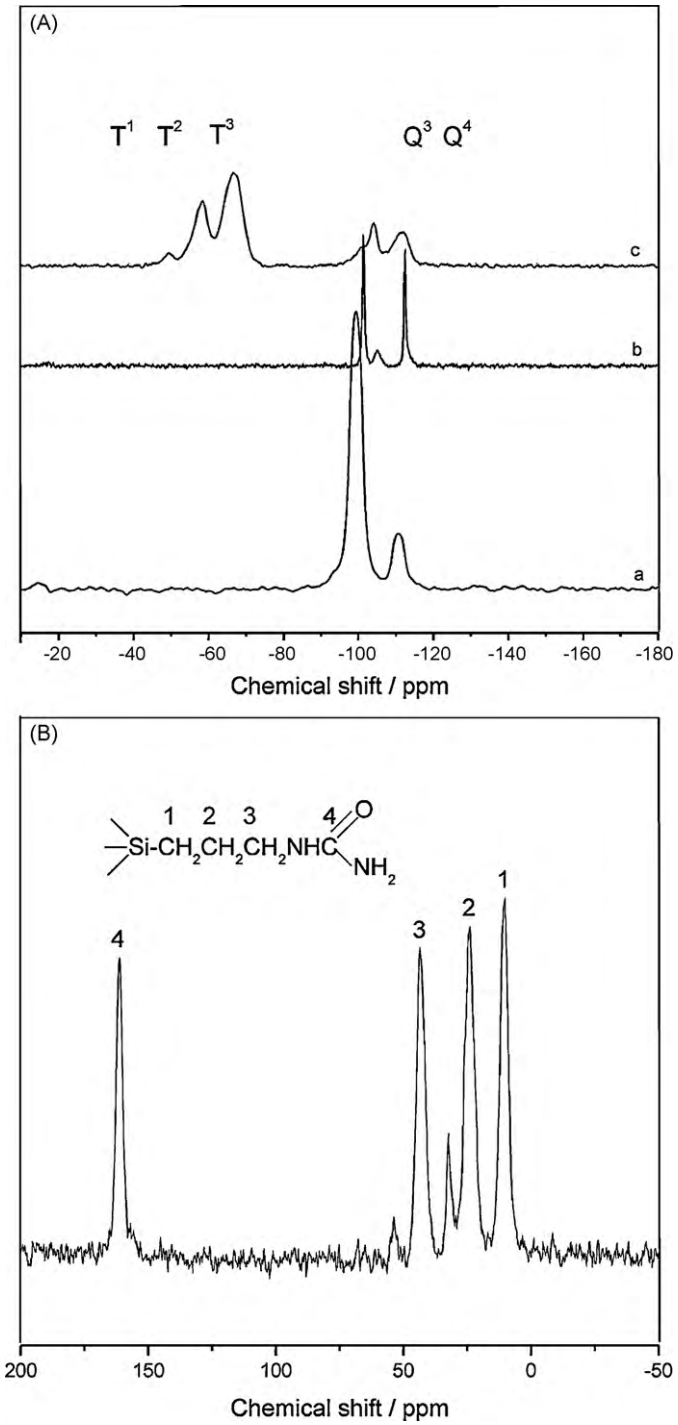

Fig. 2. (A) ^{29}Si MAS NMR of Na-RUB-18 (a), CTA-RUB-18 (b), C-RUB-U (c) and (B) ^{13}C MAS NMR of C-RUB-U materials.

The signal between at −104.8 ppm may occur when two forms of intercalation changes silicon environment [9,14].

The spectrum of the organofunctionalized inorganic–organic hybrid, as shown in Fig. 2A (c), shows signals from Q^3 and Q^4 groups at −104.2 and −111.7 ppm, respectively. The reduction of the Q^3 signal intensity was observed together with an increase in the signal intensity related to the Q^4 signal, confirming the reaction of the organic molecule with the silanol groups of the silicate surface, being converted to Q^4 sites [13]. In addition, upon covalent bond formation, three new signals are related to T^1, T^2 and T^3 environments, at −49.4, −58.3 and −66.6, respectively. Those

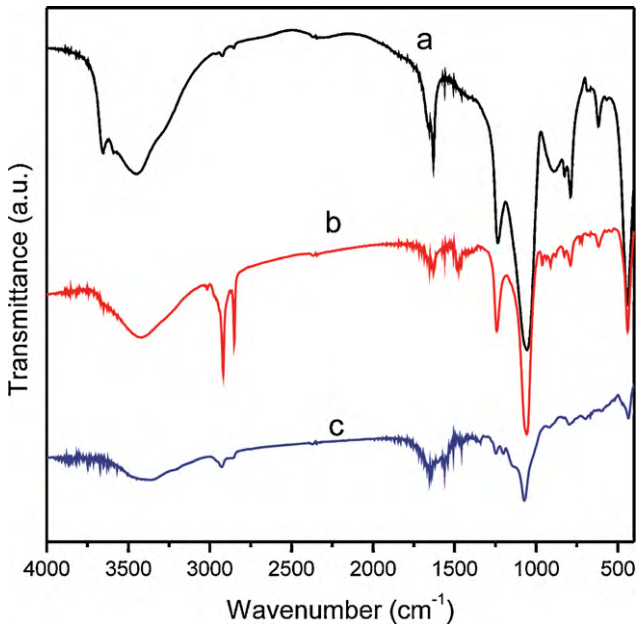

Fig. 3. FTIR spectra of Na-RUB-18 (a), CTA-RUB-18 (b) and C-RUB-U (c).

signals indicate different attachments, since T^1 corresponds to $[Si(OSi)(OH)_2R]$ to T^2 $[Si(OSi)_2(OH)R]$ and T^3 to $[Si(OSi)_3R]$, being R an organic chain [2,14,24].

^{13}C CP-MAS NMR spectrum of C-RUB-U material is shown in Fig. 2B, with the inserted structure of the organic chain covalently bonded to the inorganic framework [25]. The spectrum confirms the presence of the carbon from the silylating agent anchored to the silicate layer, and also that the surfactant was completely removed during the washing process. The signals from the organic pendant groups were seen at 12.4, 23.8, 43.9 and 161.5 ppm, in agreement with the attributions, for carbon (1) attached to the silicate sheet and chain intermediate carbons (2) and (3), with carbon (4) corresponding to the functional group, respectively.

The infrared spectrum of the Na-RUB-18 layered silicate shows the expected bands of the physisorbed water molecules on the inorganic material, represented by ν(OH) stretching frequency at 3650 cm^{-1} and the δ(OH) deformation band near 1630 cm^{-1} (see Fig. 3a). The band that appeared at 3650 cm^{-1} is also attributed to available silanol groups on the surface. The bands at the interval of 1000–500 cm^{-1} are due to frequency ν(Si–O) vibrations, from the inorganic framework. Absorption bands at 797 and 670 cm^{-1} are related to the symmetric stretching ν(SiO) of Si–O–Si groups [2]. The intercalated compound infrared spectrum shows the same bands related to the inorganic structure of the layer, with new bands detected at 2920 and 2855 cm^{-1}, associated with symmetric and asymmetric stretching $\nu(CH_2)$ respectively, and at 1474 cm^{-1} for the symmetric deformation $\delta(CH_2)$ vibrations for the intercalated organic cation $[C_{16}H_{33}N(CH_3)_3]^+$ [13,16] (see Fig. 3b). The organically modified RUB-18 structure presented bands at 2967 and at 1620 cm^{-1}, due to ν(C–H) stretching and δ(NH) deformation vibrations, respectively, and the band at 1650 cm^{-1} is attributed to ν(C=O) carbonyl stretching vibration, from the silylating agent attachment at the surface [2,14,15] (see Fig. 3c).

The scanning electron microscopy of the as-synthesized samples of CTA-RUB-18 and of the organofunctionalized C-RUB-U are shown in Fig. 4. The morphologies are similar, showing that the particles were organized forming plates typical for a layered structure [8].

3.2. Effects of acidity on adsorption

One of the most important factors in adsorption studies is the effect of the acidity of the medium [26]. Different species being adsorbed on diverse adsorbents will present divergent ranges of suitable pH regions for adsorption. The effects of initial pH on RB-5 dye adsorption capacity using C-RUB-U adsorbent was evaluated within the pH range from 2.5 to 8.5, as shown in Fig. 5A. The amount of dye adsorbed (q) was constant in the pH range from 2.5 to 3.0. From pH 3.0 to 4.0 the percentages of RB-5 dye removal decreased by 7%. With values ranging from 4.5 to 6.0, the percentages were practically constant. From pH 6.0 to 8.5, the percentages decreased on the order of 32%. Based on the present data, the initial pH of all adsorbate solutions were kept at 3.0.

The major adsorption capacity of C-RUB-U adsorbent for RB-5 adsorption occurs at pH 2.5–3.0, because at this pH range, the amino groups of the adsorbent are protonated, facilitating the adsorption of the negative charged dye (see Scheme 2).

3.3. Adsorbent mass

The investigation of the mass of adsorbent for dye removal from aqueous solution was carried out using adsorbent masses ranging from 20.0 to 200.0 mg, by fixing the initial concentration and volume of RB-5 solutions at 60.0 mg dm^{-3} and 20.0 cm^3, respectively. The highest amount of dye removal was attained for adsorbent masses of at least 50.0 mg of adsorbent, as shown in Fig. 5B (at left). For adsorbent masses higher than these values, the dye removal remained almost constant. The increase in the percentage of dye removal with adsorbent mass can be attributed to increases in

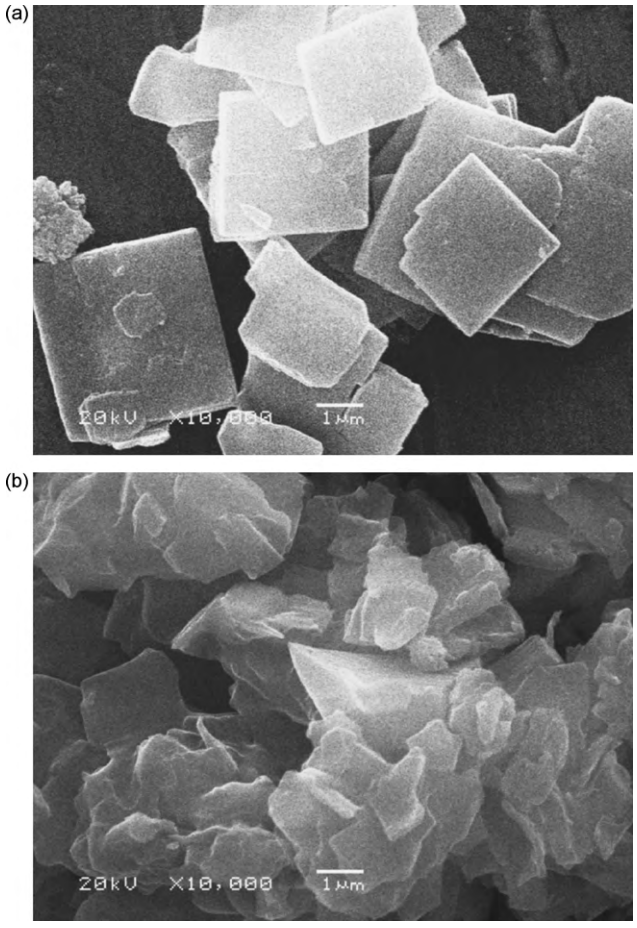

Fig. 4. Scanning electron microscopy of CTA-RUB-18 (a) and C-RUB-U (b) samples.

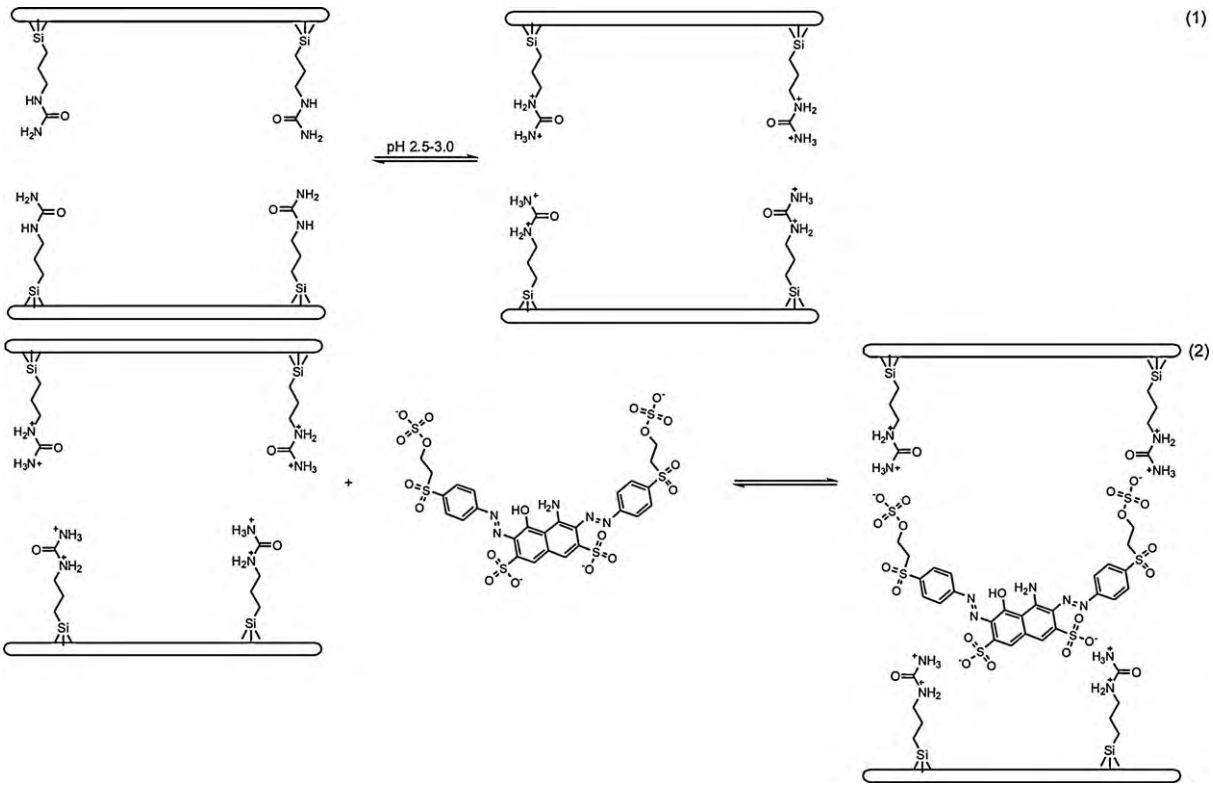

Scheme 2. Mechanism of adsorption of RB-5 by C-RUB-U adsorbent.

the adsorbent surface areas, augmenting the number of adsorption sites available for adsorption [4,5,18]. On the other hand, the increase in the adsorbent mass promotes a remarkable decrease in the amount of dye uptake per gram of adsorbent (q), as shown in Fig. 5B (at right), an effect that can be mathematically explained by combining Eqs. (1) and (2):

$$q = \frac{\%\text{Removal} \cdot C_o \cdot V}{100m} \quad (4)$$

As observed from Eq. (4), the amount of dye uptake (q) and the mass of adsorbent (m) are inversely proportional. For a fixed dye percent removal, an increase of adsorbent mass leads to a decrease in q values, since the volume (V) and initial dye concentrations (C_o) are always fixed. These values clearly indicate that the adsorbent mass must be fixed at 50.0 mg, which corresponds to the minimum amount of adsorbent that leads to constant dye removal.

3.4. Kinetic studies

Studies of adsorption kinetics are an important feature to be considered in aqueous effluent treatments as they provide valuable information on the mechanism of adsorption processes [20]. In attempting to describe RB-5 dye adsorption by the adsorbent, four kinetic models were tried, as shown in Fig. 6A and B. The kinetic parameters for the models are listed in Table 3. Based on the F_{error} values, it was observed that the Avrami the Avrami model provides the best fit to the data. The pseudo-first-order, pseudo-second-order and chemisorption kinetic models presented F_{error} values at least 3.7 times higher than the Avrami fractional kinetic model.

Additionally, it was verified that the q_e values found in the fractional-order were in good agreement with the experimental data (see Table 3). For the pseudo-first-order, pseudo-second-order and chemisorption models, the q_e fitted values were not so coincident with the q_e experimental value. This result indicates that the fractional-order kinetic model better explains the adsorption process of RB-5 uptake by C-RUB-U adsorbent.

Analyzing the values of the kinetic parameters presented in Table 3 indicates that the k_{AV} values showed a variation of 5.8%, when the initial concentration of the adsorbate increased from 60.0 to 120.0 mg dm^{-3}. On the other hand, the percentage of variation of k_S was 68.1%, when the initial concentration levels of the RB-

Table 3
Kinetic parameters for RB-5 removal using C-RUB-U as adsorbent. Conditions: temperature 298 K; pH 3.0; adsorbent mass: 50.0 mg.

	C_o (mg dm^{-3})	
	60.0	120.0
q_e experimental (mg g^{-1})	24.25	44.85
Fractional order		
k_{AV} (min^{-1})	0.01898	0.02008
q_e (mg g^{-1})	24.33	44.91
n_{AV}	0.8876	0.8738
R^2 adjusted	0.9998	0.9998
F_{error}	0.1139	0.2241
Pseudo-first-order		
k_f (min^{-1})	0.02047	0.02182
q_e (mg g^{-1})	23.78	43.82
R^2 adjusted	0.9975	0.9968
F_{error}	0.4200	0.8677
Pseudo-second-order		
k_s (g mg^{-1} min^{-1})	7.900×10^{-4}	4.700×10^{-4}
q_e (mg g^{-1})	28.29	51.72
h_o (mg g^{-1} min^{-1})	0.6321	1.257
R^2 adjusted	0.9968	0.9971
F_{error}	0.4764	0.8255
Elovich chemisorption		
α (mg g^{-1} min^{-1})	1.488	2.942
β (g mg^{-1})	0.1734	0.09513
R^2 adjusted	0.9817	0.9825
F_{error}	1.132	2.208

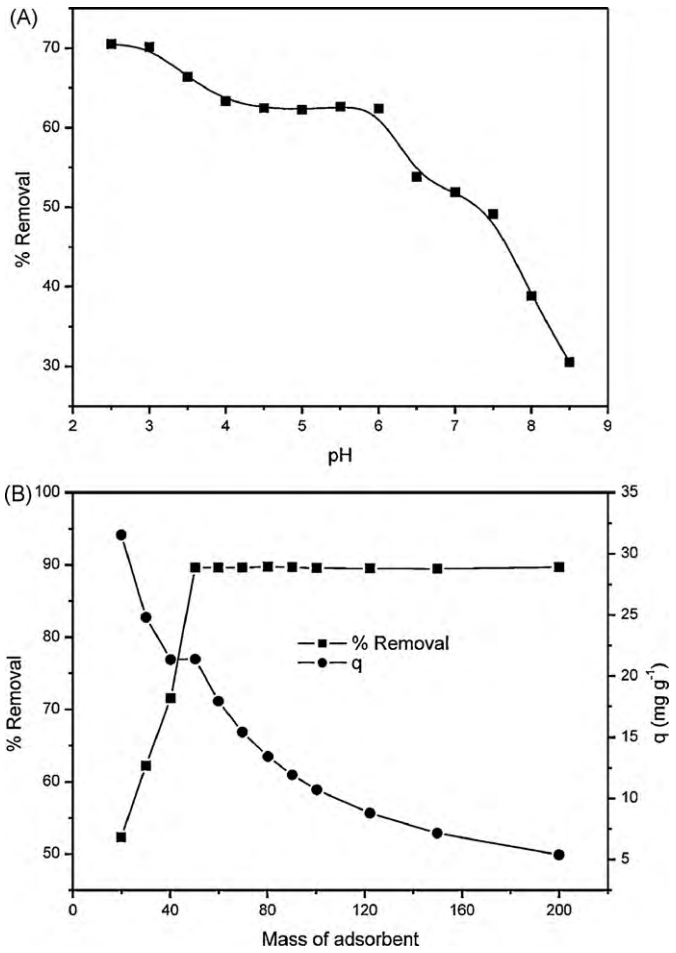

Fig. 5. (A) Effect of pH on the adsorption. (B) Effect of mass of adsorbent on the percentage removal and amount of RB-5 dye adsorbed. Initial RB-5 concentration was 40.0 and 60.0 mg dm^{-3}, for Fig. 4A and B, respectively.

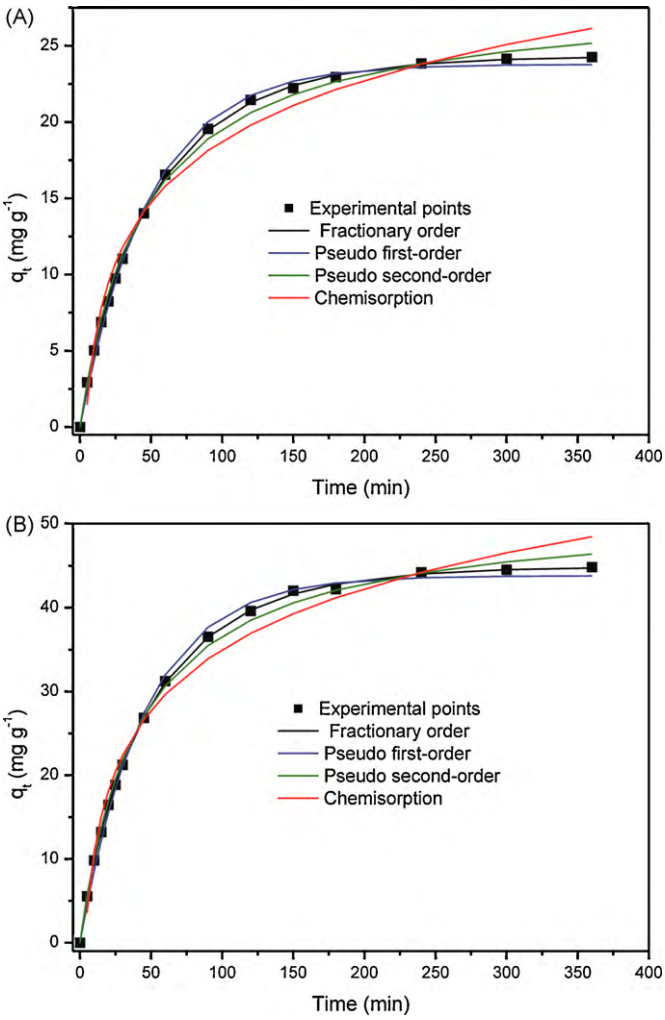

Fig. 6. Kinetic curves. (A) 60.0 mg dm^{-3}, (B) 120.0 mg dm^{-3}. Conditions: temperature 298 K; pH 3.0; mass of adsorbent 50.0 mg.

5 dye were increased from 60.0 to 120.0 mg dm^{-3}. Therefore, the fractional kinetic model provides a constant rate parameter which is much better for comparison of different kinetic constants, using several adsorbates and adsorbents, as already observed in other publications [2,4,5,17,20,21,27,28].

3.5. Equilibrium studies

The adsorption isotherm describes the amount of adsorbate uptake by the adsorbent and the adsorbate concentration that should remain in solution [21]. Therefore, many equations for analyzing experimental adsorption equilibrium data are available. The equation parameters of these equilibrium models often provide some insight into the adsorption mechanism, the surface properties and the affinity of the adsorbent. For this purpose the Langmuir [21], Freundlich [21], and Sips [29] isotherm models were assayed.

The isotherms of RB-5 adsorption on C-RUB-U adsorbent were obtained, by using the best experimental conditions, as shown in Fig. 7, and the data of the fitted models are presented in Table 4. Based on F_{error}, the equilibrium data was well fitted by Sips isotherm model when using this adsorbent for sorption of this dye. On the other hand, the Langmuir and Freundlich models failed to fit the isotherm curve, as shown by the low adjusted R^2 as well as high F_{error} values, indicating that for this specific case the Langmuir and Freundlich isotherm models were not suitable fitted. The lower the error function (F_{error}) is, the smaller will be the difference of the q calculated by the model from the experimentally measured

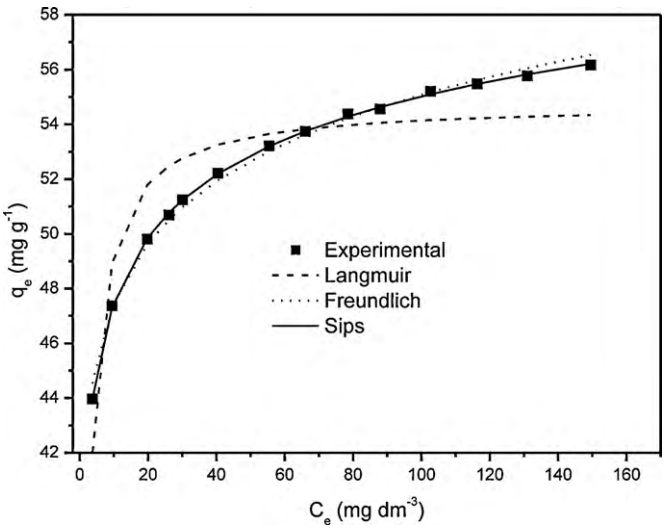

Fig. 7. Isotherm of adsorption. Conditions: temperature 298 K; pH 3.0; mass of adsorbent 50.0 mg, time of contact 300 min.

Table 4
Isotherm parameters for RB-5 adsorption, using C-RUB-U as adsorbent. Conditions: temperature 298 ± 1 K, contact time 300 min, pH 3.0 and mass of adsorbent 50.0 mg.

	C-RUB-U
Langmuir	
Q_{max} (mg g^{-1})	54.75
K_L (dm^3 mg^{-1})	0.8833
R^2 adjusted	0.8271
F_{error}	1.465
Freundlich	
K_F (mg g^{-1}(mg dm^{-3})$^{-1/n_F}$)	40.91
n_F	15.49
R^2 adjusted	0.9943
F_{error}	0.2656
Sips	
Q_{max} (mg g^{-1})	76.77
K_S ((mg dm^{-3})$^{-1/n_S}$)	1.040
n_S	5.181
R^2 adjusted	0.9997
F_{error}	0.06109

q [20–22]. Only analysis of R^2 values for the establishment of a given model is not enough, the use of the error function that evaluates the differences associated with each individual point fitted by the model, is also necessary [20–22].

Taking into account the Sips isotherm, the maximum amount of dye uptake was 76.77 mg g^{-1}, which corresponds to 0.0774 mmol g^{-1}. From the point of view of the exchange process at the solid/liquid interface, the RB-5 dye has negative sulfonate and sulfate-ethyl-sulfonate groups to ionically interact with the protonated nitrogens attached to the pendant chain covalently grafted on the silicate layer, as shown in Scheme 2. This interactive process is favored at pH < 3, as shown in Fig. 5A, when the basic nitrogen atoms are easily protonated to acquire a positive charge. In general for the adsorption process, the degree of adsorption depends both on the active sites of the adsorbent and the adsorbate properties. The results obtained suggest that the textile dye uses more than one basic center of the grafted trimethoxysilylpropylurea molecule, during the interactive process [30], as might be expected for a favorable adjustment of its size inside the pores of the adsorbent to counteract the opposing charges. When saturated an amount of 2.03 mmol g^{-1} is retained.

4. Conclusion

The synthesized crystalline layered silicic compound intercalated with surfactant, CTA-RUB-18, demonstrated efficiency in coupling a silylating agent into the free interlayer cavity. Thus, the success in grafting organic molecules depends firstly on prior basal distance expansion, which favors the intercalation process. Structural features related to silicon nuclear magnetic resonance in the solid state clearly illustrated carbon-(oxygen silicon) covalent bond formation, supporting the attachment of the pendant organic chains to the inorganic layer, by reaching the final interlayer distance of 2.43 nm. The available protonated basic atoms extract the Reactive Black 5 textile dye from aqueous solution through a batchwise process. The dye adsorption data was adjusted to the Sips isotherms model and the kinetic data was fitted to a fractional-order kinetic model. For this interactive process the basic protonated nitrogen atoms were saturated to give plateaus represented by the maximum number of moles adsorbed, for example, 76.77 mg g^{-1} (0.0774 mmol g^{-1}), given by the Sips isotherm. Based on these results, it is supposed that the textile dye uses more than one basic center of the grafted urea molecule when interacting with the available basic nitrogens to reach 0.310 mmol g^{-1}. This is expected, since the dye has two sulfonate and also two sulfatoethyl-sulfone groups, all of them possessing negative charges to interact with the positive amine groups of the organomodified material. However, this interaction may happen with different protonated amine groups of the urea, it is also necessary to consider the size of the dye molecules.

Acknowledgements

The authors are grateful to MCT, CNPq, FAPESP and CAPES for financial supports and fellowships.

References

[1] F.A. Pavan, S.L.P. Dias, E.C. Lima, E.V. Benvenutti, Removal of Congo red from aqueous solution by anilinepropylsilica xerogel, Dyes Pigment 76 (2008) 64–69.
[2] B. Royer, N.F. Cardoso, E.C. Lima, V.S.O. Ruiz, T.R. Macedo, C. Airoldi, Organofunctionalized kenyaite for dye removal from aqueous solution, J. Colloid Interface Sci. 336 (2009) 398–405.
[3] J.M. Oh, T.T. Biswick, J.H. Choy, Layered nanomaterials for green materials, J. Mater. Chem. 19 (2009) 2553–2563.
[4] B. Royer, N.F. Cardoso, E.C. Lima, T.R. Macedo, C. Airoldi, Sodic and acidic crystalline lamellar magadiite adsorbents for removal of methylene blue from aqueous solutions. Kinetic and equilibrium studies, Sep. Sci. Technol. 45 (2010) 129–141.
[5] E.C. Lima, B. Royer, J.C.P. Vaghetti, N.M. Simon, B.M. da Cunha, F.A. Pavan, E.V. Benvenutti, R.C. Veses, C. Airoldi, Application of Brazilian pine-fruit shell as a biosorbent to removal of reactive red 194 textile dye from aqueous solution. Kinetics and equilibrium study, J. Hazard. Mater. 155 (2008) 536–550.
[6] F.A. Pavan, Y. Gushikem, A.S. Mazzocato, S.L.P. Dias, E.C. Lima, Statistical design of experiments as a tool for optimizing the batch conditions to methylene blue biosorption on yellow passion fruit and mandarin peels, Dyes Pigment 72 (2007) 256–266.
[7] V. Cottier, J.P. Bellat, M.H. Simonet-Grange, A. Méthivier, Adsorption of p-xylene/m-xylene gas mixtures on BaY and NaY zeolites. Coadsorption equilibria and selectivities, J. Phys. Chem. B 101 (1997) 4798–4802.
[8] W. Schwieger, G. Lagaly, Handbook of Layered Materials, CRC Press, Germany, 2008 (Chapter 11).
[9] M. Borowski, O. Kovalev, H. Gies, Structural characterization of the hydrous layer silicate Na-RUB-18, $Na_8Si_{32}O_{64}(OH)_8{\cdot}32H_2O$ and derivatives with XPD-, NPD-, and SS NMR experiments, Micropor. Mesopor. Mater. 107 (2008) 71–80.
[10] K. Kosuge, P. Singh, Mixed-oxide pillared silicates from H-ilerite by intercalation, Chem. Mater. 12 (2000) 421–427.
[11] U. Diáz, Á. Cantín, A. Corma, Novel layered organic-inorganic hybrid materials with bridged silsesquioxanes as pillars, Chem. Mater. 19 (2007) 3686–3693.
[12] D.L. Guerra, C. Airoldi, Kinetics and modified clay thermodynamic from the Brazilian Amazon region for lead removal, J. Hazard. Mater. 159 (2008) 412–419.
[13] T.R. Macedo, C. Airoldi, Distinct features of organosilyl-grafted pendant groups attached in the RUB-18 interlayer space, Dalton Trans. 36 (2009) 7402–7409.
[14] T.R. Macedo, C. Airoldi, New inorganic–organic lamellar derivatives synthesized from H-RUB-18 and thermodynamics of cation sorption, New J. Chem. 33 (2009) 2081–2089.
[15] K. Kosuge, A. Tsunashima, New silica-pillared material prepared from the layered silicic-acid of ilerite, J. Chem. Soc. Chem. Commun. 23 (1995) 2427–2428.
[16] K. Endo, Y. Sugahara, K. Kuroda, Formation of intercalation compounds of a layered sodium octosilicate with n-alkyltrimethylammonium ions and the application to organic derivatization, Bull. Chem. Soc. Jpn. 67 (1994) 3352–3355.
[17] T. Calvete, E.C. Lima, N.F. Cardoso, S.L.P. Dias, F.A. Pavan, Application of carbon adsorbents prepared from the Brazilian-pine fruit shell for removal of Procion Red MX 3B from aqueous solution—kinetic, equilibrium, and thermodynamic studies, Chem. Eng. J. 155 (2009) 627–636.
[18] B. Royer, N.F. Cardoso, E.C. Lima, J.C.P. Vaghetti, N.M. Simon, T. Calvete, R.C. Veses, Applications of Brazilian-pine fruit shell in natural and carbonized forms as adsorbents to removal of methylene blue from aqueous solutions—kinetic and equilibrium study, J. Hazard. Mater. 164 (2009) 1213–1222.
[19] E.C. Lima, F.J. Krug, J.A. Nóbrega, A.R.A. Nogueira, Determination of ytterbium in animal faeces by tungsten coil electrothermal atomic absorption spectrometry, Talanta 47 (1998) 613–623.
[20] J.C.P. Vaghetti, E.C. Lima, B. Royer, B.M. da Cunha, N.F. Cardoso, J.L. Brasil, S.L.P. Dias, Pecan nutshell as biosorbent to remove Cu(II), Mn(II) and Pb(II) from aqueous solutions, J. Hazard. Mater. 162 (2009) 270–280.
[21] J.C.P. Vaghetti, E.C. Lima, B. Royer, N.F. Cardoso, B. Martins, T. Calvete, Pecan nutshell as biosorbent to remove toxic metals from aqueous solution, Sep. Sci. Technol. 44 (2009) 615–644.
[22] J.C.P. Vaghetti, E.C. Lima, B. Royer, J.L. Brasil, B.M. da Cunha, N.M. Simon, N.F. Cardoso, C.P.Z. Noreña, Application of Brazilian-pine fruit coat as a biosorbent to removal of Cr(VI) from aqueous solution—kinetics and equilibrium study, Biochem. Eng. J. 42 (2008) 67–76.
[23] D.W. Sindorf, G.E. Maciel, Solid-state NMR-studies of the reactions of silica surfaces with polyfunctional chloromethylsilanes and ethoxymethylsilanes, J. Am. Chem. Soc 105 (1983) 3767–3776.

[24] M.A. Melo Jr., F.J.V.E. Oliveira, C. Airoldi, Useful aminoalcohol molecules incorporated in an epoxide silylating agent for silica organofunctionalization and thermodynamics of copper removal, New J. Chem. 33 (2009) 1038–1046.
[25] C.M. Leu, Z.W. Wu, K.H. Wei, Synthesis and properties of covalently bonded layered silicates/polyimide (BTDA-ODA) nanocomposites, Chem. Mater. 14 (2002) 3016–3021.
[26] E.C. Lima, B. Royer, J.C.P. Vaghetti, J.L. Brasil, N.M. Simon, A.A. dos Santos Jr., F.A. Pavan, S.L.P. Dias, E.V. Benvenutti, E.A. da Silva, Adsorption of Cu(II) on Araucaria angustifolia wastes: determination of the optimal conditions by statistic design of experiments, J. Hazard. Mater. 140 (2007) 211–220.
[27] E.C.N. Lopes, F.S.C. dos Anjos, E.F.S. Vieira, A.R. Cestari, An alternative Avrami equation to evaluate kinetic parameters of the interaction of Hg(11) with thin chitosan membranes, J. Colloid Interface Sci. 263 (2003) 542–547.
[28] A.R. Cestari, E.F.S. Vieira, J.D.S. Matos, D.S.C. dos Anjos, Determination of kinetic parameters of Cu(II) interaction with chemically modified thin chitosan membranes, J. Colloid Interface Sci. 285 (2005) 288–295.
[29] R. Sips, On the structure of a catalyst surface, J. Chem. Phys. 16 (1948) 490–495.
[30] V.S.O. Ruiz, G.C. Petrucelli, C. Airoldi, Inorganic–organic hybrids derived from lamellar acidic kenyaite immobilizations for cation removal at the solid/liquid interface, J. Mater. Chem. 6 (2006) 2338–2346.